Fabrication of Microstructures by Powder Blasting

Henk Wensink

The research described in this thesis was carried out at the Transducers Science and Technology Group of the MESA+ Research Institute, University of Twente, Enschede, The Netherlands.

This work is part of the research programme of the 'Stichting voor Fundamenteel Onderzoek der Materie (FOM)', which is financially supported by the 'Nederlandse Organisatie voor Wetenschappelijk Onderzoek (NWO)'.

Promotiecommissie:

Voorzitter		
	prof. dr. J.H.A. de Smit	Universiteit Twente
Secretaris		
	prof. dr. J.H.A. de Smit	Universiteit Twente
Promotor		
	prof. dr. M.C. Elwenspoek	Universiteit Twente
Leden		
	prof. dr. J.E. Field	University of Cambridge
	prof. dr. M.A.M. Gijs	Swiss Federal Ins. of Tech. (EPFL)
	prof. dr. M. Wessling	Universiteit Twente
	dr. P.J. Slikkerveer	Philips Electronics N.V.
	dr. D.H.A. Blank	Universiteit Twente

Wensink, Hendrik
Fabrication of Microstructures by Powder Blasting
Ph.D. thesis, University of Twente, Enschede The Netherlands
ISBN 90-365-1698-6

FABRICATION OF MICROSTRUCTURES BY POWDER BLASTING

PROEFSCHRIFT

ter verkrijging van
de graad van doctor aan de Universiteit Twente,
op gezag van de rector magnificus,
prof.dr. F.A. van Vught,
volgens besluit van het College voor Promoties
in het openbaar te verdedigen
op vrijdag 22 februari 2002 te 16:45 uur.

door

Hendrik Wensink
geboren op 21 juli 1972
te Brummen

Dit proefschrift is goedgekeurd door de promotor:
prof. dr. M.C. Elwenspoek

- *Gefeliciteerd! Dat moet toch een bevredigend moment voor je zijn geweest.*
(…)
- Maar alleen gedurende een moment. Daarna was het zoals het altijd gaat: als je eindelijk heb bereikt wat je wilde bereiken, is het niet meer wat je wilde bereiken, maar eenvoudig datgene wat je hebt bereikt. Dan is het vanzelfsprekend geworden. Wat je wint verlies je eigenlijk, welbeschouwd. Bovendien, als je ziet wat je hebt moeten aanrichten om het te bereiken, dan vergaat de bevrediging je wel.

Harry Mulisch, De ontdekking van de hemel.

Index

Introduction

This chapter will give a short introduction to micromachining and explain why powder blasting is a useful addition to micro-technology. A general impression of the technique of powder blasting is presented.

1.1 Micromachining

Micromachining is a general term for the fabrication processes for Micro Electro Mechanical Systems (MEMS). These are sensors and actuators with a typical feature size between 1-100 μm (the thickness of a hair is about 70 μm). The advantages of making such small devices are e.g. fast response time, low weight, small volume and the utilisation of micro-scale effects. Examples of commercially successful micro devices are inkjet nozzles, airbag sensors and pressure transducers.

Traditionally, IC technologies were used for the fabrication of MEMS. Most of those techniques are based on photolithography. A light sensitive mask material is applied on top of a substrate, exposed through a mask to UV-light and developed to define the structures. Later, also other micromachining techniques were added like wafer to wafer bonding. Two

main types of techniques can be distinguished: bulk and surface micromachining. Surface micromachining concerns with the deposition and selective removal of thin films (<1 μm) on top of a substrate material. Bulk micromachining concerns etching of the substrate material and is suitable to machine feature sizes larger than 10 μm.

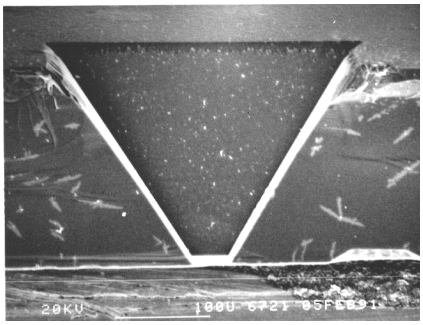

Figure 1.1 Anisotropic etch profile [1].

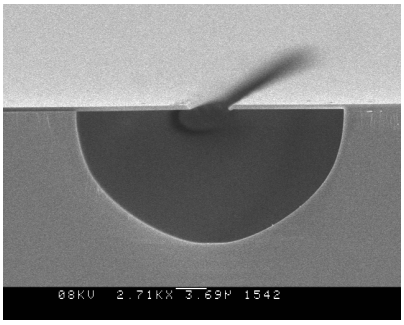

Figure 1.2 Isotropic etch profile [2].

1.2 Glass micromachining

Being an IC technology spin off, micro machining has always concentrated on silicon. Anisotropic KOH etching was an easy method to perform bulk micro machining in silicon creating channels and through holes. The dependence of the etch rate on the crystallographic directions in silicon was useful to accurately machine the substrate (Figure 1.1). Silicon is a semiconductor with a low thermal resistance. For certain applications, these properties are not wanted (see e.g. paragraph 8.3) and glass is used as the substrate material. Glass is a thermal and electrical insulator, optically transparent and chemically inert. Apart from quartz, glass is a homogeneous and amorphous material consisting of various chemical components. Thin oxide layers (SiO_2) are usually etched with wet chemical HF-etching in surface micromachining. This is also commonly used for bulk micromachining of glass wafers, although it has some serious disadvantages. Due to the highly corrosive nature of HF, ordinary mask materials can not be used. Also, this technique is an isotropic process (Figure 1.2) which results in mask underetching and low aspect ratios. Also, small local defects in the mask would allow the HF to penetrate protected areas and create large etch pits.

Alternative glass-machining methods are available but they all have certain disadvantages. Drilling or milling of glass is possible, but the minimum feature size is large (>500 μm [3]). Laser machining results in thermal stresses, material re-deposition on unexposed areas and the

equipment is expensive. Ultrasonic drilling is fast and very suitable for brittle materials [4] but complex designs are more difficult to fabricate. The Reactive Ion Etching of glass results in a very low etch rate (typically less than 1μm/min, e.g. [5]).

1.3 Powder Blasting

Sand blasting is an old technique. It was and is used for a wide variety of purposes like tombstone engraving, paint or corrosion removal, house facades cleaning, surface roughening for better adhesion, device demarking, glass decoration and (live) tooth drilling. Since the Second World War, sand blasting is used to systematically investigate the erosion resistance of materials. This field of research was important for e.g. gas turbines and pipelines and has grown very large. This provides us with a large amount of knowledge on equipment and particle-target interaction. The development of flat panel displays in the nineties caused sand blasting to be developed to an accurate machining method.
Our interest in powder blasting was raised during a cryogenic micro cooler project [6] by a review article on micro coolers where components were abrasively machined in glass using a gelatine mask [7]. Later it was found that Philips Natlab had been developing this sand blasting to a mature glass machining technique. For the production of Zeus displays [8], powder blasting was judged to be the best process to create thousands of holes at once at low cost, high speed and with a high accuracy. Currently, powder blasting is used on a large scale in Japan for the production of flat plasma displays.

1.4 Advantages and disadvantages

The costs of powder blasting equipment are relatively low. Because of the powder particles (contamination) and the large minimum feature sizes (>30μm), the process is carried out outside the clean room, which also reduces the costs. While most micromachining techniques are dedicated to a single material, powder blasting can in principle be used on any type of brittle material such as glass, silicon and ceramics. Metals and elastomers have a high resistance against powder blasting, which allows them to be used as mask materials. The minimum attainable feature size is smaller than 100 μm, which is small enough for general bulk micro machining. Because it is a directional machining technique, aspect ratios are larger than one. The removal rate of approximately 25 μm/min on a 3" wafer with one nozzle is very high and can easily be increased by e.g. using multiple nozzles, higher pressures and higher powder fluxes. Lithographic techniques can be used to define complex designs, which

makes the process similar to standard micromachining techniques. Very attractive is the ability to create through-holes in glass relatively easily.
There are also some disadvantages. Powder blasting creates rough surfaces, which can be an unwanted side effect. It is not suitable to selectively remove material for e.g. surface micromachining since it attacks all brittle materials; it is a truly bulk micromachining technique. Also, the minimum feature size is still much larger compared to other micromachining techniques. Extra safety measures for operators must be taken to prevent inhalation of small sized powders, which can cause a health risk [9].

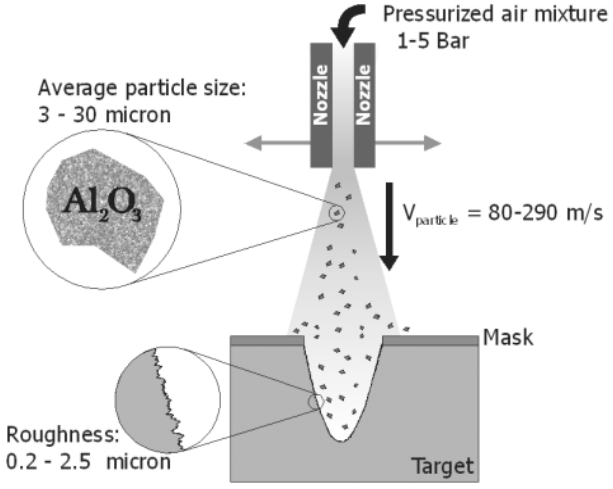

Figure 1.3 A schematic impression of the powder blast process.

1.5 Powder Blasting in practice

Powder blasting is a technology in which a particle jet is directed towards a target for mechanical material removal (Figure 1.3). The particles are accelerated towards the target with a high-pressure airflow through a circular nozzle (with a diameter of 1.5 mm). The particles hit the target with a speed up to 290 m/s (depending on the air pressure and particle size) in a ventilated box. A lateral movement ensures an evenly eroded surface while a mask, which contains the design, covers the target.

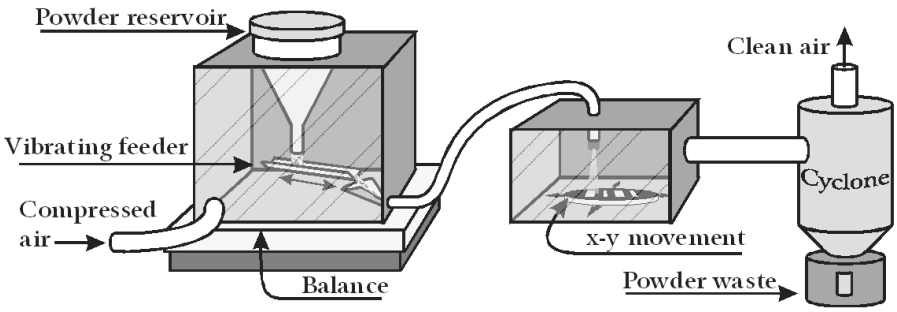

Figure 1.4 A schematic impression of the powder blast equipment.

The powder blasting equipment is build-up form three basic elements (Figure 1.4). The first element consists of a powder feeder (Texas Airsonics HP-2) and a balance (Sartorius QC 34 EDE-S) to record the amount of the powder that is being used. Second, a blasting chamber is used where the substrate or nozzle is scanned in lateral direction (custom made) to achieve an evenly eroded surface. Finally, the blasting chamber is ventilated by a cyclone (Torit VS550) to separate the particles from the airflow.

1.6 Outline of this thesis

Chapter 2 will give general information on particle-target interaction and powder blasting conditions. Most of the information is obtained by other authors from classic erosion experiments.
Powder particle velocity and kinetic energy is an important parameter for powder blasting. Chapter 3 shows how the velocity of small particles in a particle jet can be measured relatively easy.
Mask materials are used to create small and complex structures. Chapter 4 discusses some of these mask types.
The surface roughness created by powder blasting is much higher compared to other micromachining methods. Chapter 5 therefore shows how the roughness is created and how it can be manipulated.
To further decrease the minimum feature size, the average particle size also has to be decreased. However, the removal rate drops sharply if the particles become too small. Chapter 6 gives a detailed description of this transition.
In Chapter 7 the typical channel profiles that are created by powder blasting are discussed. The typical rounded v-shape of the channels gives rise to several limitations, such as the maximum aspect ratio. These

effects can be reduced by changing the particle size or the jet impact angle.
Chapter 8 will discuss most of the devices that were fabricated using powder blasting at the MESA+ research institute, and conclude with some remarks on the current position of powder blasting in micromachining.
Some final remarks on the original goals and outlooks on powder blasting will be made in Chapter 9.
The Appendix reports a case study of ceramic powder blasting.

1.7 References

1 M. Elwenspoek, H.Jansen, "Silicon Micromachining", *Cambridge University Press*, Cambridge, United Kingdom (1998)
2 R.W. Tjerkstra, "Isotropic etching of silicon in fluoride containing solutions as a tools for micromachining", *Ph.D. Thesis, University of Twente*, Enschede, The Netherlands (1999).
3 P. Heller, J. Vervest, H.Wilbrink, "Vademecum voor de glastechniek ", *Kluwer technische boeken B.V.*, Deventer, The Netherlands (1992)
4 T.B.Thoe, D.K. Aspinwall, M.L.H. Wise, "Review on ultrasonic machining ", *Int. J. Mach. Tools Manufact.* 38 (1998) pp. 239-255
5 T. Tsukada, H. Nogami, Y. Nakagawa, E. Wani, K. Mashimo, H. Sato, S. Samukawa, "SiO2 etching using high density plasma sources ", *Thin Solid Films* 341 (1999) pp. 84-90
6 J.Burger, "Cryogenic Microcooling", *Ph.D. Thesis, University of Twente*, Enschede, The Netherlands (2001).
7 W.A. Little, "Microminiature refrigeration", *Rev. Sci. Instrum.* 55 (1984) pp. 661-680
8 H.J. Ligthart, P.J. Slikkerveer, F.H. in't Veld, P.H.W. Swinkels, M.H. Zonneveld, "Glass and glass machining in ZEUS panels", *Philips J. Res.* 50 (1996) pp. 475-499
9 K. Gotoh, H. Masuda and K. Higashitani, "Powder Technology Handbook, second edition revised and expaned", *Marcel Dekker Inc.*, New York, USA (1997)

Literature review

This chapter will give an overview of the many parameters and conditions that can influence the result of powder blasting. Some of the subjects mentioned here will be further discussed and investigated in the following chapters of this thesis.

2.1 Introduction

The literature in this chapter originates mainly from papers on classic erosion experiments (determining the wear rate of materials).
First the effect of a particle impact on a target material is discussed. The result of such an impact will depend on the target material (there are three basic types of materials with respect to particle erosion), and particle properties such as e.g. shape, size and velocity. This knowledge can help us to explain the results obtained from powder blasting.
Second the transport of particles to the target by air jet will be discussed. The air flow, powder mass flux and nozzle height all have an influence on the particle velocity, which is an important parameter and has to be measured accurately.

Finally some aspect of powder blasting as a micromachining technique are discusses. Most of these subjects are explained in more detailed in the following chapters of this thesis.

2.2 Particle-target interaction

2.2.1 Brittle erosion

To predict the erosion of billions of particles impacting on a surface, often a single particle impact on a flat smooth surface is considered. When a brittle material is impacted by a hard sharp particle, the contact area is plastically deformed due to the high compressive and shear stresses. The large tensile stresses that remain after the impact (relaxation) results in lateral cracks causing the material removal (Figure 2.1).

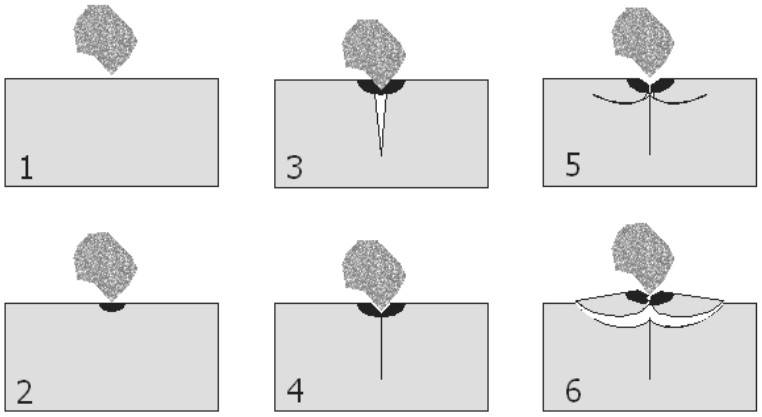

Figure 2.1 The sequence of a single particle impact (after [1]).

Such an impact event is often compared to indentations made with a standard sharp indentor (e.g. Vickers). There is no exact analytical solution to the stress state of a sharp indentation (in contrast to round indentations [1]). Over the years, several models have been published on this subject trying to relate the erosion rate to material properties [2, 3, 4]. Traditionally the erosion rate was defined by the weight of removed target divided by the weight of used powder. Nowadays, often the amount of target removed by a single particle impact is predicted or measured.

Marshall et al. empirically found a relation between indentation pressure and lateral crack length for a broad range of brittle materials [5]. Slikkerveer [6] used indentation theories to construct an analytical model based on that relation:

$$E_p = 0.0745 \frac{\rho_t E^{5/4} U_{kin}}{H^{17/12}} \left(\frac{U_{kin}^{1/6}}{K_{Ic}} - 5.34 \frac{E^{1/4}}{H^{13/12}} \right), \qquad \textbf{Eq. 2-1}$$

with E_p the brittle erosion of a single particle in grams, ρ_t the target density E the target Young's modulus, U_{kin} the particle kinetic energy, H the target hardness, and K_{Ic} the target fracture toughness. The erosion data of alumina particles on glass fitted rather well to this model. More importantly, it showed that the erosion only depends on the kinetic energy of a single particle. A recent and extensive experimental work on erosion is by Feng and Ball [7] where relations were derived for several combinations of target and powder materials.

Ceramics

In general, the lateral crack mechanism is responsible for the erosion behaviour of homogeneous brittle materials. In the case of polycrystalline ceramics the microstructure (pore size and grain size) also influences the erosion rate [8, 9]. When the ceramic consists of grains that are much smaller compared to the powder particle size, the main mechanism of material removal is the ejection of grain clusters. The particle kinetic energy is entirely used for grain boundary cracking [2, 10].

2.2.2 Impact angle dependence

When the impact angle of the particle is decreased, the change in erosion rate is very characteristic and dependent on the target material. Two main characteristics are often described in the literature: brittle and ductile erosion (Figure 2.2).

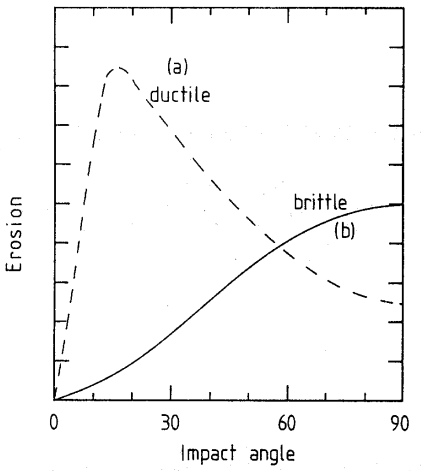

Figure 2.2 Typical ductile and brittle angle dependent erosion rate [11, 12]. Perpendicular erosion is at 90°.

Brittle erosion deals with material removal due to crack formation while ductile erosion deals with material removal due to cutting and ploughing (see next section). The difference is reflected by the impact angle dependent erosion rate. Maximum erosion for brittle materials (like glass, silicon and ceramics) is at 90° impact angle, while for ductile materials (like metals) the maximum erosion is around 20°-30° impact angle (Figure 2.2). The impact angle dependent erosion rate for brittle erosion can as an approximation be described by:

$$E \propto \sin(\alpha)^k \ , \qquad \textbf{Eq. 2-2}$$

with α the impact angle and k an exponent typically between 2 and 3. However for small angles (≤ 30°) the tangential velocity also plays a role in enhancing the lateral crack formation in the velocity direction and the erosion rate becomes larger than described by Eq. 2-2. [13].

Ductile brittle transition

It was already shown in 1966 [11] that the impact angle dependant erosion rate of glass changes from brittle to ductile for very small particles [12, 14, 15] (Figure 2.3). These particles do not have enough energy to initiate a crack, so the target is only plastically deformed. Wear maps have been developed to show the dependence of this threshold on particle size and velocity [15]. Later only the particle kinetic energy was used to calculate the threshold [6]. The ductile-brittle transition is shown in detail for Pyrex, silicon and sodalime glass in Chapter 6.

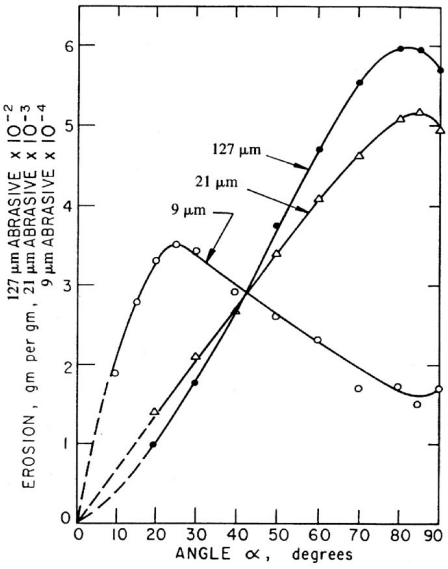

Figure 2.3 Erosion transition due to a decrease in particle size [11].

2.2.3 Ductile erosion

The ductile erosion mechanism (e.g. in the case of metal erosion) is controlled by plastic deformation. The impact angle dependent erosion rate is shown in Figure 2.4.

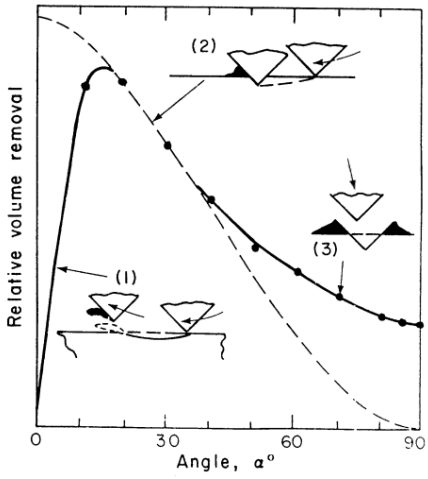

Figure 2.4 Impact angle dependent erosion rate for ductile materials [12].

At low angles, the particles graze over the surface (ploughing) and at higher angles the particle comes to rest in the surface while cutting [16, 17, 18]. The displaced material can subsequently easily be removed by other particles. Erosion at 90° impact can not be explained in this way. In reality, not all particles will impact at exactly 90° and also the rough surface results in different impact angles.
The impact angle at which maximum erosion occurs is related to the material hardness for pure metals or alloys [19]. The erosion rate of pure metals can also be related to the hardness for grazing angles [12, 20, 21] as well as for perpendicular impact [19].
The erosion rate (measured in [g/g]) does not change with particle size above a certain size threshold (<100μm) [12, 22, 23]. This particle threshold changes with impact velocity (Figure 2.5).

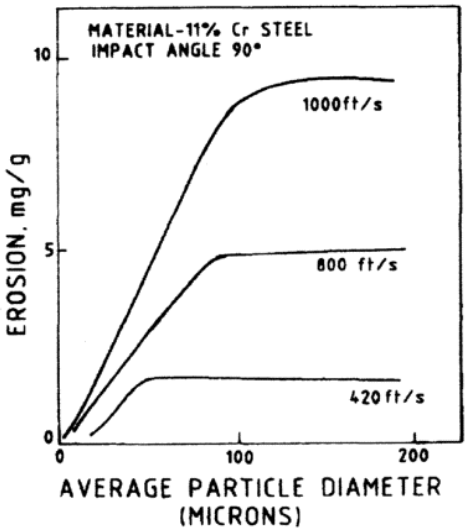

Figure 2.5 Particle threshold in the case of metal erosion at different velocities [24].

Similar to brittle erosion, the velocity dependence of the erosion rate for metals is characterised by a velocity exponent:

$$E \propto v^k, \qquad \textbf{Eq. 2-3}$$

with k between 2 and 3 [12, 24, 16]. This exponent is said to be independent [19] or dependent [17] on the impact angle. At low impact angles, ripples are formed on the surface that is a result of the tangential component of the velocity [25]. When a metal is eroded, often an initial increase in weight is observed, before the steady state erosion is obtained.

This weight increase can be explained by particles that embed in the target on impact [16].

2.2.4 Elastomer erosion

The erosion of elastomers (rubbers) is controlled by fatigue crack growth and erosive wear. This is caused by tensile stresses due to frictional traction's rather than bulk deformation of the elastomer [26, 27]. It results in a lower erosion rate at 90° impacts than at glancing impacts. The angle dependent erosion rate looks similar to that of ductile materials, although the erosion mechanisms at work are rather different. Often, there is a start-up effect in the erosion rate. First the target mass is increasing due to embedding of particles into the material. After a while this process is in equilibrium and the steady state erosion is reached. The dependence on velocity can be much higher compared to ductile or brittle materials [26]. The influence of elastomer material properties on erosion is not yet well described in the literature, probably due to the large variety of elastomer materials. A good recent literature review was made by Slikkerveer et al. [28].

2.2.5 Particle properties

Degradation

When a particle impacts on target, also the particle can fracture. This especially occurs when the particle hardness is equal to or lower than the target hardness (e.g. when blasting ceramic materials, see Appendix) and it results in a much lower erosion rate [29, 30]. Less severe degradation of particles can also lead to more rounded particles, reducing the erosion rate [31]. The amount of particle fracture also depends strongly on the impact velocity [15, 32]. Experiments with alumina particles on glass targets showed that the particles break on impact due to pre-existing flaws. So as the particles become smaller during erosion, they also become stronger since the biggest flaw is removed on first impact [32].

Size

The most important effect of the particle size on erosion properties is its influence on the kinetic energy. However, other effects have been suggested such as a difference in localised heating [33] or a difference in strain rate [34]. A wide particle size distribution will enhance the erosion rate [35].

Round particles

All particles referred to in this thesis are sharp (Figure 2.6), unless mentioned otherwise. In the case of round particles, a different crack mechanism plays a role in erosion [36]. The contact on impact is elastic and the stress distribution can be calculated using Hertz's theory [37]. Cracking now only occurs when a flaw is already present in the stressed area, whereas sharp particles create their own flaw (see Chapter 6). This plays a role in e.g. the erosion transitions [31].

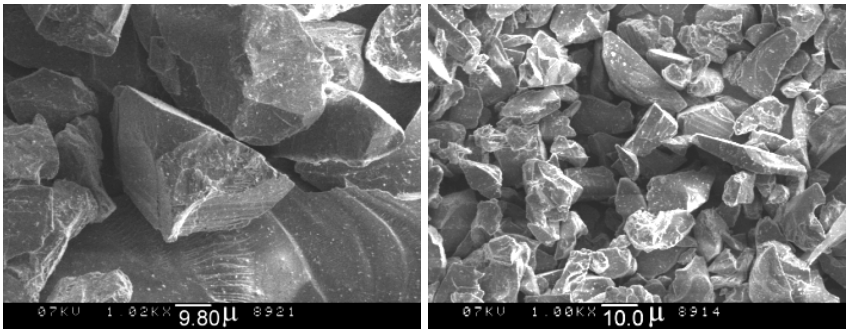

Figure 2.6 Sharp Alumina particles, average size 29.2 µm (left) and 9 µm (right).

2.3 Blast Conditions

2.3.1 Air jet flow [38]

Powder particles are accelerated by inserting them in a high velocity air jet. This air jet is produced by applying a pressure difference over a nozzle. The applied pressure differences are often larger than 1.9 bar. In that case a cylindrical nozzle is choked, which means that the air velocity at the nozzle exit is equal to the velocity of sound. (Note however that in case of a Laval-nozzle (a converging-diverging nozzle) the air velocity can increase to supersonic values.) The sound velocity at the exit of a choked cylindrical nozzle (which is now equal to the air exit-velocity) can be calculated from:

$$c \propto \sqrt{k \frac{p_e}{\rho}}, \qquad \textbf{Eq. 2-4}$$

where c is the velocity of sound, k the specific heat ratio (k = 1.4 for ideal gasses), p_e the air pressure at the nozzle exit, ρ the air density. When the

nozzle is just choked, the pressure at the nozzle exit is equal to the atmospheric pressure so the corresponding sound velocity is about 330 m/s.
When the pressure difference is increased to values above 1.9 bar, the nozzle exit pressure will also increase and become larger than atmospheric pressure The pressure at the nozzle exit can than be calculated with (for k = 1.4 and choked flow):

$$\frac{p_e}{p_r} \approx 0.5283, \qquad \textbf{Eq. 2-5}$$

with p_r the pressure in the powder reservoir.
This pressure increase also changes the local air density, because for isentropic compressible flow:

$$\frac{p_e}{\rho^k} = C_1, \qquad \textbf{Eq. 2-6}$$

with C_1 a constant, which has a value of about $69.8 \cdot 10^3$. Using Eq. 2-4 and Eq. 2-6 the sound velocity (air velocity) in a choked cylindrical nozzle exit can be calculated:

$$c = \sqrt{k C_1^{\,1/k} p_e^{\,(1-1/k)}}\,. \qquad \textbf{Eq. 2-7}$$

Using Eq. 2-5 and Eq. 2-7 it can be calculated that a reservoir pressure of $5 \cdot 10^5$ Pa results in an approximate air velocity at the nozzle exit of 378 m/s. In reality, the air jet is mixed with powder particles, which has an influence on the air jet that is very difficult to calculate. It is suggested that the exit pressure in that case becomes higher [39].

2.3.2 Gas-particle flow

When particles that are accelerated by the air jet leave the nozzle, they often have a velocity that is still lower compared to the air velocity. This means that the particles are still accelerated outside the nozzle. So the maximum particle velocity can sometimes be obtained up to a distance from the nozzle of 10 times the nozzle diameter (Figure 2.7). This is also clearly seen in the erosion rate which first increases and then decreases with increasing nozzle–target distance [39]. This effect is large when the velocity difference between particle and air jet is large, which is the case for large particles (higher mass), high air velocities and high particle fluxes (lower average velocity).

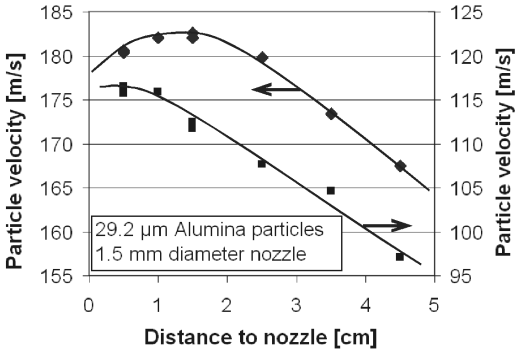

Figure 2.7 Particle velocity versus nozzle distance. Same measurement method as Figure 3.9 page 44. Mass flux is 1.4 g/min, pressure is $2.3 \cdot 10^5$ Pa (left axis) and $1.0 \cdot 10^5$ Pa (right axis).

When the air jet is projected onto a flat target, the air speed becomes zero only very close to the surface. Large and heavy particles are likely to continue their path undisturbed. Aerodynamic effects can have a large influence on the trajectory of small (<10μm) particles [40]. The air streamlines that flow around the target will interact with these particles and it can alter the impact angle and location.
Equations have been given to calculate the particle speed from the air speed [41]. Experiments show that the particle velocity v is proportional to:

$$v \propto d^{-0.285} p^{0.5}, \qquad \text{Eq. 2-8}$$

with d the particle diameter and p the air feed pressure [42] (measured for pressure up to $0.7 \cdot 10^5$ Pa, particle sizes between 70-1000 μm and cylindrical nozzle. Also see Figure 3.12 page 48.). For nozzle aspect ratios between about 30 and 130 the particle velocity is hardly effected by the nozzle length [43].

2.3.3 Particle flux properties

A higher particle flux will increase the total erosion rate. However, flux effects will at some point decrease the average erosion of a single particle [8, 44, 45]. Due to the high particle density in the jet, slow particles that rebound from the target are likely to collide with fast incoming particles. The particle-particle collisions increase the amount of particle impacts on the surface, but reduce the impact energy and change the impact angle, thereby lowering the average erosion rate. This shielding effect decreases for higher velocities because the slow rebounded particles are removed more quickly from the impact zone due to a higher air velocity [46].

Another effect of high particle fluxes is the decrease in particle velocity at a constant pressure (Figure 2.8). This is because the momentum of the air jet has to be distributed over all particles, which is also reflected in a decrease of erosion rate [39].

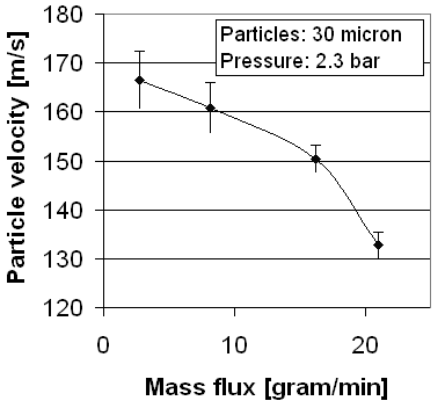

Figure 2.8 Particle velocity is decreased with flux increase. Same measurements method as in Figure 2.7

So although a higher particle flux generally decreases the total process time, it also has to be considered that the powder quantity required to remove a certain amount of target is much larger.

2.3.4 Powder supply

Powder feeding systems are used to ensure an even supply of powder to the air jet. Any discontinuity in the feeding will reflect on the erosion uniformity. Often the powder is supplied by a vibrating feeder, which is an accurate method [47]. Any water vapour in the system can coagulate the particles, so the air is dehumidified and the powder is heated up to 120°C to enhance the reliability of powder feeding [39, 50]. Next, there are two main ways to insert the powder in the high-pressure air stream:

Suction supply [48,49]

The air jet is accelerated by a narrow passage in the tube or nozzle, which creates an underpressure. Particles are supplied by an exterior tube and sucked into the nozzle (Venturi effect, Figure 2.9). The system allows an easy refill during blasting or change of powder size. It can be limited in particle velocity since the maximum air velocity is attained inside the nozzle, and not at the exit. However, the air velocity can also increase

after the narrow passage when using a carefully designed converging-diverging nozzle (Laval-type).

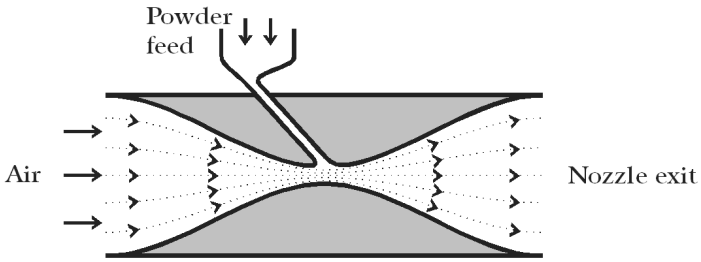

Figure 2.9 Supplying powder by using the venturi effect.

Closed system supply [39, 54, 50]

This system is also used at the MESA$^+$ institute. The powder is transported in a closed pressure system to the exit by a vibrating hopping movement. Powder refill requires decompression and powder changing requires a total cleaning of the system. However, with this closed system it is easy to obtain high particle velocities.

2.3.5 Nozzle

In our set-up, a cylindrical nozzle is mainly responsible for the acceleration of the particles. There can be a large variation in nozzle size and aspect ratio, but the inside diameter (1.5 mm in our case) is of course smaller compared to the connection tubes. The nozzle also suffers from particle impacts even though it is usually made of a hard ceramic material. This erosion makes the inner nozzle geometry divergent because the particle velocity is larger towards the nozzle exit [50]. It leads to a reduction of the particle velocity, and hence the erosion rate.

Nozzle roughness / halo effect

Even with straight nozzles, particles do not leave the nozzle parallel to the nozzle axis [51]. A turbulent air plume itself has a divergence [52], which is reflected in the particle jet. In addition to this, interaction of the particles with the inside nozzle wall can cause particles to leave the core of the jet and impact outside the main impact site (this is called the halo effect [51]). Especially if the nozzle wall roughness is large, the rebounding angle of the impacting particle on the nozzle wall will be larger. This also reduces the average particle velocity [48].

Flat Nozzle

Powder blasting with a cylindrical nozzle is like milling the target with a pointed chisel. Scanning the target results in a series of lines placed closely next to each other. Together they must form a uniformly eroded surface. To increase this uniformity, a new flat nozzle type has been introduced for powder blasting. This letterbox shaped nozzle exit distributes the particles over a wider area. Together with the scanning motion it results in overlapping eroded rectangulars, which makes it easier to achieve a uniform eroded surface. Since the core of the particle jet is still small in one direction, flux effect is smaller and the mass flux can be increased more without reducing the erosion rate [53]. The larger nozzle opening does require a higher pressurised air flow and a larger scanning motion to get the nozzle out of the working area after one completed scan.

2.3.6 Velocity measurements

Particle velocity is an important parameter in powder blasting. Although the velocity can be estimated using the air feed pressure, the exact value depends on machine set-up and can best be measured regularly. Several velocity measurement methods have been presented.

High speed photography

The shift of particles on two photographs, which are taken at a timed interval, indicates the particle speed. Also the length of a particle streak on a single photograph combined with the shutter time can provide that information. It works well with large particles, but can be time-consuming.

Double rotating disks [6, 15, 42, 54, 55, 56, 57]

In the double disk method, two disks are rotated at a high speed (Figure 2.10). The first disk contains a slit, which serves as a shutter for the particles. The place where the particles hit the second disk and a mark is created indicates the particle time of flight. Together with the distance between the disks, the velocity can be calculated. This is a cheap method of measurement. However, it is an offline and time-consuming method and has the disadvantage of creating some disturbance in the air flow pattern which introduces a systematic error which is significant for particles smaller than 100 μm. The method measures typically with an error of 10%.

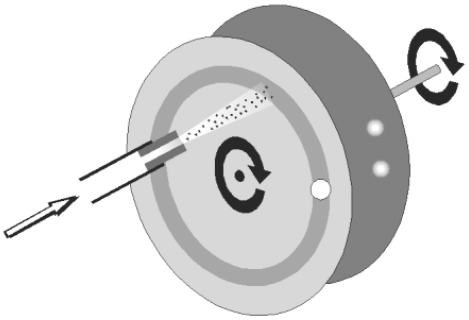

Figure 2.10 Double Disk method for velocity measurement

Optic gates [42, 48, 58]

The optic gate consists of two light emitters and receivers situated at a fixed distance from each other at the end of the nozzle. One particle consecutive passes the first and second receiver. The elapsed time between these events is measured and the velocity can be calculated. The minimum particle size that can be detected is approximately 70μm, at a low particle flux (about 40-60 particles per second).

Laser Doppler Anemometry (LDA) [6, 56, 57, 59]

In LDA, two laser beams cross each other creating interference fringes. Powder particles that cross this area reflect the pattern to an optical receiver. The frequency of the optical pulses that are received is a measure for the particle velocity. LDA is superior because it can measure the velocity of individual particles in large particle fluxes. It is an online measurement of the velocity distribution. Unfortunately, the initial equipment costs are very high.

We developed a "cross correlation method" to measure the particle velocity, which has lower initial equipment costs (described in Chapter 3). This CC-method correlates the light scattered from powder particles that are directed through two parallel laser beams. It is an accurate method, and it can be used on small (9-29μm) particles at high (up to 20 g/min) mass fluxes.

2.4 Powder blasting in micromachining

2.4.1 Mask materials

The particle jet diameter is equal to or larger than the nozzle diameter (>1mm). Therefore, mask materials are used to allow machining small feature sizes (<100 μm). Ductile materials (e.g. metals) and elastomers [28] require multiple particle impacts to remove a piece of material. This generally results in a lower erosion rate compared to brittle materials with a selectivity of about 20 to 80 (depending on process parameters). This makes them suitable to be used as a mask material.
From the industry of decorative arts, some (liquid) elastic mask materials are currently available. Due to the development of flat panel displays, for which powder blasting is an important fabrication step, the commercially powder blasting mask material BF400 was available from Japan. Fabricated by Tokyo Ohka Kogyo it comes in "Ordyl BF410" (100 μm thickness) and "Ordyl BF405" (50 μm thickness) [28, 60]. Although the erosion of this mask material is not optimal (three times faster compared to copper), it is user friendly and can be used for small feature sizes (>50μm). Also, the handling of this mask was easy and comparable to standard micromachining lithography. Other elastomeric coatings with a higher erosion resistance are also proposed for powder blasting [28]. Even a simple Scotch tape [61] or a gelatine layer [62] can be used. New candidates for mask materials should also be tested at oblique angles [28] because mask edges, were the mask is impacted at lower angles, are the first to erode during blasting.

Metals are normally used as a powder blasting mask material by means of a metal plate [63, 64]. By drilling, milling, etching or laser machining a pattern is created in a plate. The mask can simply be clamped mechanically or magnetically to the target. However, this will allow the particles to get between the mask and the target and damage the target. To prevent this, an intermediate protection/adhesion layer can be applied [63]. A metal plate mask has the advantages of a long durability (low erosion rate and large thickness) and its applicability on any kind of material. However, the disadvantages are the limitations in feature size (>50 μm [64]) and pattern constraints (ring patterns cannot be used because the inside should be` supported). Also, a thick metal mask will influence the particle stream, especially with small features. When the metal mask is very thin, the large stresses caused by the particle impacts will cause the mask to buckle if not attached properly to the target.

In order to combine the low erosion rate of a metal, and the high resolution and flexibility of a lithographic process, we introduced electroplated copper as a mask material. It has a very high resistance against powder blasting and the mask thickness can be tuned as desired. More details on the use of these masks are given in Chapter 4.

2.4.2 Side wall inclination

A problem is revealed when a part of the target is shielded from the particle jet: sidewall inclination. A powder blasted channel has slant sidewalls (Figure 2.11). The typical shapes that are created have been successfully modelled by Slikkerveer et al. [65]. This effect is responsible for a decrease in erosion rate as the channel depth increases. So it restricts the aspect ratio and results in the blast lag (wide channels become deeper compared to small channels). More details and discussions on this subject in Chapter 7.

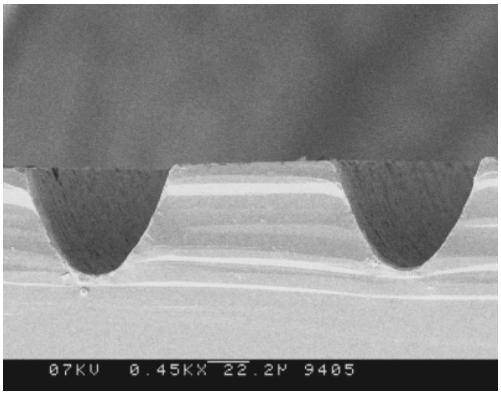

Figure 2.11 Sidewall inclination in patterned powder blasting [66].

2.4.3 Choosing particle size

A smaller feature size requires the use of smaller particle sizes. A general rule of thumb is a particle size of at most 1/3 of the minimum feature size [63]. But often a smaller particle size is chosen to get a lower roughness and smaller edge chipping of the channels. Smaller particles can also increase the aspect ratio and reduce the blast lag (see Chapter 7).

There are however several reasons why the average particle size should not be too small. First, as the particles get smaller, the erosion of a single particle impact can decrease sharply as we get closer to the ductile-brittle transition (Table 2-1, see also Chapter 6). This not only increases the

process time, but also negatively influences the selectivity with the mask. Second, small particles are more difficult to handle. Their low weight makes them more susceptible to sticking due to e.g. Van der Waals forces and humidity. This makes a smooth powder feed more difficult. Last but not least, as the particles become smaller than 10 μm, it is more dangerous for operators to accidentally inhale them [67], which has safety implications.

Table 2-1 Calculated approximate removal rates at standard blast conditions (Pyrex target, 7x7 cm blasting area, sharp alumina particles, air pressure 4.5 bar and powder flux 10 g/min).

Particle size [μm]	Speed [m/s]	Powder rate [g/cm^2·μm]	Removal rate [μm/min]
3	360	0.155	1.3
5	325	0.0315	6.5
9.0	290	0.0151	13.5
17.1	252	0.0106	19.3
29.2	220	0.00837	24.6

The decrease in erosion rate of small particles can be overcome if we could increase the kinetic energy of the small particles by accelerated them to a higher velocity. Unfortunately, our set-up does not allow a large increase in particle velocity so that the kinetic energy of a particle is mainly determined by its mass. For example, to get the same kinetic energy of a 29 μm particle with a speed of 220 m/s, a 9 μm particle would need to travel with 1275 m/s.
So the choice of particle size will determine the minimum feature size, the process time and the accuracy of the pattern transfer.

2.4.4 Surface roughness

Powder Blasting results in rough surfaces with an R_a typically up to 2.5 μm. The kinetic energy of powder particles determines the size of the lateral cracks on impact that are mainly responsible for the roughness. If the kinetic energy of the particles is low enough to prevent lateral cracks, the surface roughness is diminished. Unfortunately, in that case powder blasting does not anymore have the important advantages like a high removal rate and selectivity. The lateral crack size and hence the roughness can be predicted by erosion models [6]. Other micromachining methods (like RIE or HF etching) generally have a much lower roughness, so the effects on device performance have yet to be studied. It is clear that glass looses its optical quality after blasting, and that the roughness creates a higher contact area. In the case of micro fluidic

devices, preliminary studies show that the dispersion is higher [68] and the electroosmotic flow is opposite to normal channels [69]. The surface roughness of glass can be changed after powder blasting to a higher or lower value, these methods are described in Chapter 5.

2.5 References

1 B.Lawn, "Fracture of Brittle Solids – Second Edition", *Cambridge University press*, Cambridge, United Kingdom (1993)

2 J.E. Ritter (Ed.), "Erosion of Ceramic Materials", *Trans Tech Publications*, Zurich, Switzerland (1992)

3 M. Buijs, "Erosion of glass as modeled by indentation theory", *J. Am. Ceram. Soc.* 77 (1994) pp. 1676-1678

4 H.C. Meng, K.C. Ludema, "Wear models and predictive equations - Their form and content", *Wear* 181 (1995) pp. 443-457

5 D.B. Marshall, B.R.Lawn, A.G.Evans, "Elastic/Plastic Damage in Ceramics: The Lateral Crack System ", *J. Am. Ceram. Soc.* 65 (1982) pp. 561-566

6 P.J. Slikkerveer, P.C.P. Bouten, F.H. in't Veld, H. Scholten, "Erosion and damage by sharp particles", *Wear* 217 (1998) pp. 237-250

7 Z. Feng, A. Ball, "The erosion of four materials using seven erodents — towards an understanding", *Wear* 233-235 (1999) pp. 674-684

8 D.F. Wang, J.H. She, Z.Y. Ma, "Effect of microstructure on erosive wear behavior of SiC ceramics", *Wear* 180 (1995) pp. 35-41

9 J. Zhou, S. Bahadur, "The effect on material composition and operational variables on the erosion of alumina ceramics ", *Wear* 150 (1991) pp. 343-354

10 J.E. Ritter, L. Rosenfeld, K. Jakus, "Erosion and strength degradation in alumina", *Wear* 111 (1986) pp. 335-346

11 G.L.Sheldon, I.Finnie, "On the ductile behaviour of nominally brittle materials during erosive cutting ", *Trans. ASME* 88B (1966) pp. 387-392.

12 I. Finnie, "Some reflections on the past and future of erosion", *Wear* 186-187 (1995) pp. 1-10

13 Y. Ballout, J.A. Mathis, J.E. Talia, "Solid particle erosion mechanism in glass", *Wear* 196 (1996) pp. 263-269

14 M. Buijs, J.M.M. Pasmans, "Erosion of glass by alumina particles: transitions and exponents ", *Wear* 184 (1995) pp.61-65

15 I.M. Hutchings, "Ductile-brittle transitions and wear maps for the erosion and abrasion of brittle materials", *J. Phys. D.: Appl. Phys.* 25 (1992) pp. A212-A221

16 P. Shewmon, G. Sundararajan, "The Erosion of Metals ", *Annu. Rev. Mater. Sci.* 13 (1983) pp. 301
17 I.M. Hutchings, "Mechanisms of wear in powder technology: a review ", *Powder Technol.* 76 (1993) pp. 3-13
18 J.E. Field, I.M. Hutchings, "Impact erosion processes", *Inst. Phys. Conf.* 70 (1984) pp. 349-371, presented at *3rd Conf. Mech. Prop. High Rates of Strain*, Oxford, United Kingdum (1984)
19 Y.I. Oka, H. Ohnogi, T. Hosokawa, M. Matsumura, "The impact angle dependence of erosion damage caused by solid particle impact ", *Wear* 203 (1997) pp. 573-579
20 Y.I. Oka, M. Matsumura, T. Kawabata, "Relationship between surface hardness and erosion damage caused by solid particle impact ", *Wear* 162-168 (1993) pp. 688-695
21 G. Sundararajan, "The differential effect of the hardness of metallic materials on their erosion and abrasion resistance ", *Wear* 162-164 (1993) pp. 773-781
22 P.G. Shewmon, "Particle size threshold in the erosion of metals ", *Wear* 68 (1981) pp. 253-258
23 J. Zhou, S. Bahadur, "Effect of blending of silicon carbide particles in verying sizes on the erosion of Ti-6Al-4V ", *Wear* 132 (1989) pp. 235-246
24 G. Sundararajan, M. Roy, "Solid particle erosion behaviour of metallic materials at room and elevated temperatures,", *Tribology International* 30 (1997) pp. 339-359
25 Y.A. Ballout, J.A. Mathis, J.E. Talia, "Effect of particle tangential velocity on erosion ripple formation ", *Wear* 184 (1995) pp. 17-21
26 J.C. Arnold, I.M. Hutchings, "The mechanisms of erosion of unfilled elastomers by solid particle impact ", *Wear* 138 (1990) pp. 33-46
27 J.C. Arnold, I.M. Hutchings, "Erosive wear of rubber by solid particles at normal incidence ", *Wear* 161 (1993) pp. 213-221
28 P.J. Slikkerveer, M.H.A. van Dongen , F.J. Touwslager, "Erosion of elastomeric protective coatings", *Wear* 236 (1999) pp. 189–198
29 A.J. Sparks, I.M. Hutchings, "Effects of erodent recycling in solid particle erosion testing", *Wear* 162-164 (1993) pp. 139-147
30 P.H. Shipway, I.M. Hutchings, "The role of particle properties in the erosion of brittle materials ", *Wear* 193 (1996) pp. 105-113
31 A.J. Sparks, I.M. Hutchings, "Transitions in the erosive wear behaviour of a glass ceramic", *Wear* 149 (1991) pp. 99-110
32 P.J. Slikkerveer, H. in't Veld, M. Verspui, B. de With, D. Reefman, "Alumina Particle Degradation during Solid Particle Impact on Glass", *J. Am. Ceram. Soc.* 83 (2000) pp. 2263–2266
33 C.T. Morrison, J.L. Routbort, R.O. Scattergood, "Solid particle erosion of mullite ", *Wear* 105 (1985) pp. 19-27

34 I.M. Hutchings, "Strain rate effects in microparticle impact ", *J. Phys. D: Appl. Phys.* 10 (1977) pp. L179-L184
35 D.B. Marshall, A.G. Evans, M.E. Gulden, J.L. Routbort, R.O. Scattergood, "Particle size distribution effects on the solid particle erosion of brittle materials", *Wear* 71 (1981) pp. 363-373
36 P.J. Slikkerveer, M. Verspui, E. Skerka, "Erosion and damage by hard spherical particles on glass", *J. Am. Ceram. Soc.*, 82 (1999) pp. 3173-3178
37 S.P. Timoshenko, J.N. Goodier, "Theory of elasticity, Int. 3rd edn.", *McGraw-Hill Int. Engineering Mechanics Series*, London, United Kingdom (1970)
38 R.W. Fox, A.T. McDonald, "Introduction to fluid mechanics (third edition)", *John Wiley & Sons*, New York, USA (1985).
39 A.P. Verma, G.K. Lal, "An experimental study of abrasive jet machining ", *Int. J. Mach. Tool Des. Res.* 24 (1984) pp. 19-24
40 J.E. Fackrell, "Aerodynamic effects on PFBC erosion target experiments", *Wear* 134 (1989) pp. 237-252
41 P. Chevallier, A.B. Vannes, "Effects on a sheet surface of an erosive particle jet upon impact", *Wear* 184 (1995) pp. 87-91
42 A.N.J. Stevenson, I.M. Hutchings, "Scaling laws for particle velocity in the gas-blast erosion test", *Wear* 181-183 (1995) pp. 56-62
43 A.N.J. Stevenson, I.M. Hutchings, "The influence of nozzle length on the divergence of the erodent particle stream in a gas-blast erosion rig", *Wear* 189 (1995) pp. 66-69
44 K. Anand, S.K. Hovis, H. Conrad, R.O. Scattergood, "Flux effects in solid particle erosion", *Wear* 118 (1987) pp. 243-257
45 D.R. Andrews, N. Horsfield, "Particle collision in the vicinity of an eroding surface", *J. Phys. D: Appl. Phys.* 16 (1983) pp. 525-538
46 F.H. in't Veld, P.J. Slikkerveer, "Towards prediction of flux effects in powder blasting nozzles", *Wear* 215 (1998) pp. 131-136
47 P.J. Slikkerveer, P.C.P. Bouten, F.C.M. de Haas, "High Quality Mechanical Etching of Brittle Materials by Powder Blasting", *Sensors and Actuators* 85 (2000) pp. 296-303
48 P.H. Shipway, I.M. Hutchings, "Influence of nozzle roughness on conditions in a gas-blast erosion rig", *Wear* 162-164 (1993) pp. 148-158
49 R.H. Telling, J.E. Field "The erosion of diamond, sapphire and zinc sulphide by quartz particles", *Wear* pp. 233-235 (1999) pp. 666-673
50 R. Kumar, A.P. Verma, K. Lal, "Nozzle wear during the flow of a gas-particle mixture", *Wear* 91 (1983) pp. 33-43

51 P.H. Shipway, "The effect of plume divergence on the spatial distribution and magnitude of wear in gas-blast erosion test", *Wear* 205 (1997) pp. 169-177
52 H. Tennekes, J.L. Lumley, "A first course in Turbulence, P 4.4 "Turbulent jets", *MIT press,* Cambridge, United Kingdom (1972)
53 J.O. Steinz, "Design of a flat jet venturi nozzle for abrasive air jet machining", *M.Sc. Thesis, Delft University of Technology*, Delft, The Netherlands (2001).
54 A.W. Ruff, "Analysis of interlaboratory test results of solid particle impingement erosion", *Wear* 108 (1986) pp. 323-335
55 A.V. Levy, "The solid particle erosion behavior of steel as a function of microstructure", *Wear* 68 (1981) pp. 269-287
56 V. Ponnaganti, D.E. Stock, G.L.Sheldon, "Measurement of Particle Velocities in Erosion Processes", *Proc. Symp. Polyphase Flow and Transport Technology*, San Francisco, USA (1980) pp. 217-222
57 J.K. Patterson, A.V. Levy, "Methods for characterisation for erosion by gas-entrained solid particles", *Wear* 91 (1983) pp. 333-347
58 P.H. Shipway, I.M. Hutchings, "A method for optimizing the particle flux in erosion testing with a gas-blast apparatus", *Wear* 174 (1994) pp. 169-175
59 B. Lindsley, K. Stein, A.R. Marder, "The design of a high-temperature erosion apparatus for studying solid particle impact", *Meas. Sci. Technol.* 6 (1995) pp. 1169-1174
60 H. Fujii, H. Tanabe, H. Ishiga, M. Harayama, M. Oka, "A sandblasting process for fabrication of color PDP phosphor screens", *SID 92 digest* (1992) pp.728-731
61 A. Kruusing, S. Leppävuori, A. Uusimäki, M. Uusimäki, "Rapid prototyping of silicon structures by aid of laser and abrasive-jet machining", *SPIE proceedings 3680: Design, Test, and microfabrication of MEMS and MOEMS*, Paris, France (1999) pp. 870-878
62 W.A. Little, "Microminiature refrigeration", *Rev. Sci. Instrum.* 55 (1984) pp. 661-680
63 H.J. Ligthart, P.J. Slikkerveer, F.H. in't Veld, P.H.W. Swinkels, M.H. Zonneveld, "Glass and glass machining in ZEUS panels", *Philips J. Res.* 50 (1996) pp. 475-499
64 E. Belloy, S. Thurre, E. Walckiers, A. Sayah, M.A.M Gijs, "The introduction of powder blasting for sensor and microsystem applications", *Sensors and Actuators* 84 (2000) pp. 330-337
65 P.J. Slikkerveer, F.H. in't Veld, "Model for patterned erosion", *Wear* 233-235 (1999) pp. 377–386
66 T.T. Veenstra, F. Lim, unpublished work

67 K. Gotoh, H. Masuda and K. Higashitani, "Powder Technology Handbook, second edition revised and expaned", *Marcel Dekker Inc.*, New York, USA (1997)
68 M.T. Blom, E.F. Hasselbrink, H. Wensink, A. van den Berg, unpublished work
69 D. Solignac, A. Sayah, S. Constantin, R. Freitag, M.A.M. Gijs, "Powder blasting for the realisation of microchips for bio-analytic applications", *Sensors and Actuators A* 92 (2001) pp. 388-393

Velocity Measurements

This chapter will introduce a velocity measurement method for small particles in an air jet, which uses cross-correlation techniques. Since the particle velocity is an important process parameter, an accurate velocity measurement is essential. The method is compared to the classical double disk system, which is inaccurate for small particles.

3.1 Introduction

Erosive particle jets are widely used for erosion experiments and also for powder blasting (Abrasive Jet Machining) as a technique to machine microstructures [1][2]. Recently, the minimum feature size for powder blasted structures was decreased to about 30 μm [3]. For this, small particles (<30 μm) have to be used. The particle kinetic energy is a very important process parameter in powder blasting; therefore the particle velocity has to be accurately measured.

Several methods are available to measure particle velocity in an air jet. A well-known and simple method is the Double Disk system.

Measurements on small (<100 μm) particles with this DD-method are inaccurate, as shown in this chapter and by others. Other methods include several Particle Image Velocimetry techniques, cross-correlation methods like "Optic Gates" [4] and "laboratory correlator" [5], and the very capable, but expensive, Laser Doppler Anemometry [6] [7].
In this chapter we first improve the DD-method to attain more accurate results with small particles. This offline method however remains inaccurate and laborious. Therefore an improved cross-correlation method is also presented here. This CC-method requires a rather simple set-up, can measure (small) particle velocity easily and is suitable for online measurements on bulk particles.

3.2 Experimental set-up

3.2.1 Double Disk method [4, 7, 8, 9, 10]

The double disk method is widely used as an inexpensive and simple set-up to measure the time of flight of particles. It consists of two disks simultaneously rotating at a high frequency (Figure 3.1).

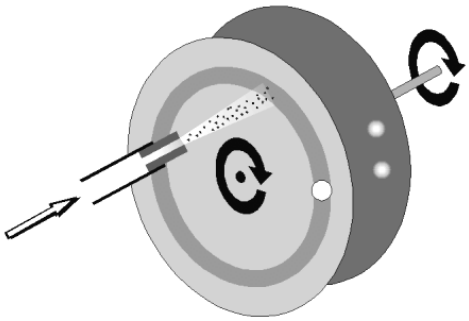

Figure 3.1 Double Disk method for velocity measurement

The first disk contains a slit, which acts like a shutter for the particles. The second disk is prepared with a thin layer of ordinary sprayed paint. The powder jet is placed in front of the first disk. As the slit passes the powder jet, some powder particles travel through the first disk towards the second disk while the disks continue to rotate. A mark is created by particle impacts on the second disk. By manually measuring the angle between this mark and a mark created at zero frequency (Figure 3.2) the particle velocity can be calculated by using the rotation frequency, and

the distance between the disks:

$$v = \frac{f \cdot d \cdot 360°}{\theta}, \qquad \textbf{Eq. 3-1}$$

with v the particle velocity, f the rotation frequency, d the distance between the disks and θ the rotated angle. The distance between the two disks is 2.1 cm. The operation frequency was measured each time using a Philips PM6667 counter, its value being approximately 500 Hz. The nozzle was placed at 1 cm from the first disk.

A more accurate but also more laboriously method, is to use a second disk of glass on which the marks are eroded by the particle impacts. The distance of these craters can then be measured using an accurate profilometer [2].

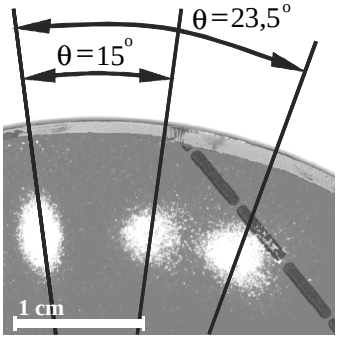

Figure 3.2 Photographic image of the typical marks on the second disk.

The first disk of the system disturbs the airflow pattern, which influences the velocity measurement, especially for particles smaller than 100 μm [4,8]. The small momentum of these particles makes their trajectory and velocity more sensitive for changes in the air jet flow.

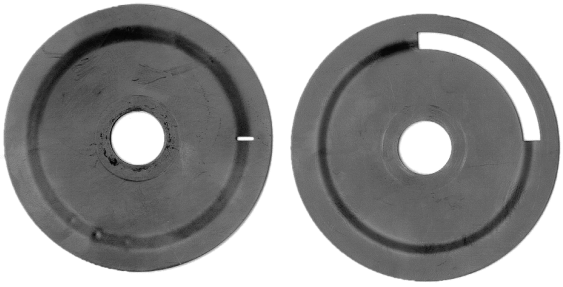

Figure 3.3 First disk from DD-method, with small (left) and long (right) slit.

To decrease this effect we also used a first disk with a long slit, as shown in Figure 3.3 (right). In that case the air stream is not immediately cut-of and it can drive the particles all the way towards the second disk. To measure the rotated angle, a different strategy is needed. First, the particle jet creates a long mark on the second disk while rotating them at the high frequency (analogous to the normal measurement). Now, manually a mark is created on the second disk (e.g. by using a knife) to indicate the start and end position of the long slit in the first disk (Figure 3.4).
It is relatively easy to determine the average position of the marks in Figure 3.2 by eye. In case of the long slit, the beginning and the ending of the mark have to be determined, which is more difficult due to the gradual change in eroded paint. To eliminate the error made by the human judgement, the angle at the begin and at the end are both measured and averaged (the difference between these two angles was never more than 6%).

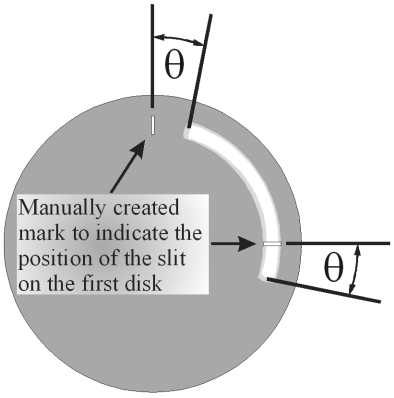

Figure 3.4 How to measure the rotated angle from the long-slit-mark on the second disk.

3.2.2 Cross-Correlation Method

Our "CC-method" consists of two scattered light signals that are cross-correlated to calculate the particles time-of-flight.
A 5 mW He-Ne laser and a beam splitter are used to obtain two parallel laser beams (width at 75% = 485 μm). The powder jet is directed through these beams to produce two scattered light signals (Figure 3.5). These signals are focused on two photodiodes (type BPX65). The non-scattered laser light is blocked at the focal point of the lenses.

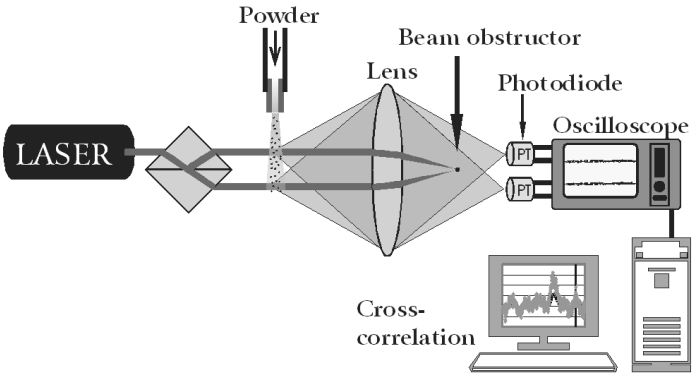

Figure 3.5 Set-up for Cross-Correlation velocity measurement.

Many particles that travel through the first laser beam are also travelling through the second beam. This means that the scattered light signal that is received by the first diode is similar to that received by the second diode, except for a time lag. By calculating the cross-correlation of the two signals this time lag, which is equal to the particles time of flight, can be found.

The distance between centre of the two laser beams was approximately 5 mm. The exact value was regularly checked using a scanning knife-edge (with an accuracy of 0.1%). The powder blast nozzle is placed 1.75 cm above the first beam to obtain the same average measurement distance as in the DD-method. When powder blasting, the particle jet is obstructed by a target, which can have an influence on the air-jet properties. Such an obstruction is not present at these CC- velocity measurements.

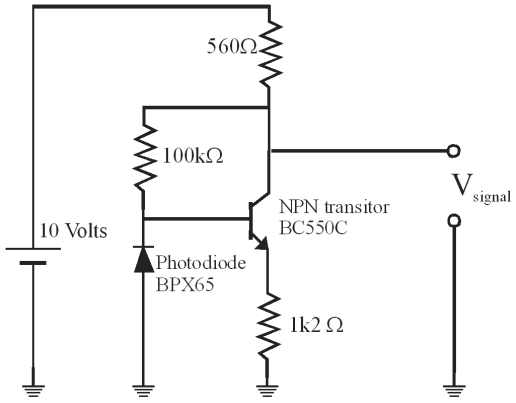

Figure 3.6 A simple one-transistor circuit to amplify the signal from the photodiode.

The two signals from the diodes are amplified by a simple one-transistor circuit (Figure 3.6) and detected by a digital oscilloscope (National Instruments 5102) for a specific time. The sample frequency was about 5-10 MHz, enough to sample the signal of a single particle travelling through one laser beam.
A computer program (programmed in Labview 6) collects the signals and calculates the cross-correlation (a standard function in Labview), the time of flight and the velocity by using the distance between the laser beams. Every velocity measurement consists of at least 10 individual measurements that are averaged.

Calibration

To calibrate the CC-method, a disk with large openings was rotated at a frequency of 50 Hz to periodically block the laser beams. Placing a small piece of transparency sheet just after the rotating disk attained the necessary scattering of the laser light. The velocity at which the disk interrupts the laser beams depends on the radius of the disk at which the beams are blocked. This radius was varied to change the velocity between 14-17 m/s. The difference of the velocity calculated from the radius and the velocity measured with the CC-method was smaller than 1%.

3.3 Results

3.3.1 CC-measurements

Figure 3.7 shows a detail of the cross-correlated signal from a typical velocity measurement, the total recorded time being 1.2 ms in this case.

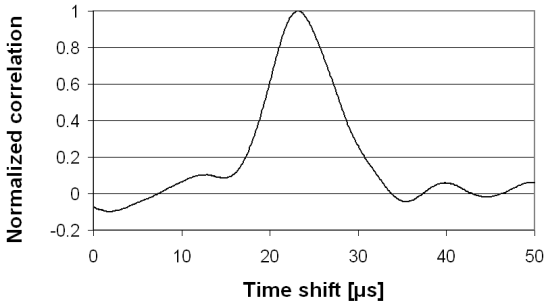

Figure 3.7 Detail of a typical single measurement result of the CC-method.

In stead of using the time of flight that corresponds with the position of the peak, it is also possible to use the average of the time values of the peak width at 75% amplitude. However, the difference between these

two results was never larger than 1%. In our case, the peak width depends mainly on the particle velocity (Figure 3.8). The width of a light peak that is generated by a single particle through a single laser beam (the time of flight through one beam) depends on its velocity. When we assume that the peak is gaussian, it can be calculated that the cross-correlated peak width is $\sqrt{2}$ times larger than the original peak width. So measuring high velocity particles results in a narrow cross-correlation peak. The solid line in Figure 3.8 indicates the peak width that should be generated by our laser beam of 485μm (at 75% peak).

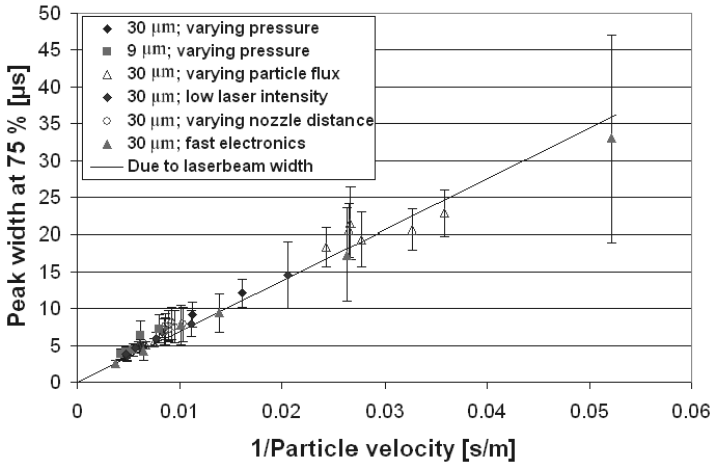

Figure 3.8 The cross-correlation peak width depends mainly on the particle velocity.

As stated, one measurement consists of the average value of several measurements. The standard deviation was in all cases about 3-7 m/s, depending on the quality of the signal.
The signal from 9 μm particles was not as good as compared to 29 μm particles when operating at the same mass flux. The cross-correlated signal improved when more particles participated in a measurement (so with increased particle flux or recorded time). A recording time of 3.2 ms. allowed us to do good measurements, while the computer could still perform the correlation twice every second.
Figure 3.9 shows that the particle velocity changes with distance from the nozzle. Therefore, when comparing the DD- and CC-method, it is important to use the same average measurement distance from the nozzle.

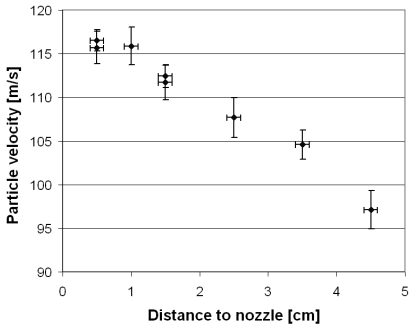

Figure 3.9 The change in particle velocity with distance to the nozzle. Mass flux is 1.4 g/min, pressure is $1.0 \cdot 10^5$ Pa.

3.3.2 Comparing DD- and CC-method

In all cases the DD-method resulted in a smaller velocity measurement. When using the small slit disk for the DD-method (Figure 3.10), it was clear that as the velocity of the 9 μm particles decreased, the time to create a clear mark on the second disk rapidly increased. The last DD measurement of the 29 μm particle at 4.5 bar deviates very strong from the rest of the measurements (this was measured several times). The reason for this is not clear, since the 9 μm particles do not show this effect. By ignoring this last point, a velocity-velocity plot is drawn to compare the two methods.

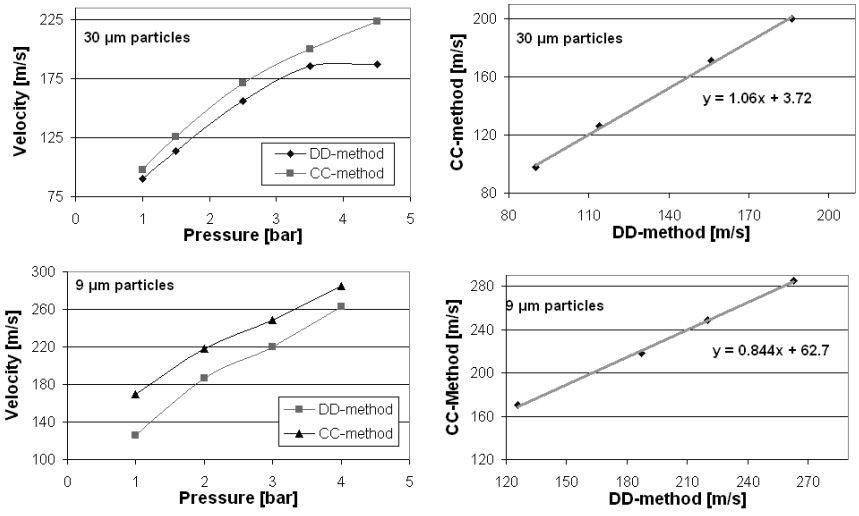

Figure 3.10 Comparison of velocity measurements with DD- and CC-method using a small slit disk.

When using the long slit disk for the DD-method, the measurements were closer to the values obtain with the CC-method (Figure 3.11). Also, the time to create a mark on the second disk was shorter and similar for all velocities. Again, a velocity-velocity plot is drawn to compare the two methods.

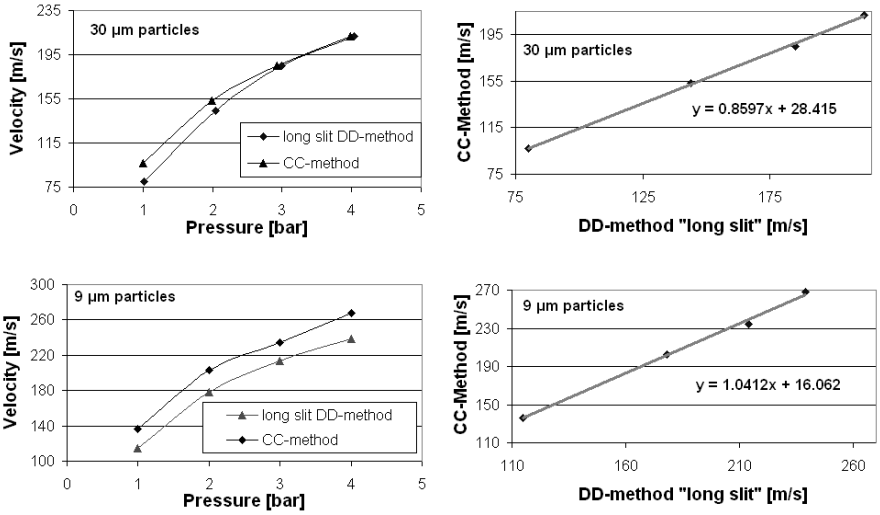

Figure 3.11 Comparison of velocity measurements with "long slit" DD- and CC-method.

3.4 Discussion

3.4.1 CC-method

The CC-method resembles the optic gates system from Stevenson [4], which could measure the velocities of 70 μm or larger particles in small mass fluxes at the end of the nozzle. Our CC-method proves to be an easy way to measure the velocity of bulk small particles at any position in the particle jet. The feed rate of our set-up was rather high (3-12 grams/min), and it can be calculated that the amount of particles simultaneously present in one laser beam varies from 2 to several hundreds (depending on particle size, speed and flux). This means that the signal consists of a superposition of several individual peaks.
Figure 3.8 shows that the peak width depends mainly on the particle velocity. So when using a single laser beam, it would be possible to calculate the particle velocity by using the peak width of the autocorrelation of the signal. However, the error bars in Figure 3.8 show that this would not be an accurate method in our set-up. One could

expect that the particle velocity distribution also influence the peak width. First of all the powder samples we use have a very narrow size distribution (sigma=1μm [11]) so the velocity distribution will also be relatively narrow (also see appendix). So apparently the width of the laser beam has a much larger influence on the peak width than the relatively small velocity distribution.

3.4.2 DD- versus CC-method

Other authors have shown that a velocity measurement with the DD-method results in a 10% lower value compared to more accurate methods [7]. This is consistent with our measurements on 29 μm particles in which the DD-method with small slit shows an average deviation of 9% compared to the CC-method.
When using 9 μm particles, the deviation compared to the CC-method increases from 8% up to 35% with decreasing velocity. It shows that the disturbance of the first disk on the air stream has a large influence on the velocity of small and slow particles.
To decrease this disturbance, we introduced a longer slit in the first disk. These measurements (Figure 3.11) indeed show a higher velocity measurement for 9 μm particles. The maximum velocity difference compared to the CC-method decreased from 35% to 18%. Long slit DD-measurements on 30 μm particles also improved. For higher velocities, the measurements even approach the values obtained with the CC-method.

Since the powder has a particle size distribution, also large and hence slower particles are present in the jet. Despite the lower velocity, they have a higher kinetic energy and can dominate in the DD velocity-measurement. However, in the appendix we calculate that this particle size distribution effect introduces an error of only 0.8% in this case. So it cannot be responsible for the large error in DD-velocity measurement that remains for the 9 μm particles. Still, for smaller particles or wider size distributions this effect can become very important. Stevenson [4] observed a higher velocity value of the DD-method compared with an optic gates method. This however can not be explained by our calculations, since a higher DD-value is only possible with a positive velocity-size exponent or an exponent which is lower than –1.5, and both are not realistic.

So other effects may still be responsible for the DD-method error. Despite the long slit, the first disk may still influence the particle jet. Also, the CC-method does not have a plate perpendicular to the particle jet (like a target or like the second disk in case of the DD-method). If a

plate would be inserted, the 9 μm particle jet and air flow will be disturbed, which can result in a lower velocity towards the plate [12].

3.5 Conclusion

Velocity measurements with the conventional DD-method on small ($<$100 μm) particles are not accurate or hardly possible. This method can be improved by replacing the small slit in the first disk with a longer slit. In this way, the air jet is not immediately cut-off and it will drive the particles all the way to the second disk. Our experiments show that this results in a more accurate velocity measurement and also enables us to measure the velocity of small and slow particles. However, it still has an unacceptable error in some cases. The particle size distribution effect can be responsible for large errors in DD velocity measurements, especially with wide particle distributions in combination with small particles. It was calculated that this effect couldn't be responsible for the error in our case, due to a narrow particle size distribution.
We introduce in this chapter an adapted CC-method for velocity measurements. The set-up requires ordinary lab equipment and the cross-correlation provides a robust and powerful measurement method. By using the scattered light from the particles, this method is capable to measure the velocity of very small particles (3 μm). There is no apparent limit to the particle size or speed that can be measured, although the signal becomes less clear when the particles get smaller or faster. The speed of the particles can be measured anywhere in the particle jet, only restricted by the distance between the laser beams (approximately 5 mm in our case). This online method is suitable when powder blasting is used as a high-resolution machining-technique with relatively high mass fluxes and small particles.

3.6 Acknowledgement

The authors would like to thank Remco Wiegerink for his support on the electrical signal processing and Henk van Wolferen for his support on the optics.

3.7 Appendix: Particle size distribution effect

Even with the long slit DD-method we still encounter an error in velocity measurement. We will calculate the effect of a particle size distribution on a DD velocity measurement to see if it can be responsible for this error. To do so, we make some assumptions:

1. The size distribution of our particles is gaussian:

$$G = \frac{1}{\sigma\sqrt{2\pi}} \exp\left(-\frac{(d - d_0)^2}{2\sigma^2} \right), \qquad \text{Eq. 3-1}$$

   with d_0 the average particle size and σ the standard deviation. Specification giving by powder supplier Treibacher [11] shows that the standard deviation of their powders is 1μm for both 9 and 29 μm particles.
2. As an approximation, we assume that an accumulated amount of kinetic energy is necessary to remove a piece of paint from the second disk. In other words, a 29 μm particle accounts for 33 particles of 9 μm at the same speed.
3. The velocity is a function of the particle size (at a constant pressure) such that:

$$v(d) = C \cdot d^n, \qquad \text{Eq. 3-2}$$

   with C a constant, n an exponent and d the particle diameter. This functional dependence was shown by e.g. Stevenson [4].

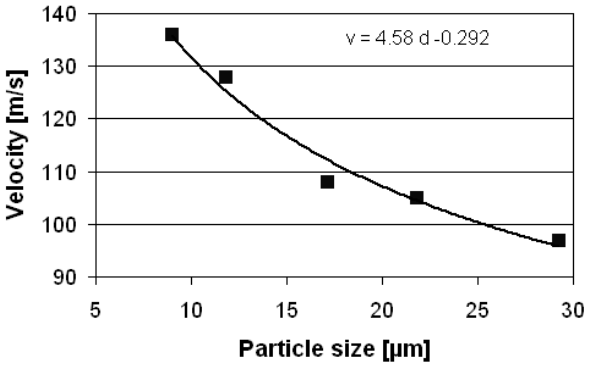

Figure 3.12 Velocity versus particle diameter, measured with CC-method at a pressure of 1 bar and a nozzle opening of 1.5 mm.

We used our CC-method to measure the velocity as a function of particle size at a pressure of 1 bar (Figure 3.12). It is fitted to a function with $C = 4.58$ and $n = -0.292$. The exponent value is comparable with the value that was measured by Stevenson [4]: -0.285. It clearly shows that larger particles are more difficult to accelerate and attain a lower velocity at the same pressure.
The mass of the particles is calculated assuming a spherical shape as an approximation. Using Eq. 3-2, the kinetic energy can be calculated:

$$U_{kin} = \frac{1}{2}mv^2, \\ = \frac{1}{2}\left(\frac{4}{3}\pi\left(\frac{1}{2}d\right)^3\rho\right)\cdot(C\cdot d^n)^2 = \frac{\pi\cdot\rho\cdot C}{12}d^{3+2n}, \qquad \textbf{Eq. 3-3}$$

with m the particle mass and ρ the specific weight.
To calculate which particle size is mainly responsible (dominant) for the mark on the second disk, we combine Eq. 3-1 and Eq. 3-3 to calculate the kinetic energy load.

$$U_{load} = \frac{\sqrt{\pi}\cdot\rho\cdot C}{24\sigma}d^{3+2n}\cdot\exp\left(-\frac{(d-d_0)^2}{2\sigma^2}\right). \qquad \textbf{Eq. 3-4}$$

The maximum of this function (where the derivative is zero) indicates the particle size d_1 that is dominant in the DD velocity measurement:

$$\frac{\partial U_{load}}{\partial d} = \frac{(3+2n)}{d}\cdot U_{load} - \frac{(d-d_0)}{\sigma^2}\cdot U_{load} = 0, \\ \Leftrightarrow \frac{(3+2n)}{d} = \frac{(d-d_0)}{\sigma^2}, \\ \Leftrightarrow d = d_1 = \frac{1}{2}\left(d_0 + \sqrt{{d_0}^2 + (12+8n)\sigma^2}\right), \qquad \textbf{Eq. 3-5}$$

(when $\sigma=0$, $d_1=d_0$ so the sign before the root is positive.) The relative shift in a DD velocity measurement can now be calculated:

$$\Delta = \frac{v(d_0) - v(d_1)}{v(d_0)},$$

Eq. 3-6

$$\Leftrightarrow \Delta = \left(1 - \left(\frac{1}{2} + \frac{1}{2}\sqrt{1 + (12 + 8n)\left(\frac{\sigma}{d_0}\right)^2}\right)^n\right) \quad .$$

By using Eq. 3-6, Figure 3.13 shows the relative velocity shift for particles sizes with a standard deviation of 1 μm, and a velocity exponent of -0.292. The shift in a velocity measurement by the DD-method for 9μm particles is only 0.8%. For smaller particles or larger standard deviations, this error can increase rapidly.

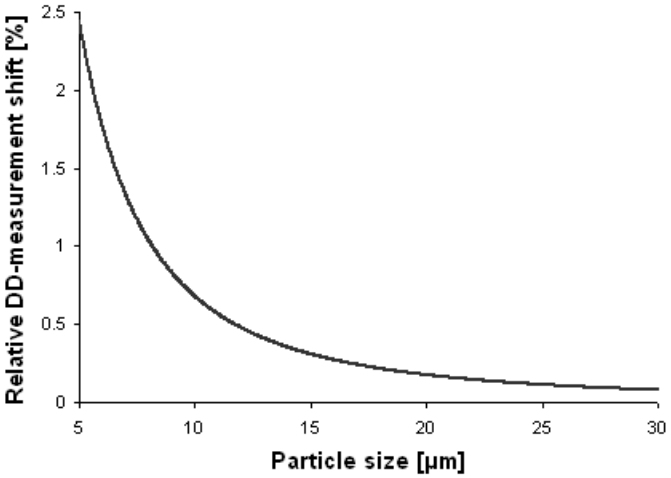

Figure 3.13 Relative velocity shift in DD-velocity measurement with a given particle size distribution.

3.8 References

1 P.J. Slikkerveer, P.C.P. Bouten, F.C.M. de Haas, "High Quality Mechanical Etching of Brittle Materials by Powder Blasting", *Sensors and Actuators* 85 (2000) pp. 296-303

2 E. Belloy, S. Thurre, E. Walckiers, A. Sayah, M.A.M Gijs, "The introduction of powder blasting for sensor and microsystem

applications", *Sensors and Actuators A: Physical* 84 (2000) pp. 330-337

3 H. Wensink, J.W. Berenschot, H.V. Jansen, M.C. Elwenspoek, "High Resolution Powder Blast Micromachining", *Proc. 13th Int. workshop on Micro Electro Mechanical Systems (MEMS2000)*, Miyazaki, Japan, (2000) pp. 769-774

4 A.N.J. Stevenson, I.M. Hutchings, "Scaling laws for particle velocity in the gas-blast erosion test", *Wear* 181-183 (1995) pp. 56-62

5 D.R. Andrews, "A versitile laboratory correlator with application to determine particle velocity in an erosion test", *J. Phys. E: Sic. Instrum.* 16 (1983) pp. 706-709

6 V. Ponnaganti, D.E. Stock, G.L.Sheldon, "Measurement of Particle Velocities in Erosion Processes", *Proc. Symp. Polyphase Flow and Transport Technology*, San Francisco, USA (1980) pp. 217-222

7 P.J. Slikkerveer, P.C.P. Bouten, F.H. in't Veld, H. Scholten, "Erosion and damage by sharp particles", *Wear* 217 (1998) pp. 237-250

8 I.M. Hutchings, "Ductile-brittle transitions and wear maps for the erosion and abrasion of brittle materials", *J. Phys. D.: Appl. Phys.* 25 (1992) pp. A212-A221

9 A.W. Ruff, "Analysis of interlaboratory test results of solid particle impingement erosion", *Wear* 108 (1986) pp. 323-335

10 A.V. Levy, "The solid particle erosion behavior of steel as a function of microstructure", *Wear* 68 (1981) pp. 269-287

11 Treibacher Schleifmittel GmbH, Ferroweg 1, D-79725 Laufenburg, Germany, Tel. +49.7763.9330

12 J.E. Fackrell, "Aerodynamic effects on PFBC erosion target experiments", *Wear* 134 (1989) pp. 237-252

Mask Materials*

Several types of mask materials will be discussed in this chapter. A small feature size and an accurate pattern transfer can be achieved when using a mask for powder blasting. Electroplated copper is introduced and studied as a new type of powder blasting mask.

4.1 Introduction

Sand blasting is an old technique, which is used to remove paint, clean house facades and decorate glass. Powder blasting, with small (<100 μm) particles, is used for e.g. device demarking in electronic industry, surface preparation prior to plating (without mask) but also rapid prototyping [1] and flat panel display production [2][3] (with mask). In research, it is widely used to determine the wear rate of industrial materials.

* Based on: H.Wensink, H.V.Jansen, J.W.Berenschot, M.C. Elwenspoek, "Mask materials for powder blasting", *J. Micromech. Microeng.* 10 (2000) pp.175-180, with an important addition to the electroplated copper section.

Powder blasting can also be used for micromachining. Being an IC technology spin off, micromachining is normally performed on silicon whereas other materials are less frequently processed. Powder blasting is suitable for machining a wide class of materials like glass, silicon and ceramics and the required equipment is relatively cheap. It is a fast process; the time to erode through a 500 μm thick 3" Pyrex wafer with one nozzle is approximately 20 min. in our set-up. It also fits very well between the common micromachining techniques due to its lithographic masking abilities, process similarities and compatibility. For the production of flat panel displays, powder blasting was judged to be the best process to create thousands of holes at once at low cost, high speed and with a high accuracy [2]. In the field of micromechanics, powder blasting has already successfully been used e.g. for making an inertial sensor [4], a selfpriming peristaltic micropump [5] and a miniaturised capillary electrophoresis chip [6]. There are several advantages in using a mask with powder blasting. The particle jet (which expands to about one cm in diameter) can be optimised for machining, while the mask defines the small and complex structures. It also allows multiple jets to be used which decreases the process time. Up to now, the minimum feature size with powder blasting is limited in practice to about 100 μm [7], a major goal of our project is to decrease it. For this, two factors are important. First, it requires the use of an average particle size of at most a third of the desired channel width (as a rule of thumb). Fortunately, sharp alumina (Al_2O_3) particles are available in large quantities with any average size. Second, it has to be possible to make a mask with small feature sizes. In this Chapter we look at mask materials for powder blasting in general, while testing them with 30 μm alumina particles, and for the possibility of making smaller dimensions in particular.

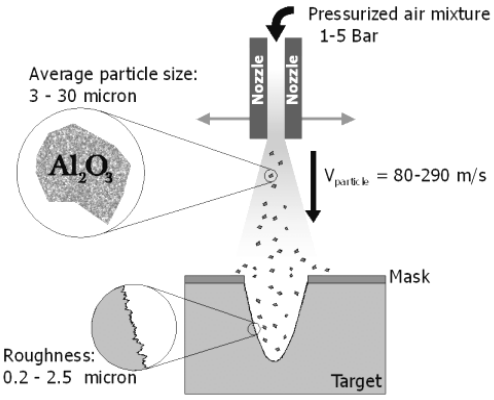

Figure 4.1 A schematic impression of the powder blast process.

4.2 Powder Blasting

Powder blasting is a technology in which a particle jet is directed towards a target for mechanical material removal (Figure 4.1). The particles are accelerated towards the target with a high-pressure airflow (Figure 4.2). The airflow is mixed with the particles by a vibrating feeder (HP-2, Texas Airsonics). The mixture is directed through a circular nozzle (with a diameter of 1.5 mm) at the end of the tube. The particles hit the target with a speed up to 200 m/s (depending on the air pressure) in a separate box. This box is ventilated by a cyclone, which removes the particles from the airflow.

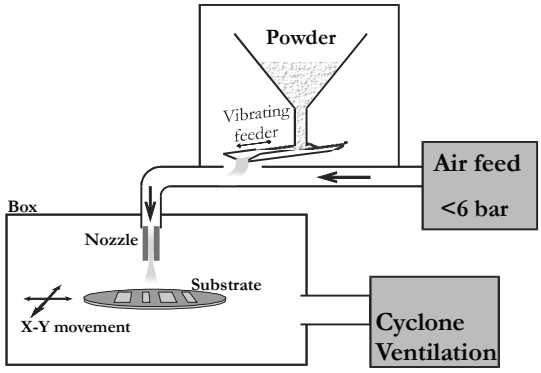

Figure 4.2 Powder blasting equipment.

A lateral movement of the target ensures an evenly powder blasted surface while a mask, which contains the design, covers the target. Figure 4.3 shows a typical result of powder blasting in Pyrex glass.

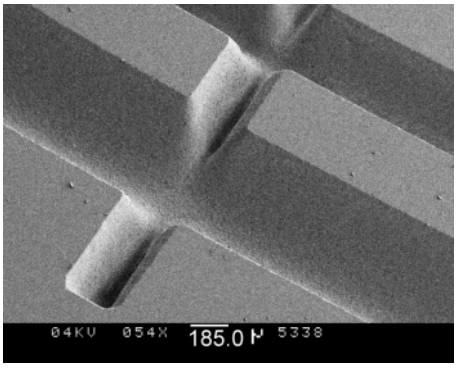

Figure 4.3 Perspective view of a typical result of powder blasting in Pyrex glass (400 μm deep).

The erosion process is usually described as the sum of many single particle impacts. There are roughly three classes of materials to be considered in powder blasting; ductile materials (like metals), elastomers (like rubbers) and brittle materials (like glass, silicon and ceramics). Ductile materials erode by cutting and ploughing, elastomers by fatigue mechanisms and brittle materials by crack growth.

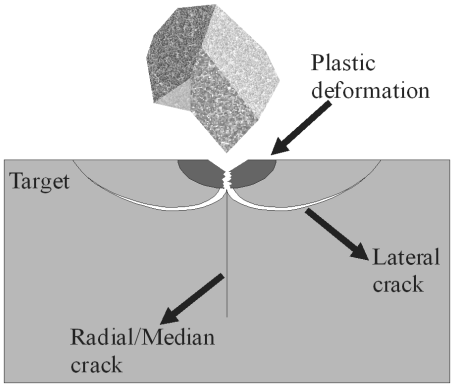

Figure 4.4 Erosion mechanism of a single particle impact.

When a brittle material is impacted by a hard sharp particle, the contact volume is plastically deformed due to the resulting high compressive and shear stresses. It leads to large tensile stresses after the impact (relaxation) at the boundary between the plastically and elastically deformed indentation. This results in lateral cracks causing the material removal (Figure 4.4) and a roughness of 0.7-2.5 μm R_a (depending on the kinetic energy of the particles [8]). The erosion mechanism of a single particle impact is more thoroughly described in erosion related papers [8][9]. Ductile materials, and also elastomers [11], have a low erosion rate (compared to brittle materials) with a local minimum at 90° impact angle (Figure 4.5).
Since the particle jet is directed perpendicular towards the target during blasting for maximum brittle erosion, ductile materials and elastomers can be suitable to be used as a mask.

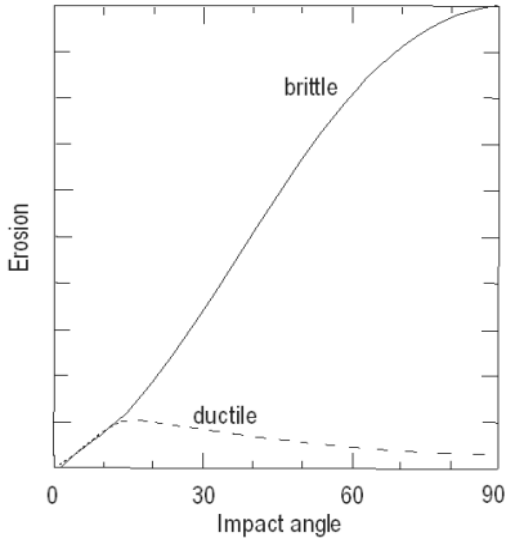

Figure 4.5 Two basic erosion characteristics in powder blasting (90° is perpendicular impact) After [10].

4.3 Mask Materials

The main qualification for a good mask material is a low erosion rate. We also look for the capability of an accurate and easy pattern transfer, and the possibility to create small feature sizes.
We first test two polymers that can be lithographically structured, and second we examined two metal masks.

4.3.1 Powder blasting foil

Ordyl BF400 is an elastic negative resist foil fabricated by Tokyo Ohka Kogyo (Japan), and specially developed for powder blasting [3][11]. There are two types: 50 μm (BF405) and 100 μm (BF410) thick, we tested the first one. The foil is applied to the target on a hot-plate (105°C). After exposure (150 mJ/cm^2), it is spray-developed with 0.2% Na_2Co_3. The resulting layer was found to be 43 μm thick. After blasting, the foil can be removed by hand, with a 10% KOH solution at room temperature or e.g. with an HNO_3 solution.
In Figure 4.6 the decrease in thickness of BF405 is shown when eroded by alumina particles with an average size of 30 μm and a speed of 180 m/s.

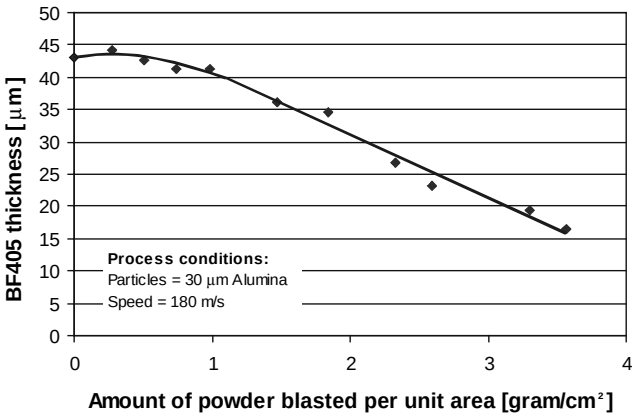

Figure 4.6 Erosion of BF405 foil.

Thickness was measured with a Dektak profiler (Sloan DEKTAK II), after blowing away the remaining particles with dry nitrogen. In the beginning of the erosion, the thickness of BF405 does not seem to decrease at all (even a small increase is observed). The foil is first degraded by the particle impacts creating subsurface cracks without actually being removed. After this incubation time, the damage becomes so severe that further blasting does decrease the resist thickness. The steady state erosion is reached, and the thickness decreases linearly. This effect is well-known and also observed by others [12, 13].
The erosion was monitored until it had a thickness of about 17 μm. Now the particles were able to penetrate the resist and damage the target. From this point on, both the target and resist are rapidly removed. This restricts the maximum powder blasted depth with this foil and these conditions to about 350 μm in Pyrex glass. Already before this breakdown, some particles are able to penetrate the foil deep enough to hit the target at undesired spots. Figure 4.7 shows such a damage.

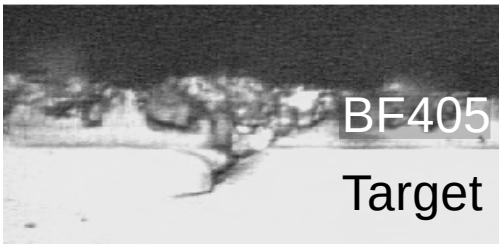

Figure 4.7 Damage underneath the BF405 foil. Remaining thickness appr. 17 μm, blasting conditions as in Figure 4.6

When powder blasting channels, another important effect occurs. The resist edges that define the channel are more vulnerable to the particle impacts and are readily withdrawing. Therefore, the top width of a channel increases during blasting, as shown in Figure 4.8. These effects are reduced to some extent when applying a postbake of 150°C or by using the thicker BF410.

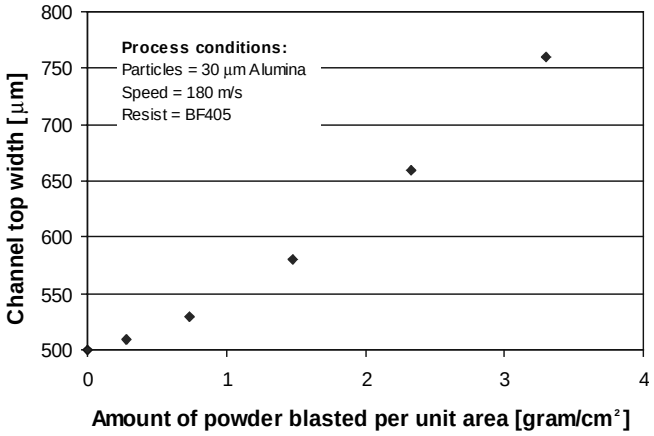

Figure 4.8 The channel width increases during blasting.

4.3.2 Polyimide

Polyimide is a negative liquid resist that is very well known for its high strength, we tested Durimide 7510 (Arch Chemicals). A thick layer was applied by spinning at 660 rpm. After exposure (300 mJ/cm^2), development and a one hour anneal in an N_2-envoriment at 350°C, the thickness was 35 μm. The erosion rate was tested by blasting the sample with alumina particles with an average size of 30 μm at a speed of 180 m/s. The decrease in thickness was measured using a Dektak surface profiler.

The polyimide clearly showed higher steady state erosion compared to BF405, approximately by a factor of 2. It also had a shorter incubation time before the steady state erosion was reached, which indicates a more brittle behaviour [14]. This high erosion rate makes polyimide less suitable for a mask material in deep and accurate powder blasting.

4.3.3 Metal plate masks

Metals are normally used as a powder blasting mask material by means of a metal plate (e.g. stainless steel) [2][4]. By drilling, milling, etching or laser machining a pattern is created in this mask. The mask can simply be

clamped directly together with the target. However, since a plate is never completely flat, there will be voids underneath the mask (Figure 4.9). This will allow the particles to get into the voids and damage the target. Also, the impact of particles on the top surface of the plate will induce great stresses, which can result in buckling of the mask (especially with very thin plates). To prevent this, the mask can be clamped magnetically to the target or an intermediate protection/adhesion layer can be applied [2]. When, in the latter case, this extra layer also covers the blast area, it should easily be removed by powder blasting.

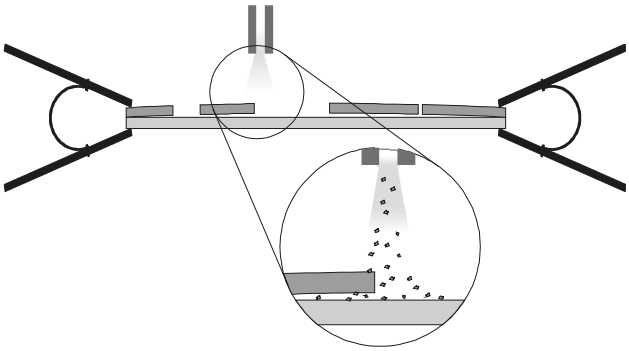

Figure 4.9 A metal plate mask clamped to the target introduces voids.

Wax seal (W100, Agar Scientific Ltd, Stansted, UK) meets the requirements to be an intermediate protection/adhesion layer. It is a brittle material, which becomes viscous at higher temperatures. At a temperature of 150°C the wax can be spread on the (also heated) mask. The target is placed on the mask and the stack is cooled down to room temperature. This results in a very tight and strong connection. Since the wax is brittle, it is very easily removed by powder blasting and it has practically no influence on uniformity (Figure 4.10).

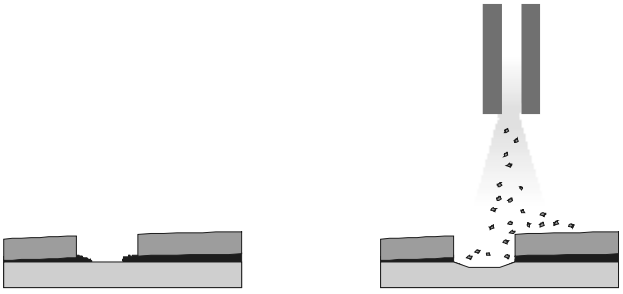

Figure 4.10 Metal mask on a target with adhesion/protection layer.

After blasting, reheating separates the mask from the target and both can be cleaned with chloroform. The positive effect of an intermediate layer is clearly seen in Figure 4.11. A relatively thick metal layer lasts for a long time, so a mask can be used on several targets.

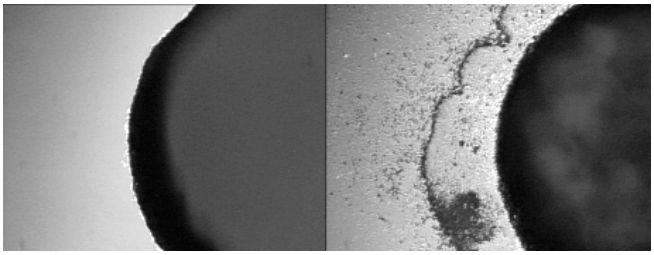

Figure 4.11 Powder blasting a 1 mm hole using a 1 mm metal mask. Resulting top view when blasted with (left) and without an adhesion/protection layer.

4.3.4 Copper

In order to combine the low erosion rate of a metal, and the high resolution of a lithographic process, a metal mask was applied on the target by electroplating. Copper was chosen as the metal, because of its wide use in electroplating and its high wear resistance against powder blasting [9].

Removal rate

The removal rate of Pyrex and copper is measured to determine the erosion resistance of the electroplated mask and the selectivity with Pyrex. Measurements are carried out at a constant pressure (4.5 bar) using 29 μm and 9 μm alumina particles. The particle velocity is measured separately at these conditions before the measurements. A silicon reference sample was simultaneously eroded in the experiments to determine the amount of powder that has been used during a measurement (see Appendix for more details). The erosion rate of silicon was available from previous experiments for a range of alumina particle kinetic energies (see Chapter 6). In this way, the relative removal rate of the different samples can be determined very accurately. The absolute removal rate will be less accurately determined, but this is also of less importance for micromachining.

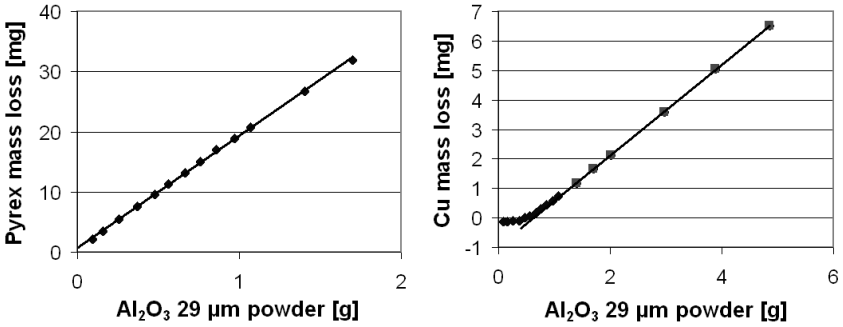

Figure 4.12 The erosion rate for Pyrex (left) and electroplated copper (right) using 29 µm Al_2O_3 particles at 270 m/s.

Figure 4.12 shows the erosion rate for Pyrex and electroplated copper measured in [mg/g] for 29 μm particles. The erosion rate of copper shows a characteristic start-up effect. Particles or particle fragments get stuck in the ductile layer, which conceals the initial erosion rate. In certain cases, even an initial weight increase is observed for metals [15]. The copper deformation and particle penetration results in compressive stress in the mask layer, which makes a good adhesion between the copper and the substrate quite critical.
Steady state removal rates are converted to [μm/min] for all measurements in Table 4-1.

Table 4-1 Steady state removal rates for several materials (for an area of 7x7 cm^2 and a powder feed of 10 g/min).

Particle type	Particle Velocity [m/s]	Removal rate Copper [μm/min]	Removal rate Pyrex [μm/min]	Selectivity Pyrex/copper
29 μm Al_2O_3	230 ± 7	0.35	25	71
9 μm Al_2O_3	270 ± 6	0.34	13.5	40

SU-8 electroplating mould

The quality of the non-conductive resist mould that is required for electroplating has a large influence on the quality of the electroplated powder blasting mask. The mould should be thick (up to 50 μm), have straight walls for a good definition of the copper mask and be resistant against the electroplating bath. EPON SU-8 (mr-L 6100exp) meets these requirements but has the disadvantage of long process times and, more

importantly, a relatively bad adhesion to the thin copper seed layer (compared to the adhesion on bare silicon).
The consequence is that small SU-8 mould structures are flushed away during development, especially at shorter exposure times. Longer exposure times do improve the adhesion during development. However, in that case the SU-8 line-width broadens and the SU-8 mould is released from the substrate after insertion in the electroplating bath. We think that an increase in internal stress due to the longer exposure times causes these structures to peel of in the acidic environment. An exposure time of 60 s (a dose of 540 mJ/cm^2) was found to be optimal for the SU-8 layer. To further reduce internal stresses, baking procedures during the SU-8 process (on a programmable hotplate) included a slow ramping down to room temperature to reduce temperature shock effects (Figure 4.13).

An RIE-N_2 plasma was used to roughen the copper surface before spinning to increase the adhesion of the SU-8 to copper. However, the larger contact area did not noticeable improve the adhesion. The SU-8 adhesion is much better when using a nickel seed layer in which case a good pattern transfer can be achieved. Unfortunately, the adhesion between the nickel and the electroplated copper is not good enough for powder blasting. The electroplated mask layer is delaminating from the nickel seed layer during powder blasting.
The channel layout and typical

Dehydration bake:
- 120°C, 10 min

Spin coat: mr-L 6100 exp
3000 rpm, 30 s
(acceleration 1000 rpm/s)
(layer thickness ≈ 50μm)

Relaxation: 10 min

Prebake:
-10 min at 70°C
-ramp to 95°C (7-8 K/min)
-90 min at 95°C
-ramp to 120°C (7-8 K/min)
-60 min at 120°C
-cool down to 25°C

Exposure:
-proximity mode
-60 s illumination

Post exposure bake:
-10 min at 60°C
-ramp to 95°C (7-8 K/min)
-60 min at 95°C
-cool down to 25°C

Development:
-mr-Dev 600, ≥5 min
-rinse with isopropanol
-spin drying

Figure 4.13 Lithography steps for SU-8

electroplating result is shown in Figure 4.14. The minimum channel width for these structures that could be electroplated is 25 μm. This is sufficient for powder blasting since the minimum feature size is also restricted by the particles sizes used for blasting.

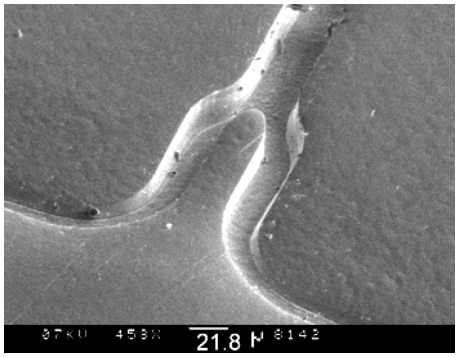

Figure 4.14 Electroplated copper masks, 25μm wide channel on silicon.

Electroplating

An intermediate titanium layer is used for a good adhesion of the copper mask with the target. Additionally, the target is cleaned with an oxygen plasma before sputtering the metal layers. It was observed that without these precautions, the copper mask buckles and releases from the Pyrex glass target during powder blasting.

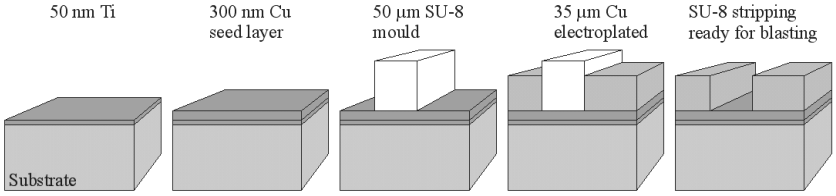

Figure 4.15 Schematic process of applying an electroplated copper mask.

Figure 4.15 shows the schematic process scheme of applying an electroplated copper mask. Substrates are first covered with a sputtered titanium layer (50 nm) and a copper seed layer (300 nm). A 50 μm thick SU-8 layer is applied on the seed layer. After exposure and development the copper is electroplated around the mould. Finally the SU-8 mould is stripped in NMP (N-methyl-2-pyrrolidinone) for 2 hours in an ultrasonic bath at 70°C. The substrate is now ready for blasting

The thin seed layer beneath the resist mould is generally not removed separately, but is easily machined during the blasting. After blasting, the remaining copper can be removed with a copper etch or a strong acid like HNO_3.

Powder Blasting

The edges of an electroplated copper mask show a very characteristic behaviour during powder blasting. The channel width during blasting as defined by the top view of the copper mask is shown in Figure 4.16.

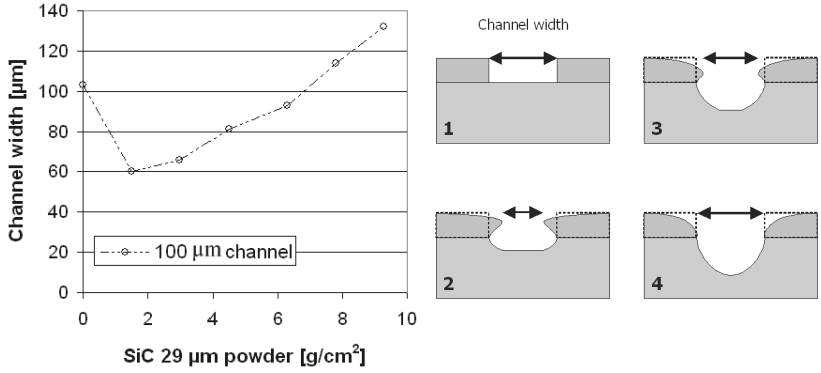

Figure 4.16 Left: Top channel width during powder blasting (mask thickness is 35 µm). Right: schematic impression of the copper mask during blasting.

It shows that during powder blasting the channel width initially decreases before it slowly increases. The edges of the copper mask are deformed due to the particle impacts, and the copper smears out over the channels decreasing the width. This effect prevents the mask opening to become wider than the original width for a long blasting time. The disadvantage is that it contributes to the blast lag (see Chapter 7). For thicker masks, the edges can even roof over the channel and close it temporarily for particles.

4.4 Discussion

The powder blasting foil Ordyl BF405 (50 µm thick) has a reasonable low erosion rate, is easy to use and very suitable for standard blasting applications with complex designs. With lithography, trenches of 70 µm wide or more can be achieved with the 50 µm thick BF405 due to the thickness and properties of the resist. An important disadvantage is that the mask edges calve of during powder blasting. This mask-widening rate is relatively high and results in a bad pattern transfer. Using the 100 µm

thick BF410 reduces these effects, but also increases the minimum attainable feature size.
When using polyimide, the mask thickness can be adjusted so a very small feature size can be obtained. However, although polyimide is known for its strength, it is more brittle compared to BF405. This results in a higher erosion rate, which makes it unsuitable to be a mask material for deep and accurate powder blasting.
A metal plate mask has the advantages of a low erosion rate and its applicability on any kind of material. However, the disadvantages are the limitations in feature size and pattern constraints (ring patterns cannot be used because the inside should be supported).
By creating a mask with electroplating, we can combine the low erosion rate of metals with the high resolution of a lithographic process. This also allows adjusting the desired thickness of the mask, which can depend on process requirements.

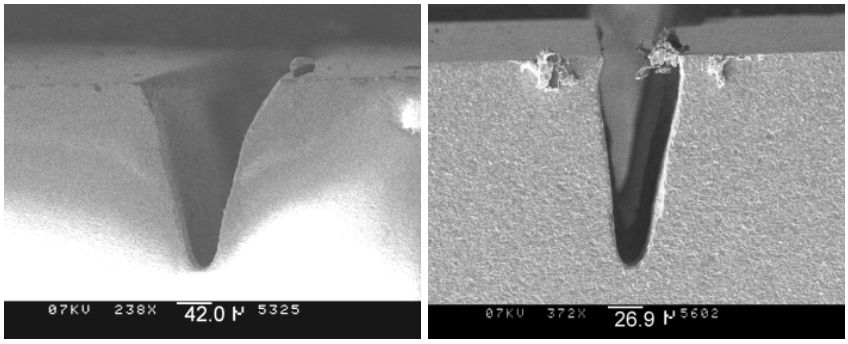

Figure 4.17 The influence of the mask on the channel profile. Left with a BF405 mask and 30 µm particles. Right with a 50 µm thick electroplated copper mask and 9µm particles. The masks were removed for both pictures.

The selectivity between copper and Pyrex is about 70 and, more importantly, the channel widening rate is much lower compared to BF405 (Figure 4.8 and Figure 4.16). This results in a more accurate pattern transfer. The difference in channel profile when powder blasting with BF405 or electroplated copper is clearly seen in Figure 4.17. Although these profiles are in this case blasted with different particle sizes, it gives a valid general idea of the accurate pattern transfer of an electroplated copper mask.

Figure 4.16 makes clear that the minimum required mask thickness is not directly determined by the selectivity between the mask and the target, since the mask edges will calve off long before the total mask is removed. The erosion rate and selectivity (at 90° and smaller impact angles) give a

good indication for the quality of mask materials, but the channel widening rate shows directly the effect of the mask material on the quality of the pattern transfer.

4.5 Conclusions

Powder blasting is a fast, cheap and accurate directional machining technique for brittle materials like glass, silicon and ceramics. It was shown that there are many possibilities with pattern transfer in powder blasting, which gives this micro technology the perspective to become a new standard tool in micromachining. The accuracy of the process depends also on the type of mask that is used. In this chapter, several mask types have been tested for this application.

The negative resist foil BF405 has a reasonable low erosion rate, is easy to use and very suitable for standard blasting applications with complex designs. The minimum feature size of this foil using lithography is restricted by its properties and standard thickness of 50 μm to about 70 μm.

With polyimide, the minimum feature size can be smaller, but the erosion rate of this negative resist is higher. A metal plate mask has a low erosion rate, but is limited in feature size and it has pattern constraints.

Electroplated copper was introduced as a new mask material for powder blasting which combines the low erosion rate of a metal with the high resolution capabilities of a lithographic process. The mask widening rate of copper, an important parameter for the comparison of mask materials, is much lower compared to the negative resist foil BF405. Electroplated copper can be used for deep and accurate powder blasting, and is a suitable mask for powder blasting feature sizes of less than 50 μm.

4.6 Acknowledgements

Jeroen Haneveld is gratefully thanked for the characterisation of the electroplated masks.

4.7 References

1 A. Kruusing, S. Leppävuori, A. Uusimäki, M. Uusimäki, “Rapid prototyping of silicon structures by aid of laser and abrasive-jet machining”, *SPIE proceedings 3680* (1999), pp. 870-878

2 H.J. Ligthart, P.J. Slikkerveer, F.H. in 't Veld, P.H.W. Swinkels, M.H. Zonneveld, “Glass and glass machining in ZEUS panels”, *Philips J. Res*. 50 (1996), pp.475-499

3 H. Fujii, H. Tanabe, H. Ishiga, M.Harayama, M. Oka, "A sandblasting process for fabrication of color PDP phosphor screens", *SID 92 digest* (1992), pp. 728-731
4 E. Belloy, S. Thurre, E. Walckiers, A. Sayah, M.A.M. Gijs, "Powder Blasting as a New Technology for Inertial Sensor Fabrication", *Eurosensors XIII* The Hague, The Netherlands (1999), pp.827-830
5 T.T.Veenstra, J.W.Berenschot, R.G.P.Sanders, J.G.E.Gardeniers, M.C.Elwenspoek, A.van den Berg, "A Simple Selfpriming Bubble-Tolerant Peristaltic MicroPump", *Eurosensors XIV*, Copenhagen, Denmark (2000) pp. 671-672
6 S. Schlautmann, H. Frank, H. Billiet, G. van Dedem, A. van den Berg, "Miniaturized Capillary Electrophoresis System with Integrated Conductivity Detector, R. Schasfoort, R. Guijt-van Duijn", *μTas 2000*, Enschede, The Netherlands (2000)
7 P.J. Slikkerveer, P.C.P. Bouten, F.C.M. de Haas, "High Quality Mechanical Etching of Brittle Materials by Powder Blasting", *Sensors and Actuators* 85 (2000) pp. 296-303
8 P.J. Slikkerveer, P.C.P. Bouten, F.H. in 't Veld, H. Scholten, "Erosion and damage by sharp particles", *Wear* 217 (1998) pp. 237-250
9 I. Finnie, " Some reflections on the past and future of erosion", *Wear* 186-187 (1995) pp. 1-10
10 J.E. Ritter (Ed.), "Erosion of Ceramic Materials", *Trans Tech Publications*, Zurich, Switzerland (1992)
11 P.J. Slikkerveer, M.H.A. van Dongen, F.J. Touwslager, "Erosion of elastomeric protective coatings" *Wear* 236 (1999) pp. 189-198
12 J.C. Arnold, I.M. Hutchings, "The mechanisms of erosion of unfilled elastomers by solid particle impact" *Wear* 138 (1990) pp. 33-46
13 S.M. Walley, J.E. Field, "The erosion and deformation of polyethylene by solid-particle impact", *Phil. Trans. R. Soc. Lond.* A 321 (1987) pp. 277-303
14 K. Friedrich, "Erosive wear of polymer surfaces by steel ball blasting", *J. Mater. Sci.* 21 (1986) pp. 3317-3332
15 P. Shewmon, G. Sundararajan, "The Erosion of Metals ", *Annu. Rev. Mater. Sci.* 13 (1983) pp. 301

Fine Tuning the Surface Roughness*

Powder blasting results in a surface roughness that is much higher compared to general micromachining techniques. This chapter shows how the roughness of a powder blasted surface can be controlled by process parameters or changed with post treatments, both quantitatively and qualitatively.

5.1 Introduction

Powder blasting is a fast and inexpensive directional machining technique for brittle materials like glass, silicon and ceramics. However, unfamiliarity with this technique sometimes causes a hesitation to use it, especially due to the uncertainty about the effect of the rough surface on the device performance [1]. It is e.g. supposed that the roughness

* Based on: H.Wensink, S.Schlautmann, M.H. Goedbloed, M.C.Elwenspoek, "Fine Tuning the Surface Roughness of Powder Blasted Glass Surfaces" Proc. Sensor Technology Conference 2001, Enschede, The Netherlands, may 14-15, pp.101-106

increases the electro-osmotic flow, fluidic mixing and hence the dispersion. Therefore it is important to be able to manipulate the roughness and study its effect on device performance.
Powder blasted surfaces are rough due to the nature of the erosion process. The erosion process is usually described as the sum of many single particle impacts. When a brittle material is impacted by a hard sharp particle, the contact area is deformed due to the high compressive and shear stresses.
The deformation leads to large tensile stresses after the impact (relaxation) that result in one or more lateral cracks originating from the plastic zone (Figure 5.1). If they are large enough they will extend to the surface removing a large heap of material and creating the rough surface.
Pyrex is an "open-structure" glass, which means that the glass is deformed by compaction of the glass, making it denser. (This is in contrast to e.g. soda-lime glass where the larger content of non-silica components results in a more plastic deformation process along slip lines [2].) Next to the lateral and radial cracks, compaction can even result in cone cracks, which are normally observed with spherical indentors and particles [3].
The erosion mechanism of a single particle impact or indentation is more thoroughly described in erosion-related papers [4, 5, 6, 7, 8, 9].

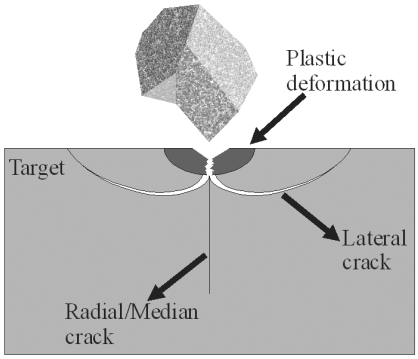

Figure 5.1 The erosion mechanism of a sharp particle.

Previous work on roughness

Models that explain the effect of a single particle impact have been used to predict the roughness created by powder blasting. Buijs [10] calculated the depth of damage due to a particle impact and related it to the roughness. Later, Slikkerveer [4] predicted the roughness by calculating the R_a of a single particle impact. His results showed good agreement and indicated that the roughness solely depends on the kinetic energy of the particle. Lateral crack size and depth decreases with decreasing kinetic

energy so also the surface roughness decreases. At some point the kinetic energy becomes low enough to prevent lateral cracks to initiate. The absence of lateral cracks results in a much lower roughness [10].

5.2 Experiments

5.2.1 Initial roughness

Figure 5.2 shows the surface roughness for different particle kinetic energies. The samples for this particular figure were taken from the experiments in Chapter 6, the roughness measurement is explained in the next section. The solid line represents the trend line ($76.9*U_{kin}^{0.272}$) and the dotted line gives the theoretical curve [4]:

$$R_a = 123101 \cdot \frac{E^{1/2}}{H^{5/6}} U_{kin}^{1/3} \quad [\mu\text{m}], \qquad \textbf{Eq. 5-1}$$

with R_a the surface roughness, E the young's modulus (68.5 ± 1 GPa), H the hardness (5.7 ± 0.3 GPa), and U_{kin} the particle kinetic energy.

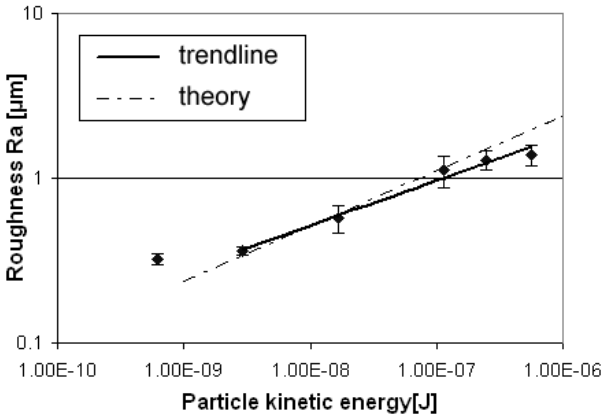

Figure 5.2 Surface roughness versus particle kinetic energy for Pyrex.

These are about the same values as measured and calculated by Slikkerveer. The first data point was omitted from the trend line because of the low kinetic energy. In this region, lateral cracking hardly occurs and the model is not valid.

5.2.2 Post-processes

To examine the post-processes, Pyrex glass wafers were blasted uniformly without structures using two alumina powder sizes: 29 μm and 9 μm with a velocity of respectively 220 m/s and 290 m/s. Samples were taken from

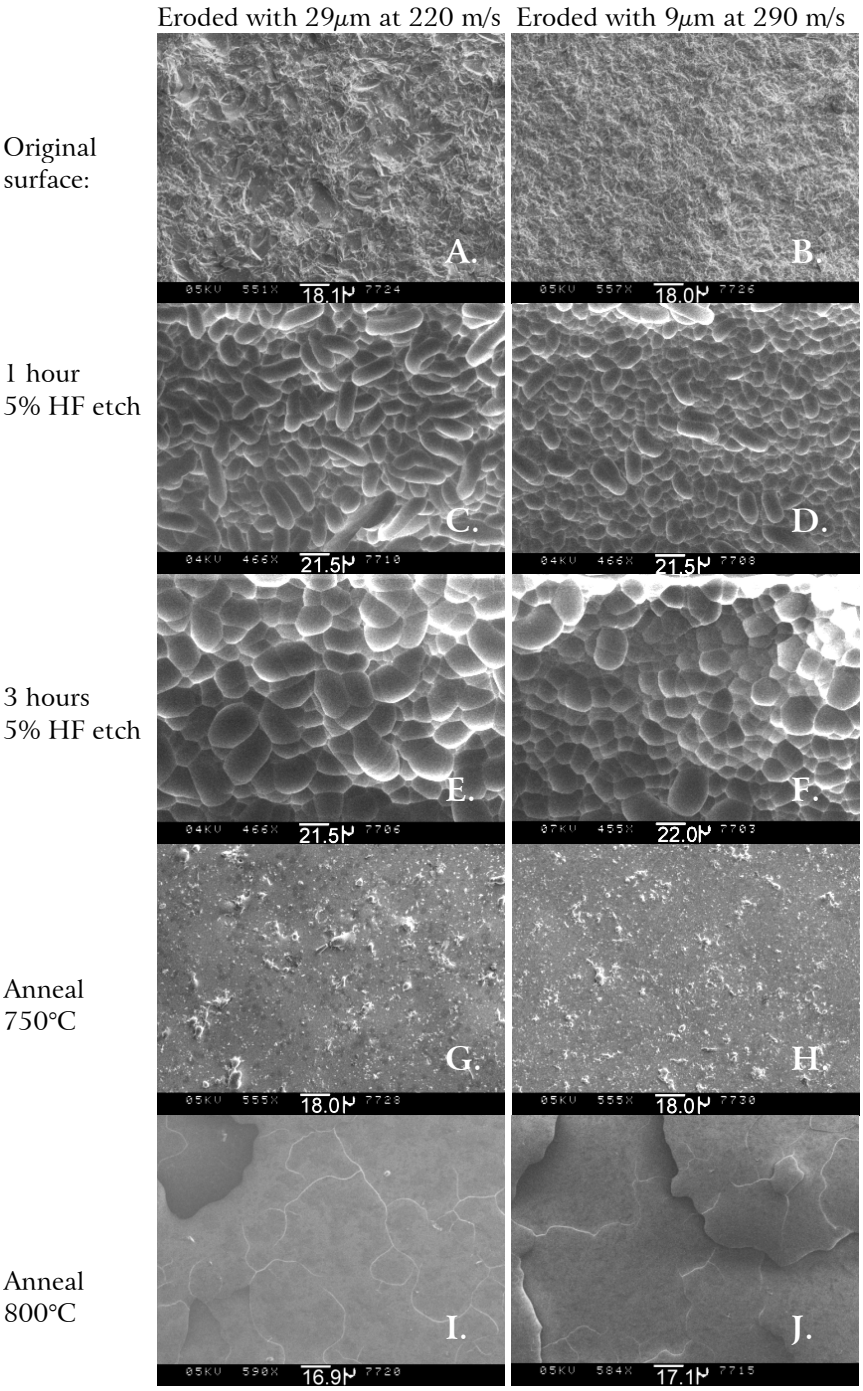

Figure 5.3 SEM pictures of the surface of original and post-processes samples (top view).

this wafer to perform one post-process. The surface roughness was determined by calculating the average R_a of 5 scans (by using the R_a function on the Sloan Dektak II surface profiler). Scan length was 1 mm, stylus tip was 2.5 μm. The R_a was chosen as a first indicator for the surface roughness, and all values are listed in Table 5-1 (the error being the standard deviation of the 5 R_a values). Additional SEM-pictures have been made to observe the roughness quality (Figure 5.3).

Table 5-1. Roughness measurements

Particle size / speed [μm]/[m/s]	**9 / 290**	**29 / 220**
R_a after blasting [μm]	1.2 ± 0.2	2.5 ± 0.6
R_a after finishing with 9 μm particles [μm]	-	2.0 ± 0.3
R_a after finishing with 3 μm particles [μm]	0.9 ± 0.2	1.8 ± 0.5
R_a after 1 hour at 5% HF [μm]	1.7 ± 0.1	3.2 ± 0.2
R_a after 3 hour at 5% HF [μm]	2.2 ± 0.1	3.9 ± 0.5
R_a after 1 hour at 700°C [μm]	1.1 ± 0.1	2.6 ± 0.5
R_a after 1 hour at 750°C [μm]	0.58 ± 0.1	1.8 ± 0.4
R_a after 1 hour at 800°C [μm]	0.091 ± 0.02	0.49 ± 0.3

Post blast

The original blasted surfaces were finished with a smaller particle size, removing approximately an additional 10 μm. As Table 5-1 shows this reduces the surface roughness of the sample.

Post HF-etch

A post HF-etch increases the surface roughness quantitatively (Table 5-1). However, the pictures in Figure 5.3 C. t/m F. show that the roughness quality has also considerably changed.

Post anneal

An anneal step at a temperature ≥750°C decreases the roughness. At 800°C the original surface morphology is almost completely destroyed (Figure 5.3 I. and J.).

5.3 Discussion

5.3.1 Post blast

Table 5-1 shows that finishing the sample with a smaller particle size can reduce the surface roughness. This is not trivial since the erosion process is not isotropic. An explanation would be that when impacting on an elevation, lateral cracks could more easily escape to the surface due to the vicinity of a slope. This can locally enhance the erosion rate, reducing the average roughness.

5.3.2 Post HF-etch

The increase of R_a after a post-HF etch can be explained in two ways. The powder blast process introduces many micro radial cracks (Figure 5.1). After particle impact, these cracks are closed and not detectable by the Dektak. HF-etching however reveals these cracks and widens them which makes the surface becomes rougher. Second, HF etching on a smooth wafer also increases the surface roughness. Next to silica, Pyrex also contains other metal oxides (e.g. aluminumoxide) which have a different etch rate in HF. Grains of this material will be revealed when the surrounding glass is etched away and act as a micro mask so the surface will be unevenly etched [11].

Figure 5.3 C. shows many elliptical ditches. We believe that these originate from the radial cracks that are formed during particle impact. Note that Figure 5.1 only shows the cross section of the radial crack. The actual crack is halfpenny shaped and perpendicular to the cross section. The widths of the ellipses are rather uniform and about 12 μm wide. This consists with the etch rate of 5% HF, which is 6 μm/hour. Vickers indentations, which are often used to predict the effect of single particle impacts, result in two radial cracks perpendicular to each other. However when using irregular shaped particles, there can be a preferable growth direction for a radial crack, resulting in one dominant radial crack. Figure 5.4 shows a single particle impact site with clearly two lateral cracks and one (dominant) radial crack in between.
The ellipse effect is less clear in Figure 5.3 D. because the radial cracks are not as deep when the surface is eroded with 9μm particles. So the elliptical ditches already have become more irregularly shaped. This is also the case for Figure 5.3 E and F.

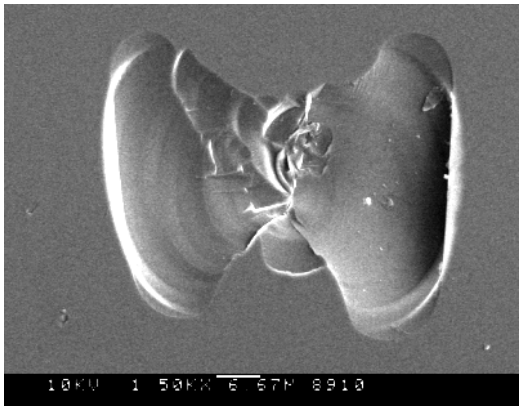

Figure 5.4 A single particle impact site on Pyrex.

5.3.3 Post anneal step

Table 5-1 shows that annealing at 700°C does not effect the surface. A temperature of 750°C does decrease the roughness and Figure 5.3 G. and H. show a smooth surface with some random irregularities. It was found that a temperature of 750°C was still low enough to keep the integrity of a 2-mm wide and 17 μm deep channel. At a temperature of 800°C, the surface becomes very smooth. However, this temperature is so high that any structures in the glass are ruined. Figure 5.3 I. and J. show that the original surface morphology is completely destroyed. In spite of the very slow temperature ramp down, these pictures show small cracks. Note that the softening point of Pyrex is 821°C [12].

5.3.4 Bonding

When making e.g. μfluidic devices, several process steps are involved such as wafer to wafer bonding. It is important to perform the tuning of the surface roughness at the correct fabrication stage, to ensure that bonding is still possible. A post-blasting naturally does not give any problems. The post-HF etch makes the bonding surface rough which can cause problems with direct bonding. Additional bonding surface protection might be necessary. In the case of post annealing, we recommend its use after bonding so that it can enhance the bond strength.

5.4 Conclusion

The surface roughness of powder blasted surfaces was successfully changed both quantitatively (Table 5-1) and qualitative (Figure 5.3) The surface roughness decreases rapidly at very low particle kinetic energies when lateral cracking hardly occurs anymore. Unfortunately, at this point

the powder blast removal rate becomes very low. To decrease the surface roughness and preserve the high removal rate, which is one of the main advantages of powder blasting, the surface can also be finished with a smaller particle size after the fast bulk machining. Post HF-etching increases the surface roughness, mainly due to micro crack widening. These cracks are also responsible for the unusual surface morphology (Figure 5.3 C. t/m F.).
A post-anneal can decrease the roughness. Especially at 800°C the surface becomes relatively smooth. However, at that temperature the macro shape of the glass also changes. An anneal step at 750°C decreases the surface roughness, and at this temperature a 2 mm wide and 17μm shallow channel still keeps its integrity.
Now that we are able to manipulate the surface roughness of a powder blasted channel, further research will be directed to the effects of the roughness on device performance.

5.5 References

1 T. Diepold, E. Obermeier, "Smoothing of ultrasonically drilled holes in borosilicate glass by wet chemical etching", *J. Micromech. Microeng.* 6 (1996) pp. 29–32
2 J.T. Hagan, S. van der Zwaag, "Plastic processes in a range of soda-lime-silica glasses", *J. Non-Crystalline Solids* 64 (1984) pp. 249-268
3 J.T. Hagan, "Cone cracks around Vickers indentations in fused silica glass", *J. Mater. Sci.* 14 (1979) pp. 462-466
4 J.T. Hagan, M.V. Swain, M.V., "The origin of median and lateral cracks around plastic indents in brittle materials", *J. Phys. D: Appl. Phys.* 11 (1978) pp. 2091-2102
5 P.J. Slikkerveer, P.C.P. Bouten, F.H. in't Veld, H. Scholten, "Erosion and damage by sharp particles", *Wear* 217 (1998) pp. 237-250
6 I. Finnie, "Some reflections on the past and future of erosion", *Wear* 186-187 (1995) pp. 1-10
7 A.W. Ruff, S.M. Wiederhorn, "Erosion by solid particle impact", *Treatise on materials Science and Technology,* 16 (1979) pp. 69-126, editor C.M.Preece, *Academic Press,* London
8 B.Lawn, "Fracture of Brittle solids – second edition", Cambridge University Press, Cambridge, United Kingdom (1993)
9 J.E. Ritter, "Erosion of ceramic materials, *Trans Tech Publications*, Zurich, Switzerland (1992)
10 M. Buijs, J.M.M. Pasmans, "Erosion of glass by alumina particles: transitions and exponents", *Wear* 184 (1995) pp. 61-65

11 A. Berthold, "Low-temperature wafer-to-wafer bonding for microchemical systems", *Ph.D. Thesis, Delft University of Technology*, Delft, The Netherlands (2001) pp. 76-79.
12 P. Heller, J. Vervest, H. Wilbrink, "Vademecum voor de glastechniek", *Kluwer technische boeken B.V.* Deventer, The Netherlands, (1992)

CHAPTER 6

The Ductile-Brittle Transition

When particle impacts become less powerful, at some point material removal in powder blasting is not achieved by cracking (brittle erosion) but by cutting and ploughing (ductile erosion). This transition, which causes a decrease in removal rate, is closely studied in this chapter for Pyrex, sodalime glass and silicon.

6.1 Introduction

Information on the solid particle erosion of materials has been available for many years now [1]. Two erosion modes are often distinguished in the literature: brittle and ductile erosion. Brittle erosion deals with material removal due to crack formation, while ductile erosion deals with material removal due to cutting and ploughing. The difference manifests itself in the impact angle dependent erosion rate. (Figure 6.1).

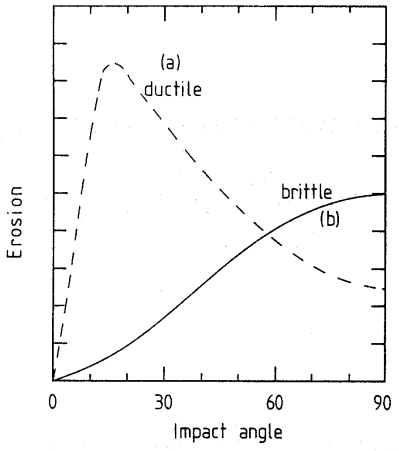

Figure 6.1 Ductile and brittle angle dependent erosion rate [7].

When a brittle material is impacted by a hard sharp particle, the contact area is plastically deformed due to the high compressive and shear stresses and a radial crack is formed. After the impact, the plastic deformation leads to large tensile stresses that result in lateral cracks causing the material removal.

Figure 6.2 gives a very simplified impression of such an event but in reality more than one lateral and redial/median cracks can be present. The exact crack mechanism is also different for "open-structured" glasses (such as fused silica and Pyrex). In that case the glass is plastically deformed by compaction of the glass, making it denser [2]. This makes the indentation more "blunt", and such an indentation can even result in cone cracks, which are normally observed for spherical particles. In the case of sodalime glass, more network modifiers are present in the glass structure and the plastic deformation process takes place along slip lines [3].

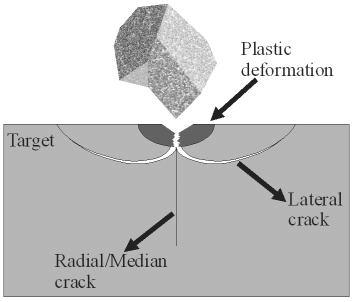

Figure 6.2 Simplified schematic drawing of crack formation from a single particle impact.

The knowledge on erosion has recently been used for the development of a new micromachining tool: Powder Blasting (or Abrasive Jet Machining). This is a fast and low cost directional machining technique for brittle materials like glass, silicon and ceramics with applications in e.g. flat panel displays [4] and μfluidics [5]. This patterned erosion creates typical V-shaped channels and this shape is maintained by the brittle erosion mode [6] (Figure 6.3). Small particles (3-30 μm) are used in powder blasting to obtain a small feature size and a low roughness.

When particle speed and size is decreased, eventually the particles are not able to initiate cracking and will only plastically deform the target. This change in erosion mode is called the ductile-brittle transition [7]. Powder blasting process conditions can get very close to this transition. The change in impact angle dependent erosion rate that accompanies ductile erosion will have an influence on the shape of powder blasted channels. Also, the erosion rate drops sharply and the selectivity with mask materials (used to pattern the target) becomes much smaller. Therefore, in this chapter we studied the erosion rate and impact angle dependent erosion rate during this transition in detail for Pyrex, Sodalime glass and <100> Silicon.

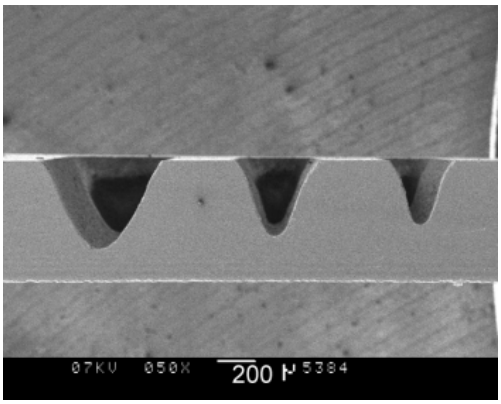

Figure 6.3 Typical channel shape obtained by powder blasting in glass.

6.2 Previous work

Sheldon and Finnie first described the ductile-brittle transition for a brittle target [7]. They demonstrated ductile erosion of "plate glass" using 9 μm SiC particles at 152 m/s and explained this ductile erosion with flaw theory. Cracking only occurs when a flaw is present in the glass.

When the size and speed of the particles is reduced, the stressed area on impact becomes very small. The chance of encountering or completely covering [8] a flaw and initiating a crack decreases. Static indentations are often used to predict the behaviour of a particle impact. For blunt indenters these flaw effects can be predicted using Hertzian models from indentation theories. It shows that the critical load for crack initiation depends on the flaw population of the surface [9].
However, for sharp indenters the critical load is insensitive to the surface state. There is a critical load for radial cracking, but this load is independent of the flaw population. This implies that sharp indenters can create their own flaws [9, 10]. If we can compare the sharp indentor with our sharp particles, than the ductile-brittle transition can not be explained by flaw theory.
Marshall et al. developed a model for lateral cracking due to sharp indentation [11]. This model comprises an "apparent threshold" for lateral cracking. Although this apparent threshold is not based on physical observations of crack initiation, they claim that the dependence on material properties is the same. Erosion is often regarded as many quasi-static single impacts. So the model can be used to extract a threshold in solid particle erosion below which lateral cracking does not occur. Hutchings derived the dependence of the apparent threshold on material properties [12]. Slikkerveer quantified the relation and calculated a value for threshold [13]. The apparent threshold refers to the minimum kinetic energy of a powder particle (U_{th}) at which cracking still occurs:

$$U_{th} = 23225 \cdot \frac{E^{3/2} K_{Ic}^{\ 6}}{H^{13/2}}, \qquad \textbf{Eq. 6-1}$$

where E is the Young's modulus, K_{Ic} the fracture toughness and H the hardness of the target (the particle mass which is used to determine the kinetic energy will be calculated assuming a spherical shape).
Although the first ductile glass erosion graph was already published in 1966, we found only a few additional measurements of this effect in the literature. These results will be compared with our results in the discussion.

6.3 Experimental procedure

The experiments are carried out in the erosion rig at the Cavendish laboratory in Cambridge. The rig consists of a 1 cm diameter barrel (4 m long) and is capable of air velocities up to 200 m/s (see [14, 15] for more details). The particle velocities were previously measured by others (as described in [15]) and small particles (<100 μm) all attain the air

velocity in this barrel. The velocity was set by controlling the airflow. The chuck that holds the samples can rotate to change the impact angle. The barrel has a suction feed powder supply. The powder was supplied through a syringe that was attached to a vibrator. An exact amount of powder is used for each measurement. As the syringe is emptied, the mass flux drops slightly. Therefore, the flux was kept low enough to avoid any flux effects [16]. Glass samples were taped to the chuck, leaving a square area of approximately 1.3x1.3 cm^2. The exact area was measured every time. Before starting the actual measurement, the sample was pre-eroded to avoid any start-up effects. Sharp Al_2O_3 particles of 3, 5 [17] and 9.0, 12.8, 17.1, 22.6, 29.2 μm [18] were used. After erosion, the sample was rinsed and cleaned with ethanol before measuring the weight. Five measurements were taken to obtain the average erosion rate. An example of such a measurement is shown in Figure 6.4.

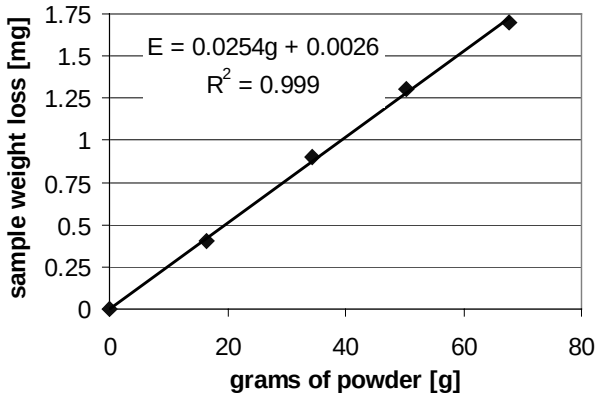

Figure 6.4 Typical erosion rate measurement. Pyrex sample, 3 μm powder, 150 m/s, 90° impact angle.

The exact amount of powder hitting a sample depends on the impact angle because the projected rectangular area is smaller and the particle density is lower outside the core of the jet (diameter ≈ 1cm). The erosion rate at 90° impact and 150 m/s of several rectangular areas were compared with the erosion rate of an un-masked glass plate to calculate the percentage of powder hitting a specific area. Others have shown that the powder distribution is constant for all velocities and particle sizes used in this article [19].

To observe ductile erosion, normally an erosion rate versus impact angle plot is created like in Figure 6.5. In that case, each kinetic energy setting would require many measurements. To do a more practical measurement, we defined the Erosion Classification Value (E_{cv}); the ratio of the erosion

rate at 45° and 90°. In the case of brittle materials this value is about 0.45 (Figure 6.5A), depending on the velocity exponent:

$$E \propto (\sin(\theta) \cdot v)^k,$$
$$E_{CV} = \frac{E_{45°}}{E_{90°}} \approx (0.707)^k, \qquad \text{Eq. 6-2}$$

with E the erosion rate, θ the impact angle, v the particle velocity and k the velocity exponent which is usually about 2.3. Normal ductile materials (for which this equation does not hold) have an E_{CV} of above 1 (Figure 6.5B).

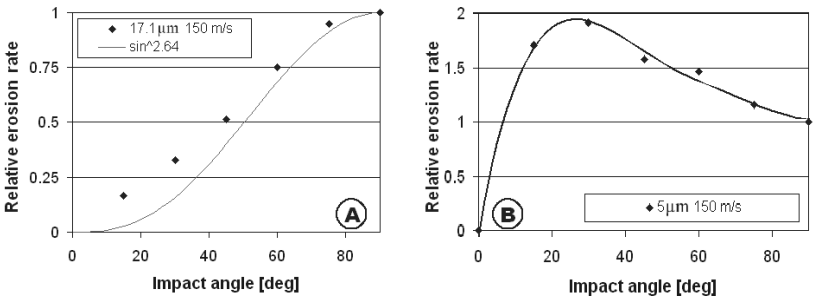

Figure 6.5 Relative erosion versus impact angle for sodalime glass, brittle (A) and ductile (B) erosion.

Since the amount of erosion only depends on the kinetic energy of the particle [13], we measure the E_{CV} and the erosion rate as a function of the kinetic energy. This allows us to use different particles sizes and velocities to measure the kinetic energy exponent (although mainly the particle size is changed). The erosion rate at 90° impact was fitted to the following relation:

$$E_p \propto U_{kin}{}^p, \qquad \text{Eq. 6-3}$$

with E_p the erosion of one particle impact, U_{kin} the particle kinetic energy and p the kinetic energy exponent. This is an approximation for small energy ranges because in theory the relationship is not purely exponential [13]. The velocity exponent k is now twice the kinetic energy exponent p.

6.4 Results

Figure 6.6, Figure 6.7 and Figure 6.8 show the E_{CV} and the erosion rate versus the particle kinetic energy for respectively Pyrex, silicon and sodalime glass.

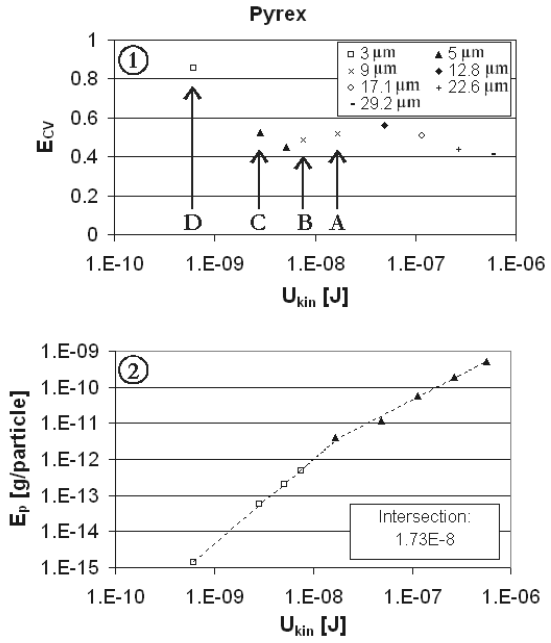

Figure 6.6 E_{CV} and erosion rate versus particle kinetic energy for Pyrex.

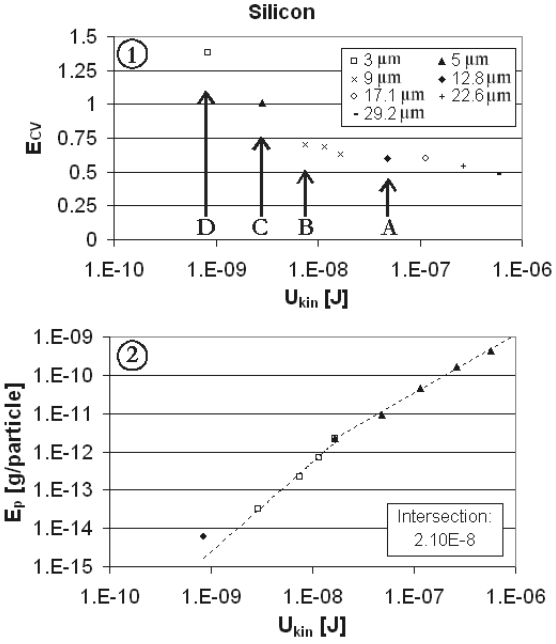

Figure 6.7 E_{CV} and erosion rate versus particle kinetic energy for Silicon.

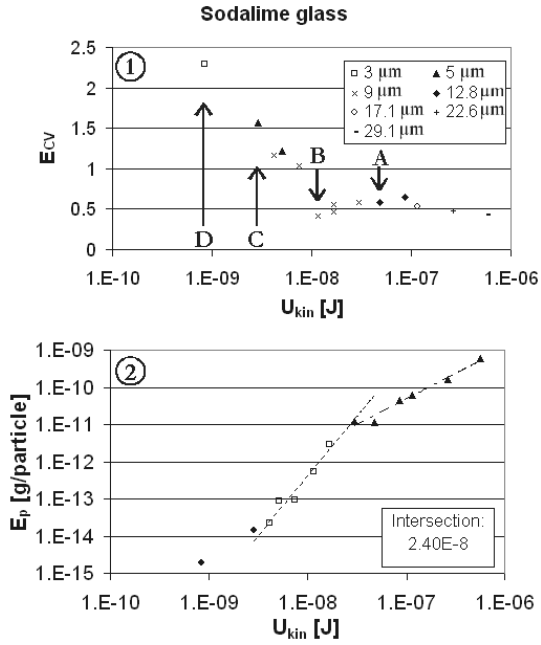

Figure 6.8 E_{CV} and erosion rate versus particle kinetic energy for Sodalime glass.

Note that the E_{CV} scale is different for each figure. Two regimes in erosion rate are clearly visible in Figure 6.6-2. The point where the two regimes meet is taken to be the start of the ductile brittle transition. This start and the erosion rate exponents are summarised in Table 6-1 for the three materials. Kinetic energy exponent p_t refers to the low energy regime, whereas p_b refers to the high-energy regime. The influence of the two regimes on the E_{CV} will be discussed in the next section. Figure 6.9 - Figure 6.11 show SEM pictures of selected experiments of Figure 6.6 - Figure 6.8.

Table 6-1 Several erosion parameters

Material	p_b	p_t	Start transition [nJ]
Pyrex	1.42	2.35	17.3
Silicon	1.53	2.35	21.0
Sodalime	1.38	3.20	24.0

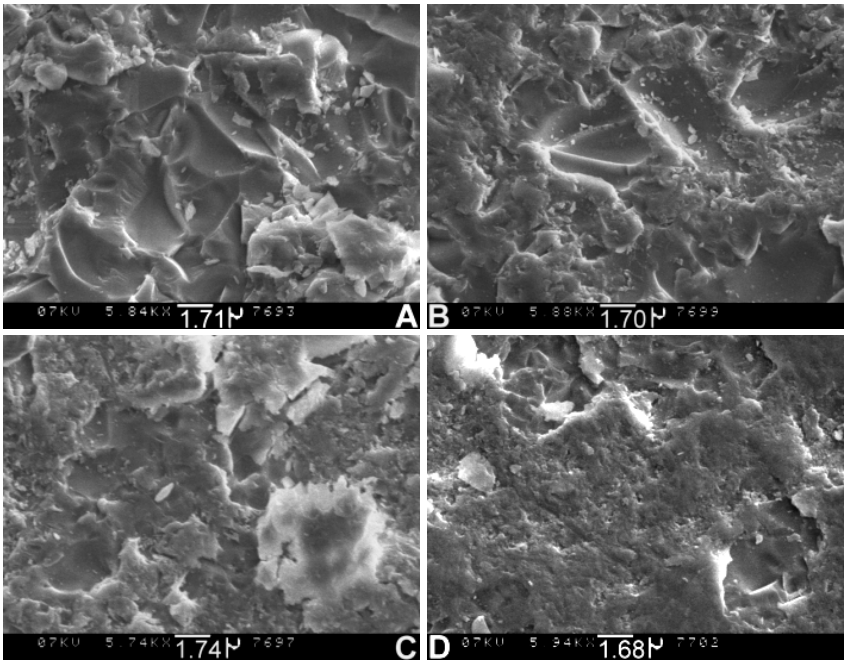

Figure 6.9 SEM pictures of eroded Pyrex, A. t/m D. refers to Figure 4

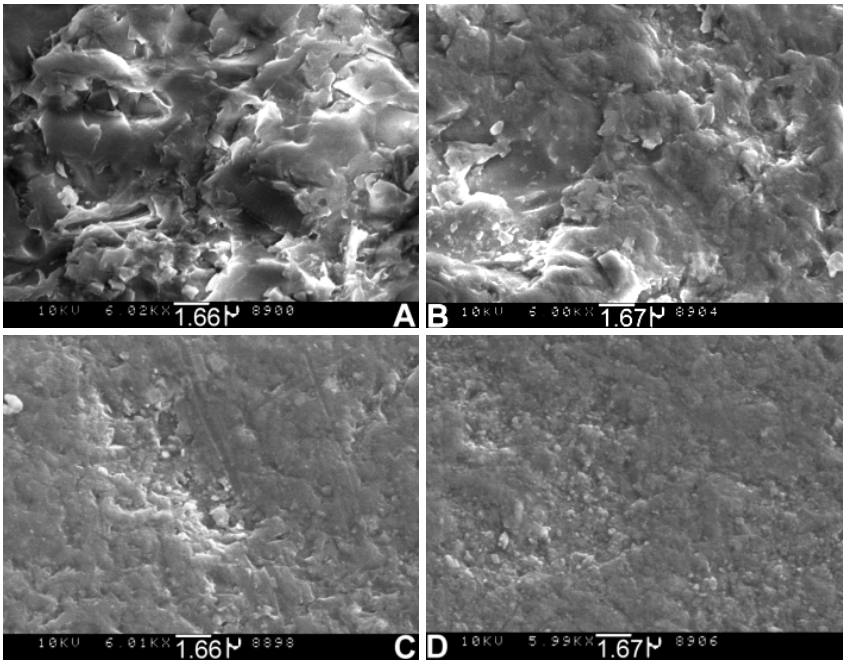

Figure 6.10 SEM pictures of eroded Sodalime glass, A. t/m D. refers to Figure 6.

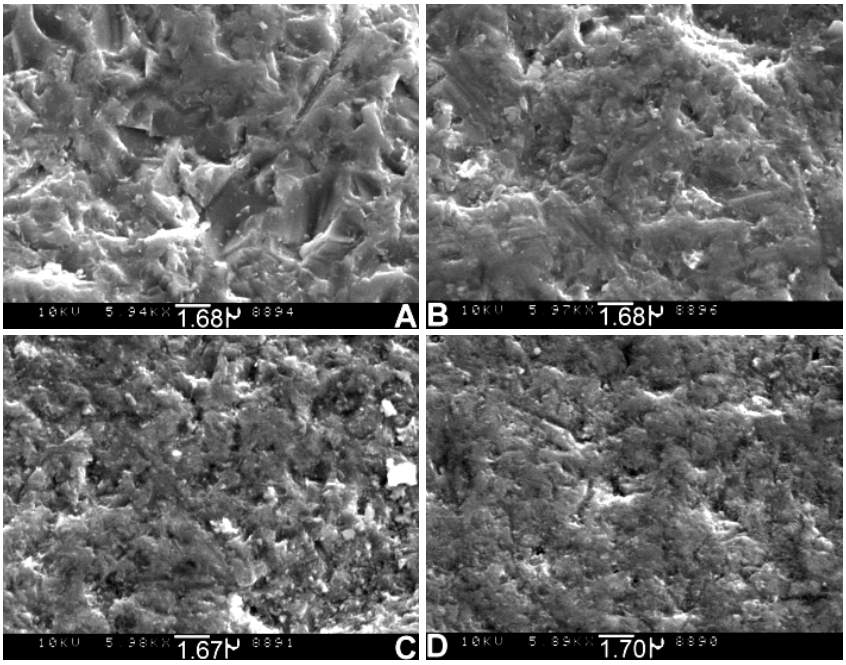

Figure 6.11 SEM pictures of eroded Silicon, A. t/m D. refers to Figure 5

6.5 Discussion

6.5.1 Kinetic energy exponent, two regimes

When the particle kinetic energy is decreased, first the erosion decreases according to a power law with exponent 1.42 for Pyrex (Figure 6.6-1 and Table 6-1). This exponent is higher compared to the one found by Slikkerveer (1.23), which was determined with energies between $1 \cdot 10^{-8}$ and $1 \cdot 10^{-4}$ J. However, we feel that those results also indicate a higher kinetic energy exponent for erosion below $1 \cdot 10^{-6}$ J. According to the theory of Slikkerveer et al., the exponent is independent of material properties for normal brittle erosion [13]. Table 6-1 lists the similar exponent values of silicon and sodalime glass. A higher velocity exponent (which we take to be twice the kinetic energy exponent) was already observed by others for smaller Al_2O_3 particles on <111> silicon [20] and mulite [21].

Below approximately $1 \cdot 10^{-8}$ J. there is a second regime which exhibits a significantly higher energy exponent. Both the first and the second regime are indicated by a trendline. The intersection of these trendlines indicates the start of the transition from only brittle erosion to only

ductile erosion (going from a high to a lower kinetic energy). In the second regime, this transition slowly takes place. This progressive transition is a result of the many unequal impact events in erosion. Particle shapes, size, velocities and impact orientations are not completely identical so each impact has a different degree of effectiveness. The lower the kinetic energy, the less the chance a positive result (= lateral crack initiation) results from a single impact. The kinetic energy exponent of silicon and sodalime even seems to restore itself to a lower value at very low energies. At this point, almost every impact event is ductile and the energy exponent should return to normal (normal erosion on ductile materials usually exhibits a velocity exponent between 2.2 and 2.4 [1])
The effect of these two regimes on the E_{CV} will now be discussed.

6.5.2 E_{CV}, three stages

The E_{CV} shows typical behaviour during the transition for all three materials investigated in this paper which we will discuss on the basis of Figure 6.6, the erosion of Pyrex.
Figure 6.6-1 can be divided into three stages. Going from high to low energy, first the E_{CV} rises to a maximum at approximately $4 \cdot 10^{-8}$ J. The erosion velocity exponent in this stage (twice the energy exponent) is 2.84, which according to Eq 2. should result in an E_{CV} of 0.37. The actual value lies between 0.41 - 0.56. Ballout [22] showed that for sharp particles (>63 μm), the lateral crack propagation is enhanced by tangential forces. This can explain the higher than expected erosion rate at 45°. The initial rise of E_{CV} could indicate a relative enhancement of this tangential effect at lower kinetic energies.
In the second stage the E_{CV} decreases to a minimum at approximately $5 \cdot 10^{-9}$ J. The change in the E_{CV} slope around $4 \cdot 10^{-8}$ J. occurs because of the change of kinetic energy exponent at $1.7 \cdot 10^{-8}$ J. as shown in Figure 6.6B. The fact that the local E_{CV} maximum lies at a higher energy compared to the exponent change is because the amount of energy that is transferred to the target by particles impacting at 45° will sooner be below the threshold.
Finally in the third stage, ductile impact events at 90° become more and more important, which increases the E_{CV} eventually to a value >1. The other two materials (Figure 6.7 for silicon and Figure 6.8 for sodalime glass) show the same qualitative behaviour, although the transitions take place at a different kinetic energy. Sodalime glass shows the most pronounced ductile behaviour at the highest energies, followed by silicon and Pyrex.

Theoretical threshold

We can calculate the apparent lateral threshold energy when using the material properties listed in Table 6-2. These values are from several literature sources and own measurements, so they can only be used as an indication of the actual value.

Table 6-2 Material propertiesselected from several literature sources

Material	E [GPa]		K_{Ic} [MPa $m^{1/2}$]		H [GPa]	
Pyrex	64	[23]	0.77	[23]	5.7±0.3	[24]
Si	130 - 187	[25]	0.9 - 1.3	[26, 27]	9.3 - 10	[28, 29]
Sodalime	86.1±0.1	[24]	0.74±0.05	[24]	5.7±0.2	[24]

In Table 6-3 we now compare the apparent lateral threshold energy (Eq. 6-1) with the start of the ductile-brittle transition found in this paper

Table 6-3 Calculated apparent lateral threshold

Material	U_{th} [nJ]	Start transition (this paper) [nJ]
Pyrex	30	17
Si	32	21
Sodalime	37	24

The U_{th} values are close to the start of the transitions as measured in this paper and the order in which the materials erode ductile is the same. However, because of the large exponents used in Eq. 6-1, a small error in material properties leads to a large error in threshold energy. The energy values are too close together to do a valid statement on the theories with these material property values.

Sodalime versus Pyrex

Although sodalime and the more open structured Pyrex behave quite different on indentation, their E_{cv} graphs are qualitatively very similar. This difference in structure will have an additional influence on the ductile-brittle threshold. Note that Eq. 6-1 does not make a difference between normal glasses, and open-structure glasses like Pyrex. Cone cracks might play a role in Pyrex erosion and their initiation can depend differently on parameters.

6.5.3 SEM study

Figure 6.10 show the surfaces of the eroded sodalime glass samples for low kinetic energies. At the highest energy, overall lateral cracking still occurs. As the energy is lowered, less lateral cracks can be observed and the erosion gets more ductile. At the lowest energy, lateral cracks were rare and never smooth (like you see when a new lateral crack removes a chip). They are already ductile eroded by many other particles, indicating that lateral cracking occurs in only a fraction of the particle impact events.

The silicon and Pyrex samples in Figure 6.11 and Figure 6.9 show similar behaviour, although lateral cracking still occurs quite often for Pyrex at the lowest energy compared to sodalime. This fits with the fact that the E_{CV} at that energy is much larger for sodalime glass (2.3) than for Pyrex (0.85).

6.5.4 Flaw theory

Although flaw-theory was not used to explain the ductile-brittle transition, flaws still have a certain effect. If pre-existing flaws are available, lateral cracking still may occur below the energy threshold. In Figure 6.12 for sodalime glass, there are still some (old) lateral cracks visible even for $E_{CV} > 1$. In the case of silicon in Figure 6.13, which can be expected to have fewer flaws, the surface appears more uniformly damaged. So flaws play a role in the surface morphology rather than in the position of the threshold of the ductile brittle transition.

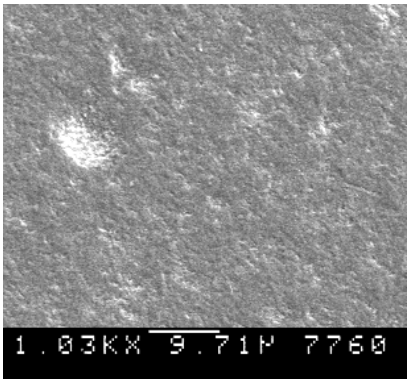

Figure 6.12 Ductile eroded sodalime glass

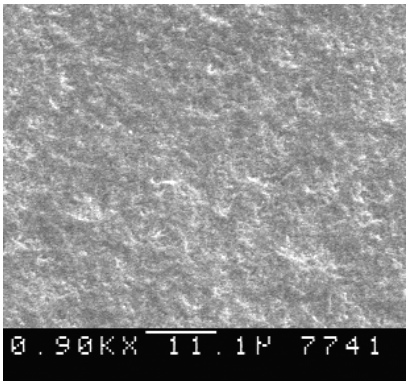

Figure 6.13 Ductile eroded silicon

6.5.5 Other work

Although the detailed look at the ductile-brittle transition as presented in this work is unprecedented, there are some reports on single ductile

erosion measurements on normally brittle materials. The particle size, speed, kinetic energy and E_{cv} are shown for each measurement in Table 6-4 if available. The values of the measurements from this paper are taken at the point were $E_{cv}=1$.

Table 6-4 Ductile erosion experiments compared

Material	Particle diameter [μm]	Speed [m/s]	U_{kin} [nJ]	E_{cv}	Reference
Pyrex	- (Al_2O_3)	-	± 0.3	1.0	This paper
Silicon	5 (Al_2O_3)	150	2.9	1.0	This paper
Sodalime glass	9 (Al_2O_3)	100	7.4	1.0	This paper
Pyrex	9 (SiC)	152	14	1.7	[1]
Plate glass	9 (SiC)	152	14	1.7	[7]
Wisdom tooth	9 (SiC)	244	36	-	[1]

All other experiments show erosion energies at which ductile erosion occurs that are larger than the ones found in this paper. Different target material properties, which were not given, as well as errors in the particle size or speed can be responsible for this.

6.6 Conclusions

In this paper, for the first time a detailed picture of the ductile-brittle transition was given. It was studied using sharp Al_2O_3 particles for different sizes and velocities (size 3-29 μm, velocity 75-200 m/s) on three materials: sodalime glass, Pyrex and silicon.
The transition does not occur suddenly, but extends over at least one decade of kinetic energy. During this transition, the kinetic energy exponent becomes much larger.

To investigate the impact angle dependent erosion rate, we introduced the Erosion Classification Value (E_{CV}) which is the ratio of the erosion at 45° over the erosion at 90° impact angle. Brittle erosion has an E_{CV} of about 0.45, whereas the E_{CV} of ductile erosion is larger than 1. It can give a quick indication of the erosion mechanism.
The large kinetic energy exponent during the transition has two effects on the E_{CV}. First, due to the higher energy exponent, the E_{CV} slightly decreases. Second, when kinetic energy is further reduced the ductile erosion mechanism becomes more and more important and the E_{CV} can eventually increase to a ductile value. This progressive transition is a result of the many unequal impact events in erosion. Particle shapes, size, velocities and impact orientations are not identical so each impact has a

different degree of effectiveness. The chance a lateral crack is initiated from a particle impact becomes smaller as the kinetic energy decreases.
The three materials that were investigated all showed this qualitatively behaviour. There was however a difference in energy transition values. Sodalime glass was the first to erode in a ductile manner and achieved the largest E_{CV}, followed by silicon and Pyrex. This order in ductility agrees with the theoretical threshold energies. However, those equations deal with large exponents, making the results very sensitive to a small deviation in material properties. The equation also does not take into account the import fact that Pyrex is an open structure glass which compacts (densifies) on impact while sodalime glass deforms due to the shear stresses along slip lines [3]. This results in different crack initiations, which can have a large impact on the ductile-brittle transition. More research is required to determine exact consequences of this effect for the transition.
In the case of powder blasting, a 25-50% higher E_{CV} around a particle kinetic energy of $4 \cdot 10^{-8}$ J. can result in steeper sidewalls, although the effect is probably small. The fast decrease in erosion rate below approximately $2 \cdot 10^{-8}$ J. is the beginning of the end of fast glass machining and practical powder blasting. As the glass erosion becomes ductile, the selectivity with mask materials (used to pattern the target) will drop, which makes this erosion mode less suitable for glass machining.

6.7 Acknowledgement

I would like to thank Prof. John Field for giving me the opportunity to stay at the University of Cambridge with his group for a few months, which allowed me to do the measurements in this chapter. Also, the personnel of the PCS Fracture & Shock Physics Group is thanked for their co-operation, especially Alun Davies who allowed me to extensively use “his” sandblasting rig.

6.8 References

1 I. Finnie,”Some reflections on the past and future of erosion”, *Wear* 186-187 (1995) pp. 1-10
2 J.T. Hagan, “Cone cracks around Vickers indentations in fused silica glass”, *J. Mater. Sci.* 14 (1979) pp. 462-466
3 J.T. Hagan, S. van der Zwaag, “Plastic processes in a range of soda-lime-silica glasses”, *J. Non-Crystalline Solids* 64 (1984) pp. 249-268
4 H.J. Ligthart, P.J. Slikkerveer, F.H. int't Veld, P.H.W. Swinkels, M.H. Zonneveld, “Glass and glass machining in ZEUS panels”, *Philips J. Res.* 50 (1996) pp. 475-499

5 S. Schlautmann, H. Wensink, R. Schasfoort, M. Elwenspoek, A. van den Berg, "Powder-blasting technology as an alternative tool for microfabrication of capillary electrophoresis chips with integrated conductivity sensors", *J. Micromech. Microeng.* 11 (2001) pp. 386-389
6 P.J. Slikkerveer, F.H. in't Veld, "Model for patterned erosion", *Wear* 233-235 (1999) pp. 377–386
7 G.L. Sheldon, I. Finnie, "On the Ductile Behaviour of Nominally Brittle Materials During Erosive Cutting", *J. Eng. Ind* nov. (1966) pp. 387-392
8 P.D. Warren, D.A. Hills, S.G. Roberts, "Influence of surface cracks on Hertzian fracture", *J.Hard Mater.* 5 (1994) pp. 213-217
9 B.Lawn, "Fracture of Brittle Solids – Second Edition", *Cambridge University press*, Cambridge, United Kingdom (1993) p. 282
10 J.T. Hagan, M.V. Swain, "The origin of median and lateral cracks around plastic indents in brittle materials", *J. Phys. D: Appl. Phys.* 11 (1978) pp. 2091-2102
11 D.B. Marshall, B.R. Lawn, A.G. Evans, "Elastic/Plastic Damage in Ceramics: The Lateral Crack System", *J.Am.Cer. Soc.* 65 (1982) pp. 561-566
12 I.M. Hutchings, "Ductile-brittle transitions and wear maps for the erosion and abrasion of brittle materials", *J. Phys. D.: Appl. Phys.* 25 (1992) pp. A212-A221
13 P.J. Slikkerveer, P.C.P. Bouten, F.H. in 't Veld, H. Scholten, "Erosion and damage by sharp particles", *Wear* 217 (1998) pp. 237-250
14 J.E. Field, Q. Sun, H. Gao, G.H. Jilbert, I.M. Hutchings, J.A. Little, "Solid particle erosion of IR-transmitting materials and diamond composites", *Wear* 186-187 (1995) pp. 195-202
15 R.H. Telling, J.E. Field "The erosion of diamond, sapphire and zinc sulphide by quartz particles", *Wear* pp. 233-235 (1999) pp. 666-673
16 F.H. in't Veld, P.J. Slikkerveer, "Towards prediction of flux effects in powder blasting nozzles", *Wear* 215 (1998) pp. 131-136
17 Buehler, 41 Waukegan Rd., Lake Bluff. IL 60044, USA.
18 Treibacher Schleifmittel GmbH, Ferroweg 1, D-79725 Laufenburg, Germany, Tel. +49.7763.9330
19 A.Davies, private communications
20 R.O. Scattergood, J.L. Routbort, "Velocity and size dependences of the erosion rate in silicon", *Wear* 67 (1981) pp. 227-232
21 C.T. Morrison, J.L. Routbort, R.O. Scattergood, "Solid particle erosion of mullite", *Wear* 105 (1985) pp. 19-27
22 Y. Ballout, J.A. Mathis, J.E.Talia, "Solid particle erosion mechanism in glass", *Wear* 196 (1996) pp. 263-269

23 P. Heller, J. Vervest, H. Wilbrink, "Vademecum voor de glastechniek", *Kluwer technische boeken B.V.* Deventer, The Netherlands, (1992)
24 Measurements made by the author in the Cavendish Laboratory, Cambridge. Hardness and fracture toughness measured using a microhardness tester (loads 100-300 grams, loading time 30 s.). Young's modulus deterimed by measuring the ultrasonic wave speed.
25 M.Madou, "Fundamentals of Microfabrication", *CRC Press*, London, United Kingdom (1997) p. 159
26 F. Ericson, J.A. Schweitz, "Micromechanical fracture strength of silicon", *J. Appl. Phys.* 68 (1990) pp. 5840-5844
27 Y.Chiang D.P. Birnie III, W.D.Kingery, "Physical Ceramics", *Wiley*, New York, USA (1997) p. 484
28 B.R. Lawn, D.B. Marshall, "Hardness, Toughness, and Brittleness: An Indentation Analysis", *J. Am. Ceram. Soc.* 62 (1979) pp. 347-350
29 P.H. Shipway, I.M. Hutchings, "The role of particle properties in the erosion of brittle materials", *Wear* 193 (1996) pp. 105-113

Blast Lag

Powder blasted structures have inclined sidewalls, which has an influence on the channel depth and aspect ratio. The effect of powder particle size and particle jet impact angle on the wall inclination is calculated and measured in this chapter.

7.1 Introduction

A mask is applied on the target surface to be able to create complex structures with powder blasting. This partial protection has an influence on the cross-sectional shape of the blasted holes and channels.

The sidewalls of a powder blasted structure are not perfectly straight but they have a certain inclination. The origin of this inclination lies probably in the inability for particles to impact infinitely close to the mask border [1]. When a particle approaches the target to impact at a distance from the mask border which is smaller than the average particle size, it is likely that the particle will be obstructed or decelerated by the mask border. This will result in a gradual removal rate decrease towards the mask border. This removal rate gradient creates the beginning of the

slant sidewall. Once this initial inclination is created, it is maintained by the brittle erosion characteristic (Figure 7.1). Particle impact at an impact angle $\varphi = 90°$ (in the middle of the channel) results in a higher removal rate compared to an impact at a lower angle (on the sidewalls).

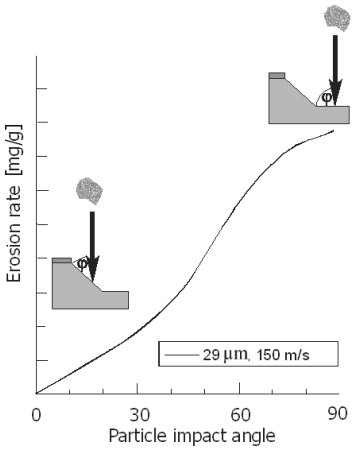

Figure 7.1 Removal rate dependence on impact angle for Pyrex.

The sidewall inclination starts at the edge and becomes larger during blasting. Three stages in the shape of the structure (a channel or hole), can be distinguished (Figure 7.2). First a flat centre section with a slant wall on each side creates a bowl shape. These sidewalls grow towards each other to create the second stage: a rounded V-shape. Continues blasting will lead to the third convex-concave shape, which arises due to second order particles impacts [2].

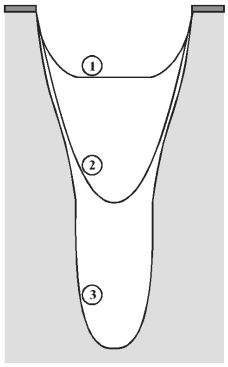

Figure 7.2 Three stages in the channel shape.

Two main problems are associated with the side wall inclination. The three stages are the same for any hole or channel, but the timing of the transition between the stages depends on the dimensions of the mask opening. A small mask opening will sooner result in a V-shaped channel. From that time on, every particle will impact on a sidewall with a small impact angle and the removal rate will decrease. A large mask opening will reach this point at a later time and at a greater depth. So side wall inclination results in what we call the blast lag: wide channels become deeper compared to smaller channels.
The decrease of removal rate in stage two makes it also more difficult to obtain high aspect ratios. Although high aspect ratios are possible since the removal rate does not vanish, the continuous decrease in removal rate in stage two puts a disproportionate strain on the mask material. The quality of the mask material therefore limits the maximum attainable channel depth. In this chapter we will discuss and show two basic methods to decrease the blast lag.

7.2 Decreasing Blast Lag

The blast lag occurs when the cross-section of one or more channels has reached a stage two shape (Figure 7.2). We will concentrate in this chapter on comparing channels that are all in stage two.

7.2.1 Smaller particles

A decrease in blast lag when using smaller particles can be expected for several reasons. The size of the area near the mask border that is not fully attacked by the powder particles (the flux boundary layer [1]) depends on the particle size. Smaller particles result in a smaller boundary layer, and consequently, the effective channel width is larger. For wider channels it takes a longer time for the two sidewalls to meet and hence the blast lag is reduced. The increase in effective channel width is relatively larger for smaller channels. Second, smaller particles can access small and narrow spots more easily and create a sharper and hence deeper V-shape cross-section, which will also decrease the blast lag. The magnitude of these two effects can easily be calculated for the simplified channel cross-section in Figure 7.3:

$$d = d_0 - r\left(\frac{1}{\tan(\alpha)} + \frac{1}{\sin(\alpha)} - 1\right), \qquad \textbf{Eq. 7-1}$$

with d the actual depth, d_0 the depth when using particles with a negligible size, r the average radius of the particles and α the side wall inclination angle. The tan-term represents the size-effect on the channel edge, and the sin-term represents the size-effect in the channel bottom.

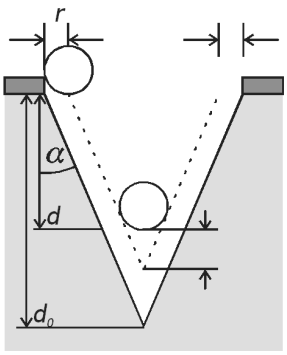

Figure 7.3. The effect of particle size on blast lag for a simplified stage two shape

This equation shows that the particle size effect increases for larger particles and for a larger α (deeper channels). Figure 7.4 shows d versus d_0 for a 100 μm wide channel and 9 and 29.2 μm particles. Note that this is only valid for channels from which the cross-section is in a stage-two shape.

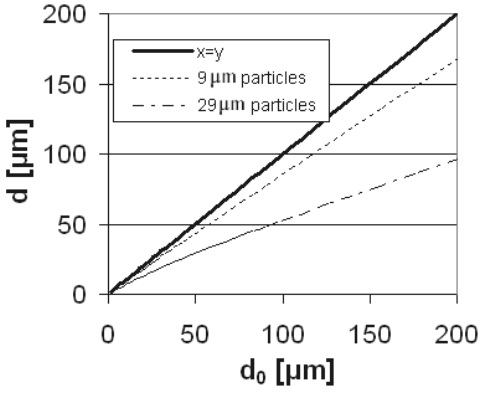

Figure 7.4. Calculated influence of particle size on blast lag for a 100µm wide channel (Eq. 7-1).

A simulation of Slikkerveer et al. indicates a possible third positive effect of small particles on the blast lag [1]. It shows that by using smaller particles (analogue to a smaller delta in that simulation) a different initiation of the sidewall may be expected. Since the flux boundary layer is smaller, the initial inclination after a certain time becomes steeper which also results in steeper sidewalls during blasting.

7.2.2 Oblique Blasting

An intuitive method to produce steeper sidewalls is by changing the jet impact angle. This will decrease the removal rate at the flat bottom of the structure, while the sidewall removal rate increases, because of the larger effective impact angle. Oblique blasting has already been studied to accurately predict the shape of powder blasted structures [3, 4]. Blasting from two sides with a lower impact angle can result in a U-shaped channel, rather than the usual V-shape [2].

The effect of a lower impact angle will be investigated using an adapted impact angle dependent removal rate graph. In such a graph, the removal rate of the sidewall (normal to the surface) relative to the removal rate of the flat bottom is shown. The removal rate is usually approximated by the following equation:

$$E \propto \sin(\varphi)^k , \qquad \textbf{Eq. 7-2}$$

with E the removal rate, φ the impact angle and k equal to 2.8 for the parameters used in this chapter (see Chapter 6). In Two-sided Oblique Blasting (TOB), two particles jets are symmetrically placed at a lower impact angle φ. The resulting sidewall removal rate perpendicular to the original flat surface is (see Figure 7.5):

$$E_w = \frac{\sin(\theta_{\max})^{k+1} + \sin(\theta_{\min})^{k+1}}{2\sin(\alpha)},$$

where,

$$\theta_{\max} = \alpha + (\frac{1}{2}\pi - \varphi), \qquad \textbf{Eq. 7-3}$$

$$\theta_{\min} = \alpha - (\frac{1}{2}\pi - \varphi),$$

with α the wall inclination angle.

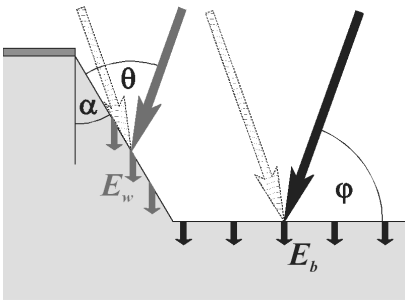

Figure 7.5 Indication of the parameters used in the equations.

The removal rate on the flat bottom decreases according to:

$$E_b = \sin(\varphi)^{k+1}. \qquad \textbf{Eq. 7-4}$$

Blasting from two fixed angles can be used to create specific parallel shapes. However, it cannot be used as a general method for complex designs. Therefore we introduce Radial Oblique Blasting (ROB, Figure 7.6).

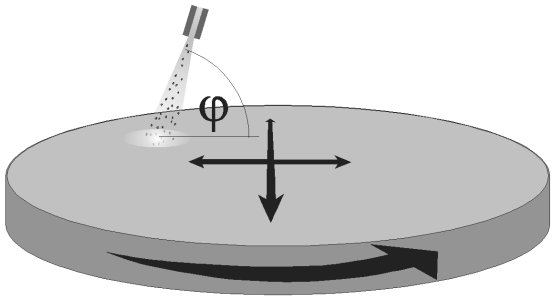

Figure 7.6 Principle of Radial Oblique Blasting.

Again, the particle jet is placed at a lower angle with respect to the flat surface. But now the target is rotated so that the particle jet impacts at a lower angle on the target from all directions. It can be calculated that the E_w changes during a rotation according to:

$$E_w = \frac{\sin(\theta)^{k+1}}{\sin(\alpha)},$$

where, **Eq. 7-5**

$$\theta = \operatorname{asin}\left(\frac{\cos(\gamma)\cos(\alpha) + \tan(\varphi)\sin(\alpha)}{\sqrt{1+\tan(\varphi)^2}}\right),$$

with the rotation angle γ between 0-360°. Integrating E_w over γ and dividing by 2π results in the average E_w. This has been done numerically for φ = 60° and a varying α. Figure 7.7 shows the removal rate of the sidewall relative to the removal rate of a flat bottom as a function of the wall inclination angle.

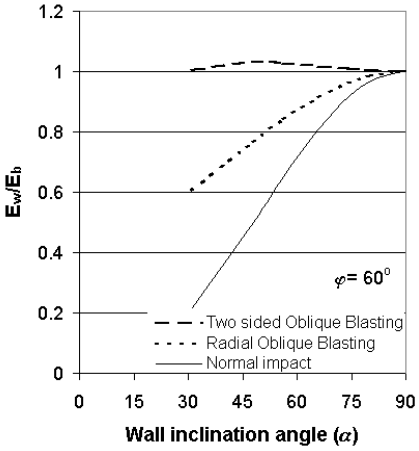

Figure 7.7 Calculated modified impact angle dependent removal rate.

Both removal rates are perpendicular to the flat surface. The curve "Two-sided oblique blasting" refers to Eq. 7-3 (two symmetrically placed particle jets) and the curve "Radial oblique blasting" refers to Eq. 7-5 (particle jet from all directions). The solid line indicates the lower bound when $\varphi = 90°$ for which both methods coincide. The equations are calculated for $90° > \alpha > 90°-\varphi$. For an even lower α the sidewall will partly shield the bottom from the particle jet which is an undesirable situation in this case. To examine the effect of ROB for different φ's, we define the Erosion Classification Value (E_{cv}); the ratio of the erosion rate at 45° and 90°. A higher E_{cv} indicates a higher side wall removal rate and hence steeper sidewalls. Figure 7.8 shows the E_{cv} as a function of φ. As can be expected, the lower impact angle enhances the relative removal rate on the walls. TOB has a stronger effect on the relative removal rate compared to ROB.

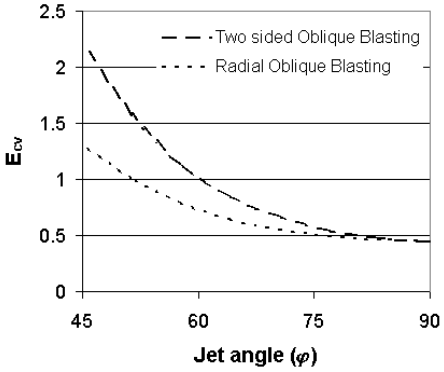

Figure 7.8 Calculated E_{CV} for oblique blasting.

7.3 Experiments

Sidewalls in powder blasting are not as well defined, as Figure 7.3 suggests. The actual slope is rounded and can therefore not be defined by one specific angle (Figure 7.2). However, straighter walls will automatically decrease the blast lag, which is also the ultimate goal of this exercise. Therefore the blast lag is measured to compare the different process settings. Channels with a width of 500, 300, 200 and 100 μm are blasted in Pyrex glass until the reference area (a unmasked part of the target) reached a depth of about 200 μm. At that time, all channels are (almost) in stage two. The depth of the channels relative to this reference depth is defined to be the blast lag. The blasting pressure was set to be 4.5 bar which results in velocities between 230-270 m/s depending on the particle size.

7.3.1 Smaller particles

Average powder sizes of 9.0, 12.8, 17.1, 22.8, and 29.2 μm [5] were used for blasting. Electroplated copper with a thickness between 14 – 16 μm was used as the mask material. The channel width increases during blasting due to the erosion of the mask edges. The rate of channel widening depends on the mask thickness and particle size. The widening did not correlate with the lag decrease and we assume that the effect on the blast lag can be ignored in this case.
The blast lag for these settings is shown in Figure 7.9.

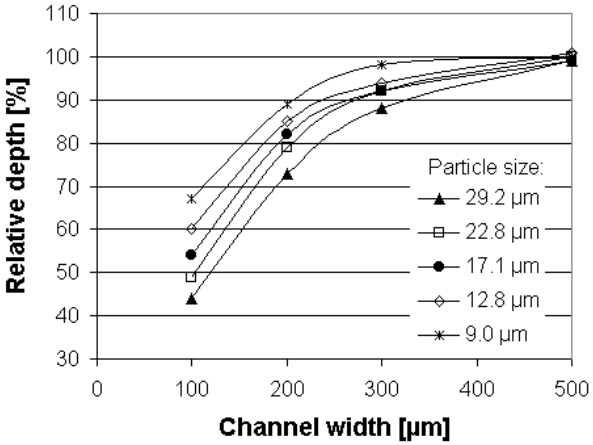

Figure 7.9 A decreasing blast lag with decreasing particle size.

7.3.2 Oblique blasting

The rotation of the target in combination with the x-y scanning movement of the nozzle can produce Lisajous patterns, which would result in an unevenly powder blasted surface. To avoid this, the rotation speed is made relatively high (210 rpm) compared to the scanning motion (1.1 by 34 strokes per minute). Average powder sizes of 9.0 and 29.2 μm were used for blasting. Electroplated copper with a thickness of about 10 or 20 μm was used as the mask material on Pyrex. The smaller impact angle will increase the erosion of copper (due to the ductile erosion characteristic), which results in faster widening rate of the mask edges. The consequences of this effect on the blast lag cannot be ignored anymore. Therefore, oblique blasting was performed on samples with a thicker mask so that the final mask widening for all samples is approximately 15 μm.
Figure 7.10 shows the effect of ROB on the blast lag. The blast lag for normal impact, which is shown as a reference, was also measured with a rotating target.

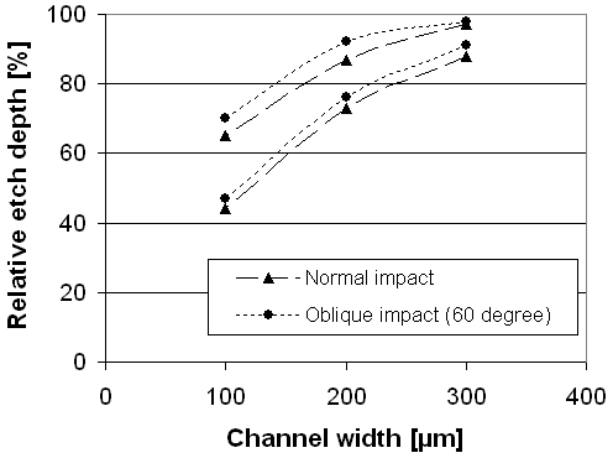

Figure 7.10 A decreasing blast lag with Radial Oblique Blasting.

7.4 Discussion

7.4.1 Smaller particles

Figure 7.9 clearly shows that the blast lag is decreased when the particle size is smaller. The depth increase can be as large as 36% when using 9 μm particles in stead of 29.2 μm particles.

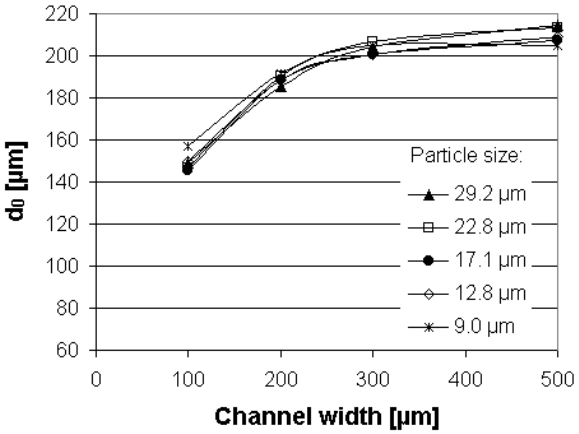

Figure 7.11 All values of d_o *calculated from Eq. 7-1 and Figure 7.9.*

Although the amount of blast lag can not be predicted from Eq. 7-1, the validity of this equation can be checked. For a fixed channel width, d_o is independent of particle size. Using the measurements of Figure 7.9, the values of d_o for each channel width can be calculated (Figure 7.11, α is approximated by using the channel width minus the particle size, and the measured channel depth).

All points are very close to each other which shows that Eq. 7-1 is a good approximation to calculate the effect of particle size on the blast lag for rounded V-shaped channels.
Smaller particles decrease the blast lag, but the disadvantage is that the selectivity of the target with the mask material and the absolute target removal rate also decreases (in case of Pyrex/copper the selectivity is 71 for 29.2 μm particles and 40 for 9 μm particles, see Chapter 4). The removal rate can partially be restored by increasing the particle speed. The erosion velocity exponent is approximately 2.8, 2.3 and 3.0 for respectively Pyrex (Chapter 6), metals [6] and the powder blasting resist foil BF410 [7]. This means that a higher particle velocity will increase the selectivity when using a metal mask, and decrease when using BF410. At very high velocities the selectivity can decrease due to the particle defragmentation which negatively influences the target removal rate.

7.4.2 Oblique blasting

Figure 7.10 shows that Radial Oblique Blasting (ROB) decreases the blast lag for both 9 and 29.2 μm particles. However the change in lag is only a few percent. The predicted effects of oblique blasting (Figure 7.7) cannot be used directly to calculate the absolute effect on the blast lag. A

blasting simulation that uses the modified impact angle dependent removal rate would be required to predict the channel profile and blast lag for oblique blasting.
A number of disadvantages are associated with ROB. The decrease of particle impact angle will increase the mask erosion rate and decrease the target removal rate, which decreases the selectivity. Also, if the channel aspect ratio becomes very large, the sidewalls shield (part of) the channel bottom from the particle jet, which is unwanted in our case. The process time after which shielding starts depends on the impact angle and the particle size. Shielding already occurs in the beginning of the process at the thick mask edges. Edge shielding decreases the effective channel width with an amount that depends on the mask thickness, impact angle and particle size. Calculations have shown that Two-sided Oblique Blasting will result in a larger decrease of the blast lag (Figure 7.7), but this technique can only be used in a very limited amount of channel designs.

7.5 Conclusions

The inclination of channel sidewalls that are formed during powder blasting results in what we call the blast lag (wide channels become deeper compared to smaller channels). This effect e.g. limits the maximum attainable aspect ratio. The inclination is caused by the relatively large size (9-29 μm) of the powder particles that are used for powder blasting.
The blast lag is reduced when the sidewall removal rate relative to the flat bottom removal rate is increased. This can be accomplished by blasting at a lower impact angle, which is confirmed by calculations. Rotating the target during blasting ensures uniform blasting. Experiments show that the steeper sidewalls that are created by this Radial Oblique Blasting result in a decreased blast lag. However, the effect is small and the application is limited due to a lower selectivity between the target and the mask material and shielding of the particle jet by the sidewalls at high aspect ratios.
A better way to decrease the blast lag is to use smaller powder particles. These can impact on the target closer to the mask edge and deeper in the bottom tip of the channel. This results in a depth increase as large as 36% when using 9 μm particles in stead of 29.2 μm particles. One disadvantage of using smaller particles is the decrease in selectivity, but that effect is much smaller compared to Radial Oblique Blasting.
Using smaller particles results in steeper sidewalls and less blast lag. However, larger particles are favourable when blasting through holes. In that case, the depth is not limited by the mask opening and blasting time but by the target thickness. The higher selectivity which accompanies

large particles allows prolonged blasting (even while the hole is already through), which will decrease the sidewall inclination.

7.6 References

1 P.J. Slikkerveer, F.H. in't Veld, "Model for patterned erosion", *Wear*, 233-235, (1999) pp. 377–386
2 P.J. Slikkerveer, P.C.P. Bouten, F.C.M. de Haas, "High Quality Mechanical Etching of Brittle Materials by Powder Blasting", *Sensors and Actuators*, 85, (2000), pp. 296-303.
3 E. Belloy, A. Sayah, M.A.M. Gijs, "Micromachining of glass inertial sensors", accepted for: *J. Microelectromech. Syst.* (2001)
4 E. Belloy, A. Sayah, M.A.M. Gijs, "Oblique powder blasting for three-dimensional micromachining of brittle materials", *Sensors and Actuators* A 92 (2001) pp. 358-363
5 Treibacher Schleifmittel GmbH, Ferroweg 1, D-79725 Laufenburg, Germany, Tel. +49.7763.9330
6 I. Finnie, "Some reflections on the past and future of erosion", *Wear* 186-187 (1995) pp. 1-10
7 P.J. Slikkerveer, M.H.A. van Dongen , F.J. Touwslager, "Erosion of elastomeric protective coatings", *Wear* 236 (1999) pp. 189–198

Application

This chapter reviews most of the devices that have been fabricated at the University of Twente using powder blasting. It gives a general idea of how powder blasting is currently used in micromachining.

8.1 Introduction

The development of powder blasting described in this thesis has been used by others to fabricate microstructures. This chapter reviews some of the devices that were made using powder blasting at the University of Twente. For each application the advantages and disadvantages of this technique will be discussed and compared to alternative techniques. Unless mentioned otherwise, all applications used Ordyl BF410 as the mask material for blasting.

8.2 Through holes

One of the most competitive applications of powder blasting is the ability of making holes easily through glass and silicon wafers. Besides the

applications that will be mentioned later in this chapter, through holes have also been blasted for the realisation of a detection cell, a reaction chamber [1], a micropipette [2], a viscosity detector [3], a centrifugal mixer [4], a gas sampling device [5] and a Modular Assembly for Total Analysis Systems (MATAS) [6]. All these applications needed through holes to access closed channels or to be able to make electrical connections after wafer to wafer bonding.

Single holes through glass or silicon can easily be blasted with a static nozzle within a few seconds. When multiple holes are required, it is easier to simultaneously blast all holes using a x-y scanning motion. The through hole shapes will be more identical in the latter case, since the amount of powder that is used for each hole (which influences the hole-shape) is more easily controlled. The top-hole diameter is generally made equal to the target thickness (Figure 8.1). The width of the bottom exit hole depends mainly on the top width but can be tuned by varying the blast time. The bottom width is always smaller than the top width, due to the slant sidewalls that are created by powder blasting. Although it limits the aspect ratio of the holes, this shape can also be beneficial for supporting and gluing capillaries. Holes with a higher aspect ratio can be blasted when using double sided masking [7] or by using a more erosion resistant mask material that allows a prolonged blasting time (see Chapter 4).

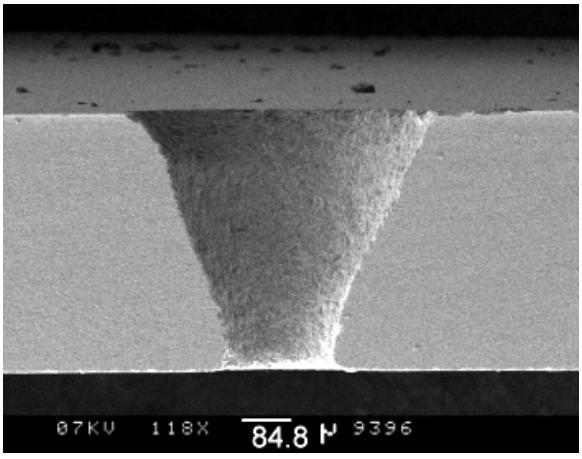

Figure 8.1 A through hole in Pyrex. Top diameter and target thickness: 500 μm, bottom diameter: 200 μm.

When the backside of the wafer has to be bonded to another wafer, it is important to protect it with a foil during blasting. If this is omitted, the heavily damaged zone around the holes makes the bonding contact area

very small. So although general bonding is still possible, the local area around the holes will not be bonded.

Alternative techniques that are capable to machining through holes such as (ultrasonic) drilling, lasermachining or RIE etching are less competitive in terms of machining time, equipment costs and reproducibility. This was already recognised by Philips [8] where powder blasting is now used to machine thousands of through holes simultaneously at a high accuracy.

8.3 Glass chips

There is a growing need to manage fluids on the microscale for chemical reactions and analyses. Microfluidics have the advantages of e.g. small sample volume, good temperature control and analysis equipment downscaling. In the case of microfluidic chips, often high voltages are required for fluid manipulation (Electro Osmotic Flow) or detection (conductivity sensors). This requires the fabrication of channels in insulating materials such as glass. Glass also has the advantage of being transparent and chemically inert.

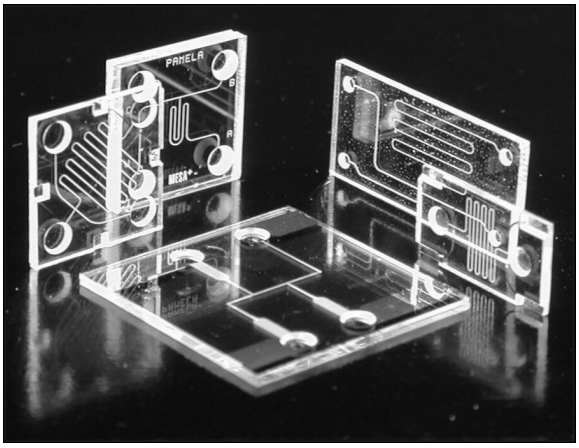

Figure 8.2 Several glass chips, which are blasted at the MESA+ research institute.

A large amount of glass chips have already been fabricated using powder blasting (Figure 8.2, [9, 10, 11, 12]). Channels and through holes are blasted in one substrate which is bonded (after a thorough cleaning step) to a second substrate to close the channels. This simple procedure results in robust glass chips. The fabrication can be carried out in a single day so it also allows for fast prototyping.

The channels can also be made by wet chemical HF etching which results in smooth and round channels. But due to the isotropic process, the aspect ratio is low and extra care and time has to be taken for the mask material in the case of deep channels (>1 μm).
As already explained in Chapter 5, the channel roughness can have an influence on the performance of the device and this subject still needs some research. One might expect some problems regarding residual particles that could prevent bonding or block channels, but non of these effects have been observed.

8.4 A Peristaltic MicroPump

A simple peristaltic micropump has been fabricated by T.T.Veenstra et al. [13] (Figure 8.3). The pump is self-priming, bubble-tolerant and it delivers a maximum flow rate of 9 ml/min.

Powder blasting was used for the connection channels (200μm wide and 180 μm deep) and the through holes (top width 850μm, bottom width about 400 μm) in the silicon bottom wafer. Together with selective anodic bonding [14], the fabrication process is extremely simple and robust and needs in principle only a single lithographic step.

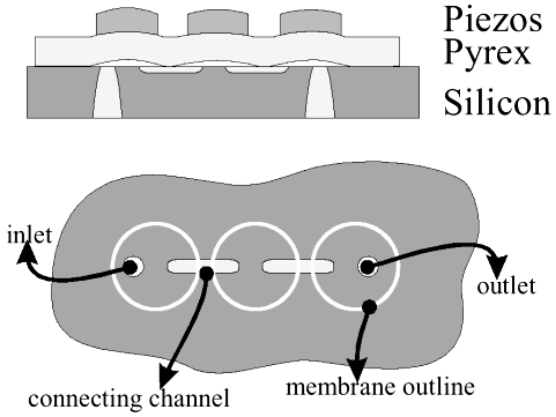

Figure 8.3 Side- and topview of the design of the peristaltic micropump..

KOH or RIE etching could have been used to make channels and inlets, but this was not necessary since the dimensions were not critical. Powder blasting was easier, faster and cheaper compared to these techniques.

8.5 Evaporator

For the realisation of a miniature fuel processor, an evaporator has been fabricated [15]. The goal is to evaporate a mixture of water and methanol at a gas rate of 3 l/min. While the mixture flows through long channels, it is heated up just above the critical evaporation temperature. The channel size is chosen such that bubble initiation will not occur and the mixture will evaporate at the channel exit.

The evaporator consist of 234 channels with a length of 6 cm and a width and depth of 70 μm placed closely together separated by 100 μm wide silicon (Figure 8.4). To blast these 70 μm narrow channels, the 50 μm thick negative resist foil BF405 was used as the mask material. The channels are closed by annodically bonding a Pyrex wafer to the silicon. Through holes in this Pyrex wafer were also made by powder blasting.

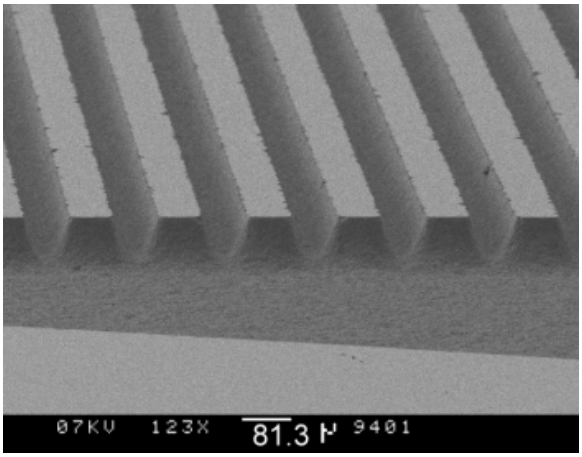

Figure 8.4 An array of 70μm wide channels in silicon for the evaporation of fluids.

Powder blasting was the most straightforward technique to fabricate these channels compared to alternative techniques like KOH or RIE etching. The channel roughness that results from the powder blasting enlarges the contact area of the fluid with the silicon causing a more efficient heat transfer.

8.6 An optical scan device

Lüttge designed a Microoptical Scan Device [16]. For this a quartz or Pyrex cantilever structure (top width 210 μm, thickness 200 – 500 μm) was fabricated using powder blasting (Figure 8.5). A wave-guide will be

placed on top of the cantilever. The beam is driven at resonance frequency to be able to scan e.g. a bar code.

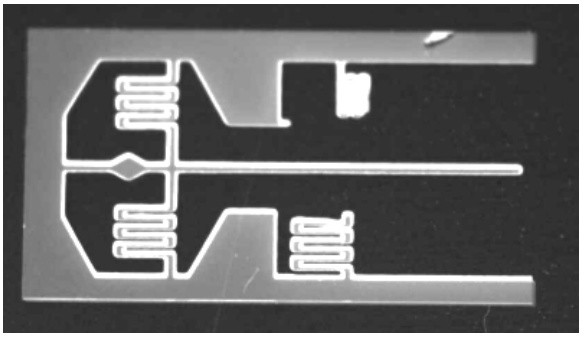

Figure 8.5 Powder blasted glass beam.

The physical forces of the air/particle jet are large enough to break the fragile cantilever when the wafer is blasted through. To support the cantilever during blasting, the substrates were either directly bonded to silicon or glued to a support wafer using ordinary resist. This also provided the necessary backside protection. The erosion rate of both fused and single crystalline quartz is smaller compared to glass (approximately two times), but the resist foil BF410 is thick enough to be able to machine through a 500 μm thick wafer.

The original design consisted of a HF- etched quartz wafer so that the piezoelectric properties of quartz can be used to drive the beam into resonance. However, it proved to be difficult to obtain a mask that could sustain such a long HF etch (over three hours). The slant side walls that result from the powder blasting causes the beam to have a trapezoidal cross-section, which decreases the maximal deflection during resonance. This effect can be decreased by oblique or prolonged blasting.

8.7 Stress release ring

M.T. Blom et al. presented local anodic bonding of a common Kovar alloy to Pyrex [17]. It is suitable for temperature-, solvent- and pressure-resistant micro fluidic connections. The different thermal expansion coefficients of Kovar and Pyrex caused some stress problems after bonding at temperatures between 200-400 °C. A stress release ring was added by powder blasting in order to release the thermal stresses induced during bonding (Figure 8.6).

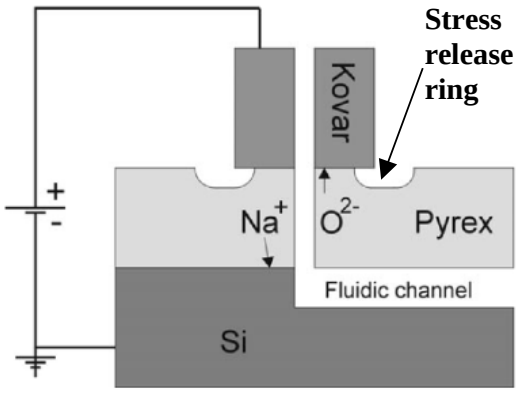

Figure 8.6 Local anodic bonding of Kovar on a bonded Pyrex–Si fluidic structure.

Together with the through holes, which were also in the design, powder blasting was done in two steps. Initially, all structures are powder blasted until the required depth for the rings is reached. Subsequently, a metal shadow mask is used to complete the through holes while protecting the rings. A ring depth of 170 μm in a 500 μm thick wafer was sufficient for a good stress release.
Powder blasting was chosen for it's ease and because the ring could be simultaneously machined with the through holes. The microflaws that are created by powder blasting did not initiate a crack due to the tensile stress that arises from the mismatch in thermal expansion coefficients.

8.8 Discussion

In the aforementioned applications, often the reason to use powder blasting is because the technique as well as the accompanying lithographics is easy, simple and fast. Even for silicon, where there are a lot of well-known machining techniques available, powder blasting was used exactly for these reasons. In the case of glass micromachining, the main alternative would be wet-chemical HF-etching. The two main disadvantages of this technique are that it etches isotropically (so aspect ratios are approximately 0.5) and to etch for a prolonged time requires extensive mask preparations. So in that case powder blasting is often the only option, especially in the case of machining through holes.
In these applications the minimum feature size is 70 μm and the maximum aspect ratio is 1. Although powder blasting is now capable of higher aspect ratios (2.5) at smaller feature sizes (30 μm) this would require an electroplated copper mask. This more laboriously process will only be used when it is really necessary.

The fabrication of glass chips shows that powder blasting does not directly affect the capability of wafer direct bonding. The substrate can easily be cleaned from the mask material (with e.g. acetone, KOH, HNO_3 or NaOH) and rinsing or an ultrasonic bath removes residual particles. After these cleaning steps, the substrate is again compatible with any micromachining technique.

8.9 Conclusion

Powder blasting is being used for machining glass in process steps that were previously impossible or avoided. It is also used for e.g. silicon machining in cases where the structure would previously have been fabricated using machines that are specialised for more specific and accurate tasks, (which is like using a pen to paint a wall). So powder blasting simplifies process steps in miromachining but also gives new opportunities.

8.10 References

1 N.R. Tas, R.E. Oosterbroek, T.T. Veenstra, M. Elwenspoek, A. van den Berg, "Microfluidics and Microtechnology for Microreactor Systems", *Proc. IMRET 5*, Strasbourg, France (2001)

2 C. Rusu, R. van't Oever, M.J. de Boer, H.V. Jansen, J.W. Berenschot, M.L. Bennink, J.S. Kanger, B.G. de Grooth, M. Elwenspoek, J. Greve, J. Brugger, A. van den Berg, "Direct integration of micromachined pipettes in a flow channel for single DNA molecule study by optical tweezers", *Journal of Microelectromechanical Systems*, 10 (2001) pp. 238 -246

3 F.H.J. van der Heyden, M.T. Blom, J.G.E. Gardeniers, E. Chmela, M. Elwenspoek, R. Tijssen, A. van den Berg, "A Micro Viscosity Detector for a Planar HydroDynamic Chromatography (HDC) System", *Micro Total Analysis Systems 2000*, Enschede, The Netherlands (2000) pp. 595-598.

4 S. Böhm, K. Greiner, S. Schlautmann, S. de Vries, A. van den Berg, "A Rapid Vortex Micromixer for Studying High-speed Chemical Reactions", *Micro Total Analysis Systems 2001*, Monterey, USA (2001) pp. 25-27

5 B.H. Timmer, J.G. Bomer, K.M. van Delft, R.P. Otjes, W. Olthuis, P. Bergveld, A. van den Berg, "Fluorcarbon Coated Micromachined Gas Sampling Device", *Micro Total Analysis Systems 2001*, Monterey, USA (2001) pp. 318-382

6 T.T. Veenstra, R.M. Tiggelaar, R.G.P. Sanders, J.W. Berenschot, J.G.E. Gardeniers, J.M. Wissink, R. Mateman, M.C. Elwenspoek, A. van den Berg, "Monolithic versus Modular Integration of a Micro-

FIA System for Ammonium Determination", *Micro Total Analysis Systems 2001*, Monterey, USA (2001) pp. 664-666

7 E.A. Dijkstra, W. Olthuis, J.G. Bomer, P. Bergveld, D.A. Kronemeijer, "Fabrication and packaging of a miniature sensor array for harsh environments", *MEMS conference*, Berkeley California, USA (2001)

8 H.J. Ligthart, P.J. Slikkerveer, F.H. in 't Veld, P.H.W. Swinkels, M.H. Zonneveld, "Glass and glass machining in ZEUS panels" *Philips J. Res.* 50 (1996) pp. 475-499

9 R.E. Oosterbroek, M.H. Goedbloed, A. van den Berg, "Optimization and Realization of Electro-osmotically driven Microsynthesis Systems", *Micro Total Analysis Systems 2001*, Monterey, USA (2001) pp. 627-628.

10 S. Schlautmann, H. Wensink, R. Schasfoort, M. Elwenspoek, A. van den Berg, "Powder-blasting technology as an alternative tool for microfabrication of capillary electrophoresis chips with integrated conductivity sensors", *J. Micromech. Microeng.* 11 (2001) pp. 386-389

11 R.B.M. Schasfoort, R. Luttge, A. van den Berg, "Magneto-hydrodynamically (MHD) Directed Flow in Microfluidic Networks", *Micro Total Analysis Systems 2001*, Monterey, USA (2001) pp. 577-578.

12 M. Brivio, N.R. Tas, R.H. Fokkens, R.G.P. Sanders, W. Verboom, D.N. Reinhoudt, A. van den Berg, "Chemical Microreactors in combination with Mass Spectrometry", *Micro Total Analysis Systems 2001*, Monterey, USA (2001) pp. 329-330.

13 T.T.Veenstra, J.W.Berenschot, R.G.P.Sanders, J.G.E.Gardeniers, M.C.Elwenspoek, A.van den Berg, "A Simple Selfpriming Bubble-Tolerant Peristaltic MicroPump", *Eurosensors XIV*, Copenhagen, Denmark (2000) pp. 671-672

14 T. T. Veenstra, J. W. Berenschot, J. G. E. Gardeniers, R. G. P. Sanders, M. C. Elwenspoek, and A. van den Berg, "Use of Selective Anodic Bonding to Create Micropump Chambers with Virtually No Dead Volume", *Journal of The Electrochemical Society*, 148, (2001) pp. G68-G72.

15 T.T. Veenstra, F. Lim, unpublished work

16 R. Luttge, A.S. Holmes, S.Schlautmann, H. Wensink, "Microoptical Scan Device", *Proceedings MME2001*, Cork, Ireland (2001) pp. 151-154

17 M.T. Blom, E. Chmela, J.G.E. Gardeniers, J.W. Berenschot, M. Elwenspoek, R. Tijssen, A. van den Berg, "Local anodic bonding of Kovar to Pyrex aimed at high-pressure, solvent-resistant microfluidic connections", *J. Micromech. Microeng.* 11 (2001) pp. 382–385

Final remarks

At the end of this thesis, it will be discussed to what extend the initial goals such as a smaller feature size and a larger aspect ratio, have been reached.

9.1 Feature Size

A main goal of this project when it started in 1997 was to decrease the minimum feature size to 10 μm. The first obstacle to accomplish this was to find a suitable resist material that was able to define such a feature size. Electroplated copper can not only be used for any feature size, it also proved to have an excellent erosion resistance. Second, to be able to blast a 10 μm channel, 3 μm particles should be used. However, using these particles results in a ductile erosion mechanism on the target due to the low kinetic energy (Chapter 6). This leads to a very bad selectivity between the mask material and the target, which makes it difficult to blast deep channels (Figure 9.1).

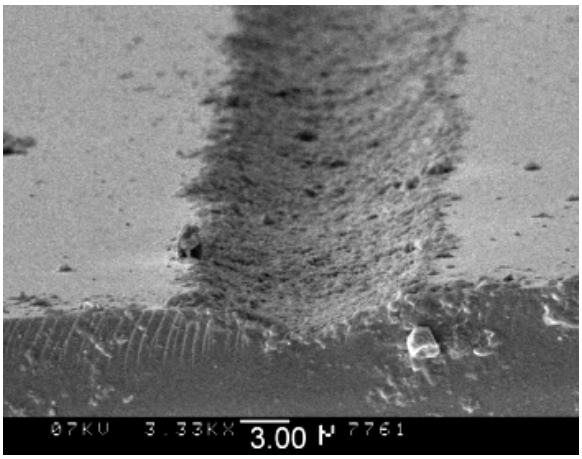

Figure 9.1 A 10 μm wide channel blasted in glass using 3 μm particles.

The particle kinetic energy at which the transition to the ductile erosion mechanism starts is 17 nJ for Pyrex. We can take this energy to be the minimum kinetic energy that is suitable for powder blasting. Table 9-1 shows some particle properties that are necessary to attain such an energy.

Table 9-1 Particle properties for a particle kinetic energy of 17 nJ.

Particle type	Density [g/cm^3]	Speed [m/s]	Remarks
5 μm Alumina (Al_2O_3)	3.9	365	
3 μm Alumina (Al_2O_3)	3.9	785	Speed not attainable
3 μm Tungsten Carbide (WC)	15.7	390	Particles not widely available

On the other hand, there is also a limit in the minimum crack length. According to Slikkerveer et al. [1], the minimum crater width (twice the minimum crack length) after impact is 12.4 μm for Pyrex and 13.1 μm for Silicon. These observations lead to a practical limit of about 30 μm wide channels (Figure 9.2).

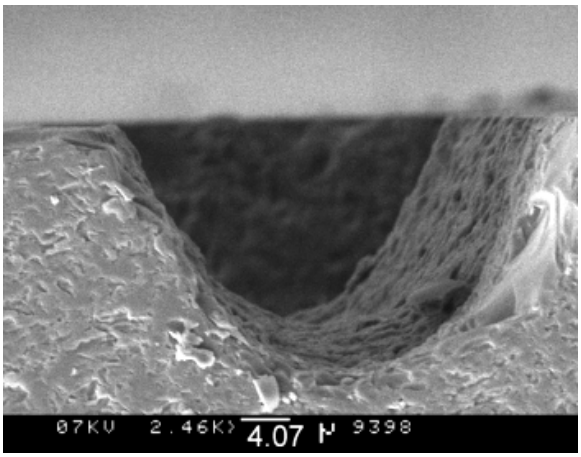

Figure 9.2 A 35 μm wide channel blasted in glass using 9 μm particles.

9.2 Aspect Ratio

Another goal of this project was increasing the aspect ratio to about 5 to be able to compete with established micromachining. The main restriction to powder blast high aspect ratios is the decrease in removal rate when the aspect ratios become larger than approximately one. The quality of the mask material now determines the blast time and hence the aspect ratio. The use of smaller particles results in steeper sidewalls, which is beneficial for the aspect ratio. Using electroplated copper, the aspect ratio could be increased to about 2.5 for channels smaller than 100 μm.

9.3 Reproducibility and predictability

Powder blasting can be regarded as a reproducible machining technique as long as the basic demands like an evenly powder flux, smooth x-y movement, constant pressure, unworn nozzle, constant particle size etc. are satisfied. In that case, depth tolerances of a magnitude close to the surface roughness can be obtained. However, the edge of the mask material will eventually calve off which strongly influences the shape of the sidewalls. The rate of mask deterioration is not a constant but depends on blasting conditions, type of mask, mask material age, mask thickness, mask treatment etc. The depth of a V-shaped channel, which is also dependent on the mask opening, is strongly influenced by these sometimes unpredictable effects. This makes the amount of blast lag very dependent on the mask quality. Electroplated copper is again the best

mask material to be used for reproducibility since it does not suffer from ageing and the erosion resistance is high.
To predict the shape of sidewalls is difficult even with a perfect mask material. Slikkerveer et al. succeeded to qualitatively predict the two-dimensional shapes that result from powder blasting [2]. However, the extensive simulations that were required obstruct a practical usage for device designing.

9.4 Outlook

Powder blasting will continue to play a role in micromachining because it simplifies existing process steps in miromachining but also gives new opportunities for glass micromachining. One reason why powder blasting would not soon be widely used by other research groups and companies is the fact that a small-scale powder blaster is not commercially available yet. This means that the equipment has to be partially home build and that there is no professional technical support.
Further research can be directed to measuring the average crack length for actual particle impacts and to adapt the existing erosion models (e.g. using two lateral cracks in stead of four, Figure 5.4 Chapter 5). Cross sections of the crack patterns (like in [3]) for the low kinetic energy particles as used in this thesis would give more information on the exact erosion mechanism. This would also clarify the differences between open-structured and normal glasses.
Using small Tungsten Carbide particles with a larger mass could be beneficial for the blast lag while the high removal rate is maintained. The consequence for the selectivity has to be investigated. A large improvement of the powder blast characteristics can be expected when there are even better resist materials available. In general, a higher erosion resistant mask material would allow a higher aspect ratio and more capabilities of blasting ceramics. It would also allow the use of smaller particles, which results in less blast lag and a lower surface roughness. A better metal mask material would be electroplated nickel, which is expected to have a 25% lower erosion rate compared to copper [4]. Improvement in the minimum feature size and erosion resistance of commercial powder blasting resist foils can be expected from the continuing growing flat panel display industry.

9.5 References

1 P.J. Slikkerveer, P.C.P. Bouten, F.H. in't Veld, H. Scholten, "Erosion and damage by sharp particles", *Wear* 217 (1998) pp. 237-250

2 P.J. Slikkerveer, F.H. in't Veld, "Model for patterned erosion", *Wear* 233-235 (1999) pp. 377–386
3 J.T. Hagan, M.V. Swain, "The origin of median and lateral cracks around plastic indents in brittle materials", *J. Phys. D: Appl. Phys.* 11 (1978) pp. 2091-2102
4 I. Finnie, "Some reflections on the past and future of erosion", *Wear* 186-187 (1995) pp. 1-10

Ceramic Powder Blasting

A.1 Introduction

Powder blasting is a directional machining technique for brittle materials like glass, silicon and ceramics. Properties of ceramic materials such as wear resistance, chemical inertness and high melting temperatures are attractive for micromechanical systems in harsh environments. Some ceramic micromachining methods like laser machining [1], ultrasonic drilling [2], and isotropic etching [3] are already available. The advantage of powder blasting is that it is suitable for different brittle materials, the design can be defined by lithography and there are no large residual thermal stresses like in laser machining (although there are small localised residual stresses due to the particle impacts [4]). To investigate the possibilities of powder blasting as a ceramic micromachining technique, channels are powder blasted in an Alumina (Al_2O_3) substrate as a case study.

Alumina substrates can be obtained in a much larger variety compared to silicon or glass. There is not only a difference in surface roughness and thickness but also in e.g. grain size, density and alumina content. Properties are more standard when acquiring single crystalline alumina (sapphire), but the costs are much higher in that case. Some properties of the polycrystalline alumina that is used for this study are listed in Table A-1.

Table A-1 Alumina properties [5]

Material	Alumina A-476
Thickness	500 μm
Alumina content	96%
Density	3.7 g/cm^2
Grain size	$\approx$ 2 μm
Surface roughness	R_a = 0.2-0.8 μm
Vickers hardness	13.7 Gpa
Young's modulus	330 Gpa

In this appendix we will first determine the erosion rate of the mask material and alumina target after which channels will be blasted in alumina.

A.2 Mask Material

Several types of mask materials can be used for powder blasting. An electroplated copper mask is used in this case of ceramic powder blasting because it has a very low erosion rate (see Chapter 4).
The channel layout and electroplating results are shown in Figure A.1. The minimum channel width for these structures that could be electroplated is 100 μm for alumina. SU-8 channel moulds on alumina that are smaller than 100 μm are flushed away during development. The adhesion of SU-8 to the copper seed layer is worse when using alumina as a substrate compared to a silicon substrate. A possible explanation for this is that the irregular bottom surface of the SU-8 moulds (as a result of the rough alumina surface) has a bad influence on the SU-8 adhesion.

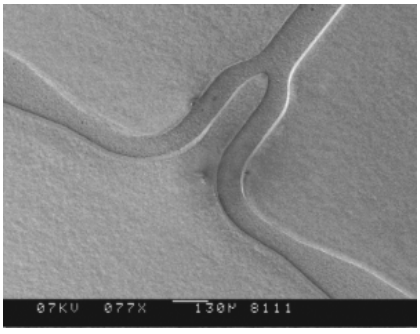

Figure A.1 Electroplated copper masks, 100 μm wide channel on Alumina.

A.3 Blasting Experiments

A.3.1 Erosion rate

The erosion rate is measured at a constant pressure using 9 and 29 μm particles of alumina and SiC, with a hardness of 17 GPa and 25 GPa and a density of 3.9 g/cm^3 and 3.2 g/cm^3 respectively. The particle velocity is measured separately at these conditions before the measurements. Erosion rates are usually measured by exposing a piece of target to a fixed amount of powder at constant blasting conditions. The amount of powder that is used during blasting is measured with an accuracy of 0.5 grams in our case. To perform an accurate erosion measurement with such a large absolute error in powder weight would require relatively large and many pieces of target which were not available to us. Therefore we choose to use a silicon reference sample to determine the amount of powder that has been used during a measurement. The erosion rate of silicon was available from previous experiments for a range of alumina particle sizes (Chapter 5). We assume that the silicon erosion rate depends on the particle kinetic energy and not on the particle material. In this way, the relative removal rate of the different samples can be determined very accurately. The absolute erosion rate will be less accurately determined, but this is also of less importance for micromachining.

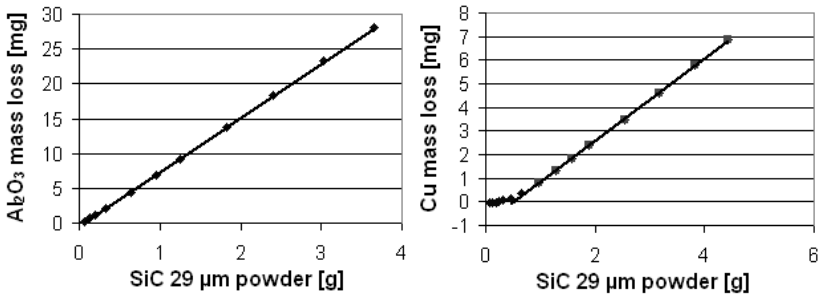

Figure A.2 The erosion rate for Alumina and electroplated copper.

Up to five samples were placed in line, all leaving the same area exposed to the particle jet. The jet is scanned over the samples in one direction and the weight loss is measured at intervals and compared to the silicon weight loss. The removal rate is subsequently calculated from these measurements. Figure A.2 shows the erosion rate for alumina and electroplated copper measured in [mg/g.] Removal rates are converted to [μm/min] for all measurements in Table A-2. The surface roughness was

determined by calculating the average R_a of 5 Dektak scans with a length of 1 mm. These results are also listed in Table A-2 (the error being the standard deviation of the 5 R_a values). The data for Pyrex is shown for comparison.

Table A-2 Surface roughness R_a and steady state removal rates for several materials (for an area of 7x7 cm^2 and a powder feed of 10 g/min).

	29 μm SiC	**29 μm Al_2O_3**	**9 μm SiC**	**9μm Al_2O_3**
Particle velocity [m/s]	254 ± 6	230 ± 7	267 ± 10	270 ± 6
Removal rate Al_2O_3 [μm/min]	4.3	1.7	1.3	0.72
Removal rate Cu [μm/min]	0.40	0.35	0.26	0.34
Selectivity Al_2O_3/Cu	10.8	4.9	5.0	2.1
R_a Al_2O_3 [μm]	1.23 ± 0.09	0.97 ± 0.09	1.10 ± 0.12	0.98 ± 0.13
Removal rate Pyrex [μm/min]	-	25	-	13.5
R_a Pyrex [μm]	-	2.5 ± 0.6	-	1.2 ± 0.2

A.3.2 Channels

Square samples of Alumina (6x6 cm^2) were prepared with a 35 μm thick electroplated copper mask. The 29 μm SiC particles are used for powder blasting since they are small enough to machine the 100 μm channels and ensure a high selectivity between alumina and copper (Table A-2).
Figure A.3 shows the results of powder blasting with the remaining copper mask still on. The depth in the channels is approximately 80 μm. A separate metal plate mask containing 1 mm holes is manually aligned and clamped to the substrate for the blasting of the 1 mm holes. Blasting is carried out at a fixed nozzle position above a single hole for about 90 s to machine through the 500 μm thick alumina.

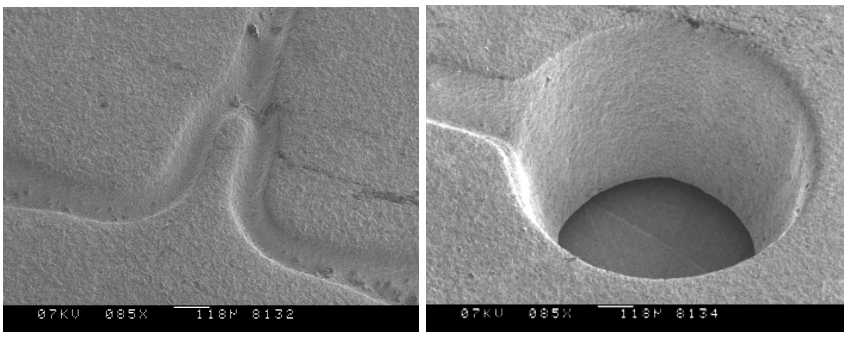

Figure A.3 Powder blasted ceramic structures. Left: 100 μm wide and 80 μm deep powder blasted channels. Right: through hole.

The powder blasted depth was monitored during the process (Figure A.4).

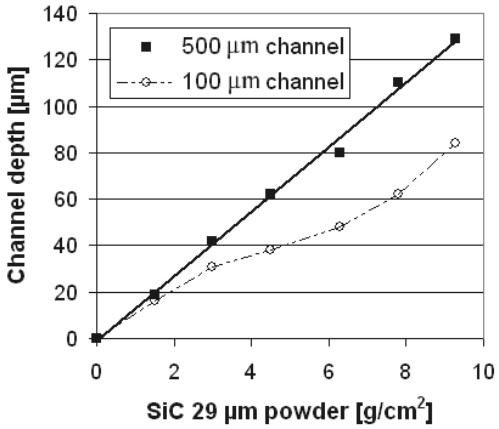

Figure A.4 Channel depth during powder blasting.

A.4 Discussion

The powder particle size and hardness has a strong influence on the alumina erosion rate, while the copper erosion rate does not change very much (Table A-2). The hardness of the SiC particles is higher compared to the alumina substrate, which results in a higher removal rate [6]. So the selectivity between copper and alumina depends mainly on the erosion rate of alumina. As a rule of thumb, the particle size is taken to be at most a third of the minimum channel width. Often a smaller size is

chosen to achieve a smoother finish, but in this case the largest possible particle size is chosen to obtain a high selectivity.

The surface roughness of the alumina samples is between 1 - 1.2 μm (Table A-2). Normally, when a homogeneous brittle material (glass or silicon) is blasted at comparable conditions the surface roughness varies between 1.2 and 2.5 μm. The dependence of the roughness on the particle kinetic energy in that case can be attributed to the erosion mechanism which is defined by the lateral crack system (see Chapter 5). The small variation in roughness for alumina implies that the lateral crack system is not the (only) erosion mechanism for alumina. The erosion mechanism will be influenced by the microstructure of polycrystalline alumina, which contains numerous grain boundaries. These boundaries are relatively weak which makes it easier to eject grains from the target [see e.g. 7].

Figure A.3 shows that the resulting powder blasted channels are well defined. Figure A.4 shows that the removal rate of a 100 μm wide channel is slower compared to wider channels. This is called the blast lag and is a normal phenomenon in powder blasting (Chapter 7). However, the lag is enhanced by the fact that the copper mask opening temporarily becomes narrower during powder blasting. The absolute erosion rate of alumina if determined from this graph (the 500 μm channel depth) is 35% lower compared to the erosion rate measurements. This is probably due to the inaccurate determination of absolute erosion rate by using a silicon reference sample

A.5 Conclusion

The erosion rate of Alumina depends mainly on the powder particle size (or kinetic energy) and the particle hardness as expected. The best selectivity is attained for particles that are harder than the target material and with the largest size that is allowed by the minimum feature size.
The surface roughness that results from the powder blasting is between 1-1.2 μm. The small variation in roughness at different blasting conditions indicates that the erosion mechanisms is not (only) defined by the lateral crack mechanism.
The adhesion of the SU-8 mould to the copper seed layer is even worse when using a rough alumina substrate. This limits the minimum feature size to about 100 μm channels in case of an SU-8 thickness of 50 μm.
Channels with a width of 100 μm and a depth of 80 μm have been powder blasted in Alumina. Through holes of 1 mm have been fabricated using a separate metal shadow mask.

As with isotropic etching and laser machining, powder blasting is capable of machining complex designs in ceramic. It has the advantage of being a directional and cold process, which avoids thermal stresses. However, the selectivity with mask materials is low which limits the application of ceramic powder blasting.

A.6 Acknowledgement

Jeroen Haneveld is gratefully thanked for his contribution to this work.

A.7 References

1 M. Mendes, V. Oliveira, R. Vilar, F. Beinhorn, J. Ihlemann, O. Conde, "XeCl Laser Ablation of Al2O3-TiC Ceramics" *Applied Surface Science* 154-155 (2000) pp. 29-34

2 T.B. Thoe, D.K. Aspinwall, M.L.H. Wise, "Review on ultrasonic machining", *Int. J. Mach. Tools Manufact.* 38 (1998) pp. 239-255

3 E. Makino, T. Shibata, Y. Yamada, "Micromachining of Fine Ceramics by Photolithography" *Sensors and Actuators* A 75 (1999) pp. 278-288

4 M.V. Swain, "A note on the residual stress about a pointed indentation impression in a brittle solid", *J. Mat. Sci. Letters* 11 (1976) pp. 2345-2348

5 Kyocera Fineceramics GmbH, Hammfelddamm 6 D-41460 Neuss, Germany, Phone: +49-213116910, Fax: +49-2131129340

6 P.H. Shipway, I.M. Hutchings, "The role of particle properties in the erosion of brittle materials ", *Wear* 193 (1996) pp. 105-113

7 J.E. Ritter (Ed.), "Erosion of Ceramic Materials", *Trans Tech Publications*, Zurich, Switzerland (1992)

Summary

This thesis deals with the use of powder blasting as a micromachining technique to create micro systems. Powder blasting is a technology in which small particles, accelerated by an air jet, are directed towards a brittle target for mechanical material removal. It is especially useful for glass machining due to the limitations of other glass micromachining techniques.

Particle jets have been used for many years to test the wear resistance of materials. Chapter 2 gives a literature overview of this research field. Only recently have particle jets been used as a machining technique.

An important parameter for powder blasting is the average particle velocity. In Chapter 3 a method is presented that is able to measure the velocity of small particles in an air jet (< 30 μm) that are used to machine very small structures (< 100 μm).

By partially shielding the target from the particle jet using a mask, small and complex structures can be fabricated. Three types of mask materials are discussed in Chapter 4; a pre-machined metal plate, commercially available thick negative resist foil and electroplated copper.

The surface roughness of powder blasted structures is much higher compared to other micromachining techniques. Chapter 5 shows how the roughness depends on the powder blasting parameters, and how it can be manipulated afterwards.

Powder blasting smaller structures requires the use of smaller powder particles. As the particle size is decreased, the erosion mechanisms will change (the ductile-brittle transition) and the removal rate and selectivity with mask materials will drop sharply. This transition is studied in detail for silicon, Pyrex and sodalime glass in Chapter 6.

The sidewall of a powder blasted channel is not straight but has a certain inclination. This inclination restricts the maximum aspect ratio of the

channel, and it results in the blast lag: wider channels become deeper compared to smaller channels. Chapter 7 shows how blasting with a smaller impact angle and by using smaller particles can reduce this blast lag.
Chapter 8 shows some of the micro systems that have been fabricated with the help of powder blasting, and it discusses why powder blasting was chosen in those cases.
Chapter 9 gives some final remarks on the limitations of powder blasting as a micromachining technique.

Samenvatting

Dit proefschrift gaat over het gebruik van poederstralen als een micro-bewerkingstechniek voor de fabricage van microsystemen. Poederstralen is een techniek waarbij kleine deeltjes, versneld door een luchtstroom, worden gericht op een bros werkstuk om mechanisch materiaal te verwijderen. Het is in het bijzonder geschikt om glas mee te bewerken, vanwege de beperkingen van alternatieve bewerkingstechnieken voor glas.

Het stralen met deeltjes is jarenlang gebruikt om de slijtage van materialen te testen. Hoofdstuk 2 bevat een literatuuroverzicht van dit onderzoeksveld.

Een belangrijke parameter voor poederstralen is de gemiddelde deeltjessnelheid. In hoofdstuk 3 wordt een methode gepresenteerd waarmee de snelheid gemeten kan worden van kleine deeltjes in een luchtstroom ($<30\ \mu$m) die worden gebruikt om zeer kleine structuren te fabriceren ($<100\ \mu$m).

Door het werkstuk gedeeltelijk af te schermen met een masker kunnen kleine en complexe structuren gemaakt worden. Drie soorten maskers worden besproken in hoofdstuk 4; een voorbewerkte metalen plaat, een commercieel verkrijgbare dikke fotogevoelige folie en elektrodepositie van koper op het werkstuk.

De oppervlakteruwheid van gepoederstraalde structuren is groter in vergelijking met andere micro-bewerkingstechnieken. Hoofdstuk 5 laat zien hoe de ruwheid afhangt van de poederstraal parameters, en hoe deze na het poederstraal proces kan worden veranderd.

Om zeer kleine structuren te fabriceren zijn zeer kleine deeltjes nodig. Als de deeltjes kleiner worden, verandert het erosiemechanisme (de “bros naar week” overgang) waardoor de graafsnelheid sterk afneemt (zowel

absoluut als in vergelijking met het masker). Deze overgang wordt in hoofdstuk 6 nauwkeurig bestudeerd voor sodalime glas, Pyrex glas en silicium.
De wanden van een gepoederstraald kanaal zijn niet loodrecht, maar hebben een zekere helling. Deze helling beperkt de maximale breedte-diepte verhouding van de kanalen en resulteert ook in de "graafvertraging": brede kanalen worden onder dezelfde omstandigheden dieper dan smallere kanalen. Hoofdstuk 7 laat zien hoe de graafvertraging verminderd kan worden door het gebruik van kleinere deeltjes of door de invalshoek van de poederstraal te verminderen.
In hoofdstuk 8 worden enkele microsystemen getoond die gefabriceerd zijn met behulp van poederstralen, en er wordt uitgelegd waarom poederstralen daarvoor als fabricagetechniek werd gekozen.
Hoofdstuk 9 geeft enkele laatste opmerkingen met betrekking tot de beperkingen van poederstralen als een micro-bewerkingstechniek.

Dankwoord

Ondanks dat op de voorkant van dit boekje mijn naam prijkt, ben ik geenszins alleen verantwoordelijk voor de resultaten die er in staan. Ik was slechts de top van een grote piramide zullen we maar zeggen. Die piramide ga ik nu bedanken.

Allereerst diegenen die het dichts bij het project betrokken waren. Miko Elwenspoek, mijn begeleider en promotor. Bedankt dat je me veel vrijheid gaf, het project in goede banen leidde maar vooral omdat je me altijd bleef steunen.
Henri Jansen, mijn eerste begeleider. Wat betreft het onderzoek konden we soms behoorlijk van mening verschillen (ik denk aan het vacuüm stralen), ook daarvan heb ik veel geleerd.
Jeroen Haneveld, mijn enige afstudeerder. We hadden zoveel gemeen in werkwijze en op het persoonlijke vlak, dat ik je helaas moeilijk kon aanvullen.

De volgende mensen hebben grootte en kleine dingen gedaan voor mij en mijn project.
Remco Sanders maakte de eerste opstelling, en toen wisten we zeker dat we er beter één konden kopen. Henk van Wolferen liet toe dat er optica in de stofkamer gezet mocht worden, en dacht er zelfs aan mee. Erwin Berenschot had dat ene geweldige masker idee. Stefan Schlautmann was de eerste poederstraal volgeling. Meint de Boer begeleidde Uwe en Jeroen toen ik in Cambridge zat. Uwe Matheis hat das erste plating bath aufgebaut und wir benutzen es noch immer. Joost Visser produceerde uiteindelijk een schuinstraler, maar vraag niet hoe. Tijs Lammertink, Maarten Jacobs, Gerard Slootweg, Mathieu Odijk maakten een heuse kolommenklopper.

Verder wil de overige mensen van de micmec bedanken voor de bijzondere werksfeer.
Robert Zwijze, meer cleanroomgenoot dan kamergenoot. Remco Wiegerink, maakte een voor hem eenvoudige en voor mij ingewikkelde transistor schakeling. Theo Veenstra was met name in de laatste maanden een bron van steun en promotie informatie (een slecht beoefenaar maakt een goede leraar). Willem Tjerkstra, daar waar Linux wel gewoon werkt. Roald Tiggelaar, ook wel Twheo maar met een duidelijker fatsoensnorm. Niels Tas, je zal blij zijn dat mijn opstelling nu naar boven gaat. Saravanan S., cricket goeroe. Edin Sarajlic, van de lekkere chiwachichi (goed gespeld?). Cristina Russu, de eerste gaatjes zaten in jouw device. Edwin Oosterbroek, niet omvallen op die motor. Ronny van 't Oever, met zijn pion Niko Bloemendaal (succes jongens). Wietze Nijdam, ain't no mountain high enough. Jasper Nijdam, not always User Friendly. Zakaria Moktadir, always smiling. Regina Lüttge, wordt bedankt voor de ginger-wine. Florian Lim, yet another Gronauer. Pele Leusink nam me in het begint aan het handje toen er aan de opstelling geknutseld moest worden. Theo Lammerink, succes met de DSP's. Toon Kuijpers, graag hoor ik nog eens een gitaar concert van je. Gijs Krijnen, karaoke bleek niet je sterkste punt. Marieke Janssen, young blue eyes. Joost van Honschoten, doe nog eens een tentje-boompje. Hien Duy Tong, let's play some more soccer! Martijn Goedbloed, ga alsjeblieft nog eens kanalen poederstralen. Han Gardeniers, speel nog eens FC Twente – Roda JC. Martin van Es, jouw PHP-scrips kwamen zowel privé als op de UT goed van pas. Philip Ekkels, bonking dolphin. Dick Ekkelkamp, de oudste der micmeccers. Han van Egmond, liep het nu spaak of niet? Koen van Delft, alleen micmeccer bij vlaai. Deladi, I like your first name better. Johannes Burger, stond niet zozeer aan als wel bij de wieg van dit project. Monica Brivio, ciao tesorino mio. Marko Blom, weet je nog de Okonomiyaki? Judith Beld en inmiddels -Kuipers, de hoedster der micmeccers. John van Baar, de dolende.

Ook hulde aan het financiële team Ingrid Boers, Dirk de Groot, Simone Heideman en Jose Nijhuis.

De hele MESA$^+$ staf wordt bedankt voor de hulp als ik weer eens in de cleanroom vertoefde. Jullie zullen blij zijn dat mijn opstelling daar niet stond. Speciale dank voor Samantha Geerdink voor de chemicaliën die ik mocht meesmokkelen, en natuurlijk Bert Otter voor de SEM foto's en alle verhalen over Ierland die tijdens de sessies loskwamen.

I would like to thank John Field for letting me wander around the Cavendish for three months and Alun Davies for letting me get in his

way and use the erosion rig. Please send my regards to the whole PCS fracture group.

Wat er ook allemaal gebeurde in de afgelopen jaren, er was één constante factor waarop ik altijd kon terugvallen: mijn directe familie. Ik hoop dat dat voor altijd zo blijft.

Annemieke, wij gaan nu echt beginnen (K).

Henk Wensink,
Enschede, januari 2002